



**UNIVERSITÀ DEGLI STUDI DI TRIESTE**

**XXVII CICLO DEL DOTTORATO DI RICERCA IN  
NANOTECNOLOGIE**

**TARGETING NATURAL ANTIOXIDANT  
COMPOUNDS TO THE BRAIN: A  
METABOLOMIC ASSESSMENT**

Settore scientifico-disciplinare: BIO/10

**DOTTORANDO  
STEFANO FORNASARO**

**COORDINATORE  
PROF. LUCIA PASQUATO**

**SUPERVISORE DI TESI  
PROF. SABINA PASSAMONTI**

**TUTOR  
DR. FULVIO MATTIVI**

**TUTOR  
DR. LOVRO ŽIBERNA**

**ANNO ACCADEMICO 2013 / 2014**

The research presented in this doctoral thesis was supported by the European Regional Development Fund, Cross-Border Cooperation Italy-Slovenia Programme 2007-2013 (project AGROTUR).

## Abstract

A diet rich in fruits and vegetables has been associated with a decreased risk of brain diseases. Some plant-specific compounds occurring in fruits and vegetables, such as flavonoids, have been found to exert neuroprotection, thus decreasing neurological disease risk. The current hypothesis is that neuroprotection is due to the antioxidant properties of flavonoids.

The main aims of this PhD thesis were: i) to assess whether some flavonoids are transported from the blood into the brain across the blood-brain barrier, ii) to understand if neuroprotection is mediated by an impact on brain metabolism.

The first part of the thesis describes *in vivo* experiments with cyanidin 3-glucoside (C3G), implementing different metabolomics analyses approaches. Mean Time (MT) parameters are reported as useful indicators of the retention properties of C3G in peripheral tissues. The second part deals with the development and characterization of a selective and sensitive analytical method, based on Surface-Enhanced Raman Spectroscopy (SERS), enabling the assessment of reactive oxygen species (ROS) and reactive nitrogen species (RNS) in living cells.

## Abstract

Una dieta ricca in frutta e verdura è stata associata a un ridotto rischio di malattie neurodegenerative, e alcuni composti antiossidanti presenti in frutta e verdura, come i flavonoidi, sono stati riconosciuti come agenti neuroprotettivi. Gli obiettivi principali dell'attività di ricerca riportata in questa tesi sono stati la valutazione del passaggio dal sangue al cervello, attraverso la barriera emato-encefalica, di alcuni flavonoidi, la comprensione del loro impatto sul metabolismo del cervello e del loro meccanismo d'azione come agenti neuroprotettivi. La prima parte della tesi descrive diversi approcci di analisi metabolica utilizzati in esperimenti in vivo con cianidina 3-glucoside (C3G). Parametri di tempo medio sono riportati come utili indicatori delle proprietà di ritenzione di C3G nei tessuti periferici.

La seconda parte presenta lo sviluppo e la caratterizzazione di un metodo analitico, basato sulla spettroscopia Raman amplificata da superfici (SERS), per la determinazione di specie reattive dell'ossigeno e dell'azoto (ROS/RNS), in cellule viventi.

# Abbreviations

<b>Abbreviation</b>	<b>Description</b>
A	$T_0$ intercept of distribution kinetics; dependent on dose and PK properties
$\alpha$	Exponent of the polyexponential equation (slope factor)
$\beta$	Exponent of the polyexponential equation (slope factor)
ABAP	2,2'-azobis (2-amidinopropane) dihydrochloride
AIC	Akaike's information criteria
$AUC_{0-\infty}$	Area under curve out to infinity;
AUMC	Area Under the first Moment Curve from time 0 to infinity
AuNPs	Gold nanoparticles
B	$T_0$ intercept of elimination phase; dependent on dose and PK properties
C(t)	Drug concentration at time t
$C_0$	Back-extrapolated drug concentration following rapid bolus iv administration
C3G	Cyanidin-3-glucoside
$CL_d$	Distribution clearance; a measure of the ability of a drug to pass into and out of the tissues of the peripheral compartment. Constant of proportionality between rate of distribution and rate of redistribution
$CL_T$	Total body clearance; a measure of the ability of the organs of elimination to remove drug from the plasma; proportionality constant between rate of elimination and plasma concentration
$C_{max}$	Maximum observed concentration
$C_{min}$	Minimum observed concentration over a dosing interval
D3G	Delphinidin-3-glucoside
DCM	Dichloromethane
DMEM	Dulbecco's Modified Eagle's Medium
DMSO	Dimethylsulphoxide
EMA	European Medicines Agency
ESI	Electrospray ionisation
FBS	Fetal bovine serum

FCS	Fetal calf serum
FDA	Food and Drug Administration
FDR	False Discovery Rate
GSH	Glutathione (reduced form)
GSSG	Glutathione (oxidized form)
HEPES	4-(2-hydroxyethyl)-1-piperazineethanesulfonic acid
HPLC	High performance liquid chromatography
IC	Number of circulations. Average number of times molecules return to the central compartment after passage through it.
isoPN3G	Iso-peonidin-3-glucoside
K <sub>p</sub>	Measure of relative distribution of drug over the two compartments.
k <sub>10</sub>	rate constant for elimination of drug from central compartment to outside body
k <sub>12</sub>	rate constant for distribution of drug from central compartment to peripheral compartment
k <sub>21</sub>	rate constant for redistribution of drug from peripheral to central compartment
LC/MS	Liquid chromatography mass spectrometry
LTQ	Linear trap quadrupole
M3G	malvidin-3-O-glucoside
MPA	3-mercaptopropionic acid
MRT	Mean Residence Time; the average time spent in the body by a drug molecule
MRTC	Mean Residence Time in the central compartment
M RTP	Mean Residence Time in the peripheral space
MTT	Meat Transit Time;
MTT <sub>i</sub>	Mean Transit Time in a specific tissue <i>i</i>
NCA	Non-Compartmental Analysis
NPs	Nanoparticles
PBS	Phosphate Buffered Saline
PCA	Principal component Analysis
PG3G	Pelargonidin-3-O-glucoside
PK	Pharmacokinetic(s)

PN3G	peonidin-3-O-glucoside
PT3G	Petunidin-3-O-glucoside
RNS	Reactive Nitrogen Species
ROS	Reactive Oxygen Species
RPMI	Roswell Park Memorial Institute medium
SC	Schwartz criteria
SERS	Surface-enhanced Raman Scattering
SPR	Surface Plasmon Resonance
$t^{1/2}$	Terminal elimination half-life or apparent terminal elimination half-life, for compounds presenting release/absorption as limiting steps
$t^{1/2d}$	Distribution half-life. Takes 1 $t^{1/2}$ for distribution to go to 50% completion and 3-5 $t^{1/2}$ for distribution to go to completion
$t^{1/2e}$	Elimination half-life. Takes 1 $t^{1/2}$ to eliminate 50% of dose and 3-5 $t^{1/2}$ for elimination to go to completion
TEM	Transmission electron microscopy
$t_{last}$	Time of Clast
$t_{max}$	Time of occurrence of $C_{max}$
$t_{min}$	Time of occurrence of $C_{min}$
ToF	Time-of-Flight
Uv-vis	Ultra violet-visible
$V_1$	Volume of central compartment; volume of distribution at $T_0$ ; entire dose in $V_1$
$V_2$	Volume of peripheral compartment
$V_{ss}$	Volume of distribution at steady state following iv administration. At steady state rate of distribution equals rate of redistribution and volume of distribution = $V_1 + V_2$
WSSR	Weighted sum of square of residuals
$V_z$	Apparent volume of distribution during terminal phase
$\lambda_z$	First order terminal elimination rate constant

# Synopsis

A diet rich in fruits and vegetables has been associated with a decreased risk of brain diseases. Some plant-specific compounds occurring in fruits and vegetables, such as flavonoids, have been found to exert neuroprotection, thus decreasing neurological disease risk. The current hypothesis is that neuroprotection is due to the antioxidant properties of flavonoids.

The main aims of this PhD thesis were: i) to assess whether some flavonoids are transported from the blood into the brain across the blood-brain barrier, ii) to understand if neuroprotection is mediated by an impact on brain metabolism.

For the illustration of the above work, this PhD thesis has been divided in four sections.

- Section I provides the theoretical background and a survey of the analytical techniques, instrumentation, and data processing techniques used.
  - Chapter 1 reviews the literature on the putative role of flavonoids as antioxidant agents in the contest of neurodegeneration and dementia-related diseases. Bioavailability and pharmacokinetic issues are discussed.
  - In chapter 2 various analytical approaches in metabolomics are reviewed. Specifically, attention is paid to common platforms and strategies to data acquisition, data pretreatment, preprocessing and multivariate analysis of metabolomics data.
- Section II describes *in vivo* experiments implementing different metabolomics analyses approaches.
  - Chapter 4 presents the relationship between plasma C3G values and C3G amounts in the rat brain in the very early phase (i.e. 0-20 min) after C3G administration. Mean Time (MT) parameters are reported as useful indicators of the retention properties of C3G in peripheral tissues;
  - Chapter 5 discusses a method validation for an untargeted profiling of rat brain.
- Section III deals with the development and characterization of a selective and sensitive analytical method, based on Surface-Enhanced Raman scattering (SERS) spectroscopy, enabling the assessment of reactive oxygen species (ROS) and reactive nitrogen species (RNS) in living cells.

- Chapter 6 examines three possible novel nanosensors (NS) composed of oxidation-sensitive reporter molecules, adsorbed onto the surface of gold nanoparticles (Au-NPs). The rationale is that various ROS/RNS can induce a chemical change in the structure of the adsorbed molecules that is reflected in specific spectral differences, thus allowing measurement of specific ROS/RNS under versatile experimental conditions;
- In Chapter 7 one SERS-based NS has been further refined for SERS-imaging technique with the ultimate goal to enable real-time intracellular observations in living cells.

Conclusions and recommendations for future work are discussed in Section IV.



# Table of contents

ABSTRACT .....	1
ABBREVIATIONS.....	2
SYNOPSIS .....	5
TABLE OF CONTENTS.....	7
<b>INTRODUCTION .....</b>	<b>9</b>
<i>The grand challenge of healthy ageing in the European Union .....</i>	<i>10</i>
<i>Diet and healthy ageing: State-of-the-art of the scientific knowledge .....</i>	<i>11</i>
Bibliographic references .....	13
<b>SECTION I .....</b>	<b>16</b>
CHAPTER 2. SCIENTIFIC BACKGROUND .....	17
<i>Neurodegeneration, brain pathology and dementia syndrome.....</i>	<i>18</i>
Oxidative stress and neurodegenerative disorders.....	19
Oxidative damage and protein conformational diseases .....	21
<i>Flavonoids as neuroprotectors.....</i>	<i>24</i>
Antioxidants.....	24
Anthocyanins.....	26
Bioavailability and Pharmacokinetic Issues .....	29
Bibliographic references .....	36
CHAPTER 3. REVIEW OF ANALYTICAL TECHNIQUES.....	43
<i>Metabolomics .....</i>	<i>44</i>
Types of analyses.....	46
<i>Metabolomics Workflow .....</i>	<i>48</i>
Statistical analyses .....	49
Analytical platforms .....	54
Bibliographic references .....	57
<b>SECTION II - A METABOLOMIC AND PHARMACOKINETIC STUDY ON CYANIDIN-3-GLUCOSIDE .....</b>	<b>60</b>
CHAPTER 4. SHORT-TERM PHARMACOKINETIC OF CYANIDIN-3-GLUCOSIDE (C3G).....	61
Chapter Overview .....	61
<i>Experimental section .....</i>	<i>62</i>
Materials.....	62
Study design and protocol .....	62
Organ collection and extract preparation.....	64
Quantitative analysis.....	64
Recovery and residual blood correction .....	65
Pharmacokinetics analysis .....	66
<i>Results and discussion .....</i>	<i>70</i>
Plasma Pharmacokinetics of C3G .....	72
Tissue pharmacokinetics of C3G and its metabolites .....	76
Significance of C3G in the brain.....	77
<i>Conclusions.....</i>	<i>80</i>
Bibliographic References .....	81
CHAPTER 5. A DATA ANALYSIS PIPELINE FOR AN UNTARGETED METABOLOMIC WORKFLOW .....	83
Chapter Overview .....	83
<i>Experimental section .....</i>	<i>84</i>
Materials.....	84
Study design and protocol .....	84
Ultra performance liquid chromatography–quadrupole time-of-flight analysis.....	86
Quality control .....	88
Data Analysis Workflow .....	88

<i>Results and discussion</i> .....	90
Efficiency of extraction solvent .....	90
Data preprocessing .....	92
Extraction and number of features .....	92
Quality assessment .....	94
Univariate and multivariate statistical methods.....	99
Conclusions .....	101
Bibliographic references .....	107
<b>SECTION III - DEVELOPMENT AND CHARACTERIZATION OF A SERS METHOD FOR THE ASSESSMENT OF ROS/RNS IN LIVING CELLS .....</b>	<b>109</b>
CHAPTER 6. REACTIVE OXYGEN SPECIES (ROS) DETECTION IN AQUEOUS ENVIRONMENTS WITH SERS-BASED NANOSENSORS.....	110
Chapter Overview.....	110
<i>Experimental section</i> .....	111
Materials.....	111
Raman Instrumentation.....	112
Cit-AuNPs preparation .....	112
Preparation of functionalized-AuNPs .....	112
Nanoparticles characterization .....	114
Measurement for ROS specificity and sensitivity .....	114
Generation of ROS/RNS .....	114
Data Processing .....	115
<i>Results and discussion</i> .....	117
Characterization .....	120
Ligand exchange.....	120
Specificity and sensitivity of ROS detection.....	122
Stability in physiological buffer .....	125
Bibliographic references .....	127
CHAPTER 7. CELLULAR RESPONSE AND SENSOR DEVELOPMENT.....	128
Chapter overview .....	128
<i>Experimental section</i> .....	129
Materials.....	129
Cit-AuNPs preparation .....	130
Preparation of Au-nanoparticles coated with 6-Amino-6'-hydroxy-3H-spiro[2-benzofuran-1,9'-xanthene]-3,3'(9a'H)-dione (6AF) .....	130
Nanoparticles characterization .....	130
Raman Instrumentation.....	131
Cell culture.....	132
Toxicity Assay.....	132
Cellular Uptake .....	133
Intracellular SERS experiments.....	134
Antioxidant screening.....	134
Data Processing .....	134
<i>Results and discussion</i> .....	136
Nanoparticle Tracking Analysis (NTA) .....	136
Cytotoxicity and cellular uptake .....	137
Intracellular Surface-Enhanced Raman Spectroscopy with 6AF-AuNPs.....	139
Assays of oxidative stress .....	141
Conclusions .....	142
Bibliographic references .....	143
<b>SECTION IV - CONCLUSIONS &amp; FUTURE DIRECTIONS.....</b>	<b>145</b>
<i>Targeting natural antioxidant compounds to the brain</i> .....	146
<i>Future Direction</i> .....	147
<b>ACKNOWLEDGMENTS.....</b>	<b>148</b>

# **Introduction**

## **The grand challenge of healthy ageing in the European Union**

One of the most recent documents on population aging released by the European Commission claims that “Europe is the oldest region in the world” (Marcowycz & Futurage Team, 2011). Population aging has been a policy priority at both the member state and European Union levels for more than two decades and in recent years has been promoted to the level of a “grand challenge”: the number of Europeans aged 65 and older is expected to increase by 45% between 2008 and 2030 and will exceed 30% of the total population by 2060.

Old age is characterized by an increased risk for multiple chronic diseases (e.g., hypertension, atherosclerosis, coronary syndromes, dementia-related disorders). Therefore, it is important to determine approaches that can be used today to promote healthy aging, forestall the onset of these chronic diseases, and create conditions favorable for obtaining a “longevity dividend” in both financial and human terms.

Aside from the cardiovascular system, the brain is affected most significantly by the lifelong impact of stressors such as reactive oxygen and nitrogen species (ROS and RNS, respectively). Several cellular and molecular events are also thought to be related to oxidative stress, including impaired mitochondrial function, activation of neuronal apoptosis, deposition of aggregated proteins, and excitotoxicity. The majority of drug treatments for neurodegenerative disorders are ineffective, and consequently, there is an urgent need to develop alternative therapies for preventing the progressive loss of specific neuronal populations (Desai et al., 2010).

As one of the most important lifestyle factors, diet can strongly influence the incidence and onset of neurodegenerative disorders. Epidemiological studies have demonstrated the positive effect of a fruit- and vegetable rich-diet on pathologies strictly linked with an imbalance in redox status, including aging, cancer, cardiovascular disease, and some degenerative diseases (Campbell et al., 1998; Jin et al., 2011). Detailed investigations into the specific dietary components of these foods have consistently suggested that a group of phytochemicals known as flavonoids is highly effective in reversing age-related declines in neurocognitive performance. In particular, foods rich in three specific flavonoid subgroups—flavanols, anthocyanins, and flavanones—seem to have the greatest potential to act on cognitive processes (Bohm et al., 1998). The consumption of flavonoid-rich foods and beverages reportedly limits the neurodegeneration associated with a variety of neurological disorders and prevents or reverses normal and abnormal deterioration in cognitive performance (Steele

et al., 2007).

In addition, a growing number of flavonoids have been shown to inhibit the development of Alzheimer's disease (AD)-like pathology and reverse deficits in cognition. These effects suggest that flavonoids may have potential therapeutic utility in dementia-related disorders (Dragicevic et al., 2011; Spencer, 2008b).

### **Diet and healthy ageing: State-of-the-art of the scientific knowledge**

Ageing is associated with many common chronic neurodegenerative diseases; however, the precise cause of the neuronal degeneration underlying these diseases, and indeed normal brain aging, remains unclear (Desai et al., 2010). Because the neuropathology of many neurodegenerative diseases has been linked to increases in brain oxidative stress, strong efforts have historically been directed at exploring antioxidant strategies for combating neuronal damage. Recently, intense interest has developed in the potential of flavonoids—anthocyanins in particular—to modulate neuronal function and prevent age-related neurodegeneration (Spencer, 2010). For example, red wine is a rich source of flavonoids (Mattivi et al., 2006), and its moderate consumption is associated with a decreased risk for cardiovascular (Dohadwala & Vita, 2009; Karatzi et al., 2009; Walzem, 2008) and neurodegenerative (Collins et al., 2009; Panza et al., 2009) diseases.

Flavonoids may exert their positive effects via several mechanisms—e.g., (i) neuroprotection against neurotoxins (Spencer, 2008a), (ii) suppression of neuroinflammation (Vafeiadou et al., 2007), and (iii) enhancement of the cellular pathways linked to memory, learning, and cognitive function (Spencer, 2008b, 2009, 2010). In recent years, the classic view of flavonoids as antioxidants via direct scavenging of ROS and RNS (Rice-Evans et al., 1996; Terao, 2009) has been replaced by a more realistic view that they act as modulators of key enzymes involved in metabolic and signaling pathways, thereby allowing fine control of endogenous ROS formation (Alvarez et al., 2010; Androutsopoulos et al., 2010; Chalopin et al., 2010; Gokara et al., 2010; Huang et al., 2010; Londono-Londono et al., 2010; Ochiai et al., 2009; Ragazzon et al., 2009; Rashidi & Nazemiyeh, 2010; Sheng et al., 2009; Sirk et al., 2009). Nonetheless, information about the capacity of flavonoids to pass through or interact with the blood–brain barrier is lacking (Faria et al., 2011), and our studies have attempted to address this gap.

Together these observations make an even more urgent case for explaining the available

epidemiological data, which thus encourages a better understanding of flavonoid bioactivity. In turn, such scientific knowledge is needed to provide human populations with sound guidelines for choosing diet and lifestyle.

Some studies have succeeded in filling knowledge gaps concerning the rapid absorption of grape anthocyanins (wine pigments) in the stomach (Passamonti, Vrhovsek, Vanzo, et al., 2003) and their fast distribution in tissues such as the brain (Passamonti et al., 2005), liver (Passamonti, Vrhovsek, Terdoslavich, et al., 2003), and kidneys (Vanzo et al., 2008). The amounts of anthocyanins recovered and measured in these tissues are very low, however—i.e., too low to justify ROS scavenging—and thus suggest that their biological activities might be due to a highly specific interaction with the active sites of cellular enzymes, their regulation, or both. “Omics” approaches are undoubtedly the most suitable for obtaining a global view of the impact of anthocyanins on enzyme function (Fiehn, 2002; Kell, 2006; Weckwerth & Fiehn, 2002). However, the time window in which anthocyanins have peak impact on cells is very short (less than a few minutes). Therefore, the effects of anthocyanins are unlikely to be detected as changes at the transcriptome or proteome levels. Only changes at the metabolome level can reasonably be expected.

## Bibliographic references

- Alvarez, A. I., Real, R., Perez, M., Mendoza, G., Prieto, J. G., & Merino, G. (2010). Modulation of the activity of ABC transporters (P-glycoprotein, MRP2, BCRP) by flavonoids and drug response. *J Pharm Sci*, 99(2), 598-617. doi: 10.1002/jps.21851
- Androutsopoulos, V. P., Papakyriakou, A., Vourloumis, D., Tsatsakis, A. M., & Spandidos, D. A. (2010). Dietary flavonoids in cancer therapy and prevention: substrates and inhibitors of cytochrome P450 CYP1 enzymes. *Pharmacol Ther*, 126(1), 9-20. doi: 10.1016/j.pharmthera.2010.01.009
- Bohm, H., Boeing, H., Hempel, J., Raab, B., & Kroke, A. (1998). [Flavonols, flavone and anthocyanins as natural antioxidants of food and their possible role in the prevention of chronic diseases]. *Z Ernahrungswiss*, 37(2), 147-163.
- Campbell, T. C., Parpia, B., & Chen, J. (1998). Diet, lifestyle, and the etiology of coronary artery disease: the Cornell China study. *Am J Cardiol*, 82(10B), 18T-21T.
- Chalopin, M., Tesse, A., Martinez, M. C., Rognan, D., Arnal, J. F., & Andriantsitohaina, R. (2010). Estrogen receptor alpha as a key target of red wine polyphenols action on the endothelium. *PLoS One*, 5(1), e8554. doi: 10.1371/journal.pone.0008554
- Collins, M. A., Neafsey, E. J., Mukamal, K. J., Gray, M. O., Parks, D. A., Das, D. K., & Korhuis, R. J. (2009). Alcohol in moderation, cardioprotection, and neuroprotection: epidemiological considerations and mechanistic studies. *Alcohol Clin Exp Res*, 33(2), 206-219. doi: 10.1111/j.1530-0277.2008.00828.x
- Desai, A. K., Grossberg, G. T., & Chibnall, J. T. (2010). Healthy brain aging: a road map. *Clin Geriatr Med*, 26(1), 1-16. doi: 10.1016/j.cger.2009.12.002
- Dohadwala, M. M., & Vita, J. A. (2009). Grapes and cardiovascular disease. *J Nutr*, 139(9), 1788S-1793S. doi: 10.3945/jn.109.107474
- Dragicevic, N., Smith, A., Lin, X., Yuan, F., Copes, N., Delic, V., . . . Bradshaw, P. C. (2011). Green tea epigallocatechin-3-gallate (EGCG) and other flavonoids reduce Alzheimer's amyloid-induced mitochondrial dysfunction. *J Alzheimers Dis*, 26(3), 507-521. doi: 10.3233/JAD-2011-101629
- Faria, A., Pestana, D., Teixeira, D., Couraud, P. O., Romero, I., Weksler, B., . . . Calhau, C. (2011). Insights into the putative catechin and epicatechin transport across blood-brain barrier. *Food Funct*, 2(1), 39-44. doi: 10.1039/c0fo00100g
- Fiehn, O. (2002). Metabolomics--the link between genotypes and phenotypes. *Plant Mol Biol*, 48(1-2), 155-171.
- Gokara, M., Sudhamalla, B., Amooru, D. G., & Subramanyam, R. (2010). Molecular interaction studies of trimethoxy flavone with human serum albumin. *PLoS One*, 5(1), e8834. doi: 10.1371/journal.pone.0008834
- Huang, Z., Fang, F., Wang, J., & Wong, C. W. (2010). Structural activity relationship of flavonoids with estrogen-related receptor gamma. *FEBS Lett*, 584(1), 22-26. doi: 10.1016/j.febslet.2009.11.026
- Jin, Y., Alimbetov, D., George, T., Gordon, M. H., & Lovegrove, J. A. (2011). A randomised trial to investigate the effects of acute consumption of a blackcurrant juice drink on markers of vascular reactivity and bioavailability of anthocyanins in human subjects. *Eur J Clin Nutr*, 65(7), 849-856. doi: 10.1038/ejcn201155

- Karatzis, K., Papaioannou, T. G., Papamichael, C., Lekakis, J., Stefanadis, C., & Zampelas, A. (2009). Red wine, arterial stiffness and central hemodynamics. *Curr Pharm Des*, 15(3), 321-328.
- Kell, D. B. (2006). Systems biology, metabolic modelling and metabolomics in drug discovery and development. *Drug Discov Today*, 11(23-24), 1085-1092. doi: 10.1016/j.drudis.2006.10.004
- Londono-Londono, J., Lima, V. R., Jaramillo, C., & Creczynski-Pasa, T. (2010). Hesperidin and hesperetin membrane interaction: understanding the role of 7-O-glycoside moiety in flavonoids. *Arch Biochem Biophys*, 499(1-2), 6-16. doi: 10.1016/j.abb.2010.04.023
- Marcowycz, A., & Futurage Team. (2011). FUTURAGE. A Road Map for European Ageing Research.
- Mattivi, F., Guzzon, R., Vrhovsek, U., Stefanini, M., & Velasco, R. (2006). Metabolite Profiling of Grape: Flavonols and Anthocyanins. *J Agric Food Chem*, 54, 7692-7702.
- Ochiai, H., Takeda, K., Soeda, S., Tahara, Y., Takenaka, H., Abe, K., . . . Kawamura, M. (2009). Epigallocatechin-3-gallate is an inhibitor of Na<sup>+</sup>, K(+) -ATPase by favoring the E1 conformation. *Biochem Pharmacol*, 78(8), 1069-1074. doi: 10.1016/j.bcp.2009.06.007
- Panza, F., Capurso, C., D'Introno, A., Colacicco, A. M., Frisardi, V., Lorusso, M., . . . Solfrizzi, V. (2009). Alcohol drinking, cognitive functions in older age, predementia, and dementia syndromes. *J Alzheimers Dis*, 17(1), 7-31. doi: 10.3233/JAD-2009-1009
- Passamonti, S., Vrhovsek, U., Terdoslavich, M., Vanzo, A., Cocolo, A., Decorti, G., & Mattivi, F. (2003). *Hepatic uptake of dietary anthocyanins and the role of bilitranslocase*. Paper presented at the 1st International Conference on Polyphenols and Health, Vichy - France.
- Passamonti, S., Vrhovsek, U., Vanzo, A., & Mattivi, F. (2003). The stomach as a site for anthocyanins absorption from food. *FEBS Lett*, 544(1-3), 210-213. doi: S0014579303005040
- Passamonti, S., Vrhovsek, U., Vanzo, A., & Mattivi, F. (2005). Fast access of some grape pigments to the brain. *J Agric Food Chem*, 53(18), 7029-7034. doi: 10.1021/jf050565k
- Ragazzon, P. A., Iley, J., & Missailidis, S. (2009). Structure-activity studies of the binding of the flavonoid scaffold to DNA. *Anticancer Res*, 29(6), 2285-2293. doi: 29/6/2285 [pii]
- Rashidi, M. R., & Nazemiyeh, H. (2010). Inhibitory effects of flavonoids on molybdenum hydroxylases activity. *Expert Opin Drug Metab Toxicol*, 6(2), 133-152. doi: 10.1517/17425250903426164
- Rice-Evans, C. A., Miller, N. J., & Paganga, G. (1996). Structure-antioxidant activity relationships of flavonoids and phenolic acids. *Free Radic Biol Med*, 20(7), 933-956.
- Sheng, R., Lin, X., Zhang, J., Chol, K. S., Huang, W., Yang, B., . . . Hu, Y. (2009). Design, synthesis and evaluation of flavonoid derivatives as potent AChE inhibitors. *Bioorg Med Chem*, 17(18), 6692-6698. doi: 10.1016/j.bmc.2009.07.072
- Sirk, T. W., Brown, E. F., Friedman, M., & Sum, A. K. (2009). Molecular binding of catechins to biomembranes: relationship to biological activity. *J Agric Food Chem*, 57(15), 6720-6728. doi: 10.1021/jf900951w
- Spencer, J. P. (2008a). Flavonoids: modulators of brain function? *Br J Nutr*, 99 E Suppl 1, ES60-77. doi: 10.1017/S0007114508965776



- Spencer, J. P. (2008b). Food for thought: the role of dietary flavonoids in enhancing human memory, learning and neuro-cognitive performance. *Proc Nutr Soc*, 67(2), 238-252. doi: 10.1017/S0029665108007088
- Spencer, J. P. (2009). The impact of flavonoids on memory: physiological and molecular considerations. *Chem Soc Rev*, 38(4), 1152-1161. doi: 10.1039/b800422f
- Spencer, J. P. (2010). The impact of fruit flavonoids on memory and cognition. *Br J Nutr*, 104 Suppl 3, S40-47. doi: 10.1017/S0007114510003934
- Steele, M., Stuchbury, G., & Munch, G. (2007). The molecular basis of the prevention of Alzheimer's disease through healthy nutrition. *Exp Gerontol*, 42(1-2), 28-36.
- Terao, J. (2009). Dietary flavonoids as antioxidants. *Forum Nutr*, 61, 87-94. doi: 10.1159/000212741
- Vafeiadou, K., Vauzour, D., & Spencer, J. P. (2007). Neuroinflammation and its modulation by flavonoids. *Endocr Metab Immune Disord Drug Targets*, 7(3), 211-224.
- Vanzo, A., Terdoslavich, M., Brandoni, A., Torres, A. M., Vrhovsek, U., & Passamonti, S. (2008). Uptake of grape anthocyanins into the rat kidney and the involvement of bilitranslocase. *Mol Nutr Food Res*, 52(10), 1106-1116. doi: 10.1002/mnfr.200700505
- Walzem, R. L. (2008). Wine and health: state of proofs and research needs. *Inflammopharmacology*, 16(6), 265-271. doi: 10.1007/s10787-008-8027-6
- Weckwerth, W., & Fiehn, O. (2002). Can we discover novel pathways using metabolomic analysis? *Curr Opin Biotechnol*, 13(2), 156-160. doi: S0958166902002999 [pii]

# **Section I**

# Chapter 2. Scientific Background

**Part of this chapter was published on:** Ziberna, Lovro, Fornasaro, Stefano, et al. (2013). *Bioavailability of Flavonoids: The Role of Cell Membrane Transporters*. R. R. Watson, V. R. Preedy and S. Zibadi. San Diego, Academic Press: 489-511.

## **Neurodegeneration, brain pathology and dementia syndrome**

The Alzheimer's Association (Prince et al., 2014) defines dementia as “a group of disorders that cause irreversible cognitive decline as a result of various biological mechanisms that damage brain cells.” This definition appropriately describes neurodegenerative disorders in general, in which neurons are lost due to biological malfunction. However, although many neurodegenerative conditions are recognized, there is no fine line that separates one from another (Ubhi et al., 2010). For instance, symptoms such as motor impairment, memory loss, hallucinations, and agitation may occur in several types of neurodegenerative disorders. No diagnostic biomarkers of dementia-related brain damage have been established (Frisoni et al., 2013), and the mechanisms that link this damage to the expression of dementia symptoms are not fully understood (Savva et al., 2009). Thus, clinical diagnoses are usually based on qualitative evaluations of symptoms.

Similar to the systemic changes in other chronic conditions such as cardiovascular disease and cancer, neuronal loss in neurodegenerative disorders begins decades before the onset of clinical symptoms, which may be a transition point in the accumulation of brain damage over time. Accordingly, the brain may have a certain “buffering” capacity that maintains acceptable cognitive function even during progressive pathological neurodegeneration (McDowell et al., 2007; Mortimer, 1997).

The four most common subtypes of dementia-type disorders in order of frequency are AD, vascular dementia, Lewy body dementia, and frontotemporal dementia (Table 2.1). However, evidence from neuropathological studies challenges the notion of “one disease, one pathology”: mixed pathologies are much more common than “pure” ones (Langa et al., 2004; Neuropathology Group. Medical Research Council Cognitive & Aging, 2001; Schneider et al., 2007). The brains of individuals with one form of neurodegeneration can also have the pathological markers of another because two disorders may share risk factors as well as pathological events.

Aging has been established as a major risk factor for neurodegenerative diseases, and neurodegeneration appears to accompany accelerated or dysfunctional aging (Prince et al., 2014). Hypercholesterolemia, hypertension, atherosclerosis, coronary heart disease, smoking, obesity, and diabetes are also linked to the development of underlying neuropathologies because they are vascular risk factors that affect the effective supply of blood to the brain (Luchsinger & Mayeux, 2004; Shobab et al., 2005). Other risks factors include high intake of

salt (Gandy & DeKosky, 2013) and of saturated and trans fats (Gillette Guyonnet et al., 2007).

On the contrary, evidence from cross-sectional studies suggests that compared with adults with dementia, older people with normal cognitive function tend to consume a healthier diet that is richer in fruits and vegetables and have a higher intake of homocysteine-related vitamins (vitamin B12 and folate), antioxidants such as flavonoids, and omega-3 polyunsaturated fatty acids (Blennow et al., 2006; Luchsinger & Mayeux, 2004). From this perspective, a growing consensus has emerged in recent years that dementia is preventable to some extent through the modification of environmental and behavioral factors (Standridge, 2004).

### **Oxidative stress and neurodegenerative disorders**

All neurodegenerative disorders, are characterized by the progressive atrophy of neurons. Although the mechanisms responsible for neuronal death remain to be completely elucidated, advances in systems biology have allowed our understanding of aging and neurodegeneration to accumulate. Many studies have suggested that a central biochemical feature of the implicated pathology of this atrophy is an unbalanced accumulation of oxidative stress linked to mitochondrial dysfunction (Folbergrova et al., 2012; Higgins et al., 2010; Moreira et al., 2010; Nagley et al., 2010; Sims & Muyderman, 2010). Oxidative stress is a condition in which the balance between the production of intracellular small-molecule reactive species (Wang et al., 2012) and the level of endogenous antioxidants is significantly disturbed.

Oxygen is essential for the normal function of eukaryotic organisms. Approximately 2% of the oxygen that enters living cells is converted into ROS and RNS amid a system of reactions that constantly consumes these species (Boveris et al., 1972). However, cells that produce reactive species at a greater rate than can be consumed by related intracellular systems enter a state of hyperoxia, which produces toxicities that include neurotoxicity (Ahdab-Barmada et al., 1986; Danilov & Fiskum, 2008; Hinkelbein et al., 2010).

The toxicity and chemical reactivity of oxygen rely on its electronic structure. The identical electron spin states of its two outer-orbital electrons make oxygen kinetically stable except in the presence of catalysts that disturb these spin states to produce partially reduced forms of oxygen, mostly ROS and RNS (Valko et al., 2007). During cellular oxidative stress, free radical forms of ROS or RNS steal electrons from lipids, proteins, carbohydrates, or nucleic

acids, thereby damaging these essential biomolecules. To protect cells from ROS/RNS-induced oxidative insults, aerobic organisms have evolved an array of antioxidant defense systems: (i) enzymatic antioxidants (e.g., superoxide dismutase [SOD], catalase, peroxidases, and heme oxygenase), and (ii) non-enzymatic redox-regulating antioxidants (e.g., glutathione and vitamin C) (Droge, 2002).

ROS/RNS toxicity is a primary pathogenic factor not only in neurodegenerative disorders such as AD, Parkinson's disease (PD), and amyotrophic lateral sclerosis (ALS) (Gandhi & Abramov, 2012; Halliwell, 2006; Mhatre et al., 2004) but also in many non-degenerative brain diseases—e.g., cerebral stroke (Chen et al., 2011), epilepsy (Aguilar et al., 2012; Shin et al., 2011), hepatic encephalopathy (Skowronska & Albrecht, 2013), and brain dysfunction related to heavy metal toxicity (Farina et al., 2013).

Increases in ROS concentrations in the brain seem not to be caused by elevations in oxidative

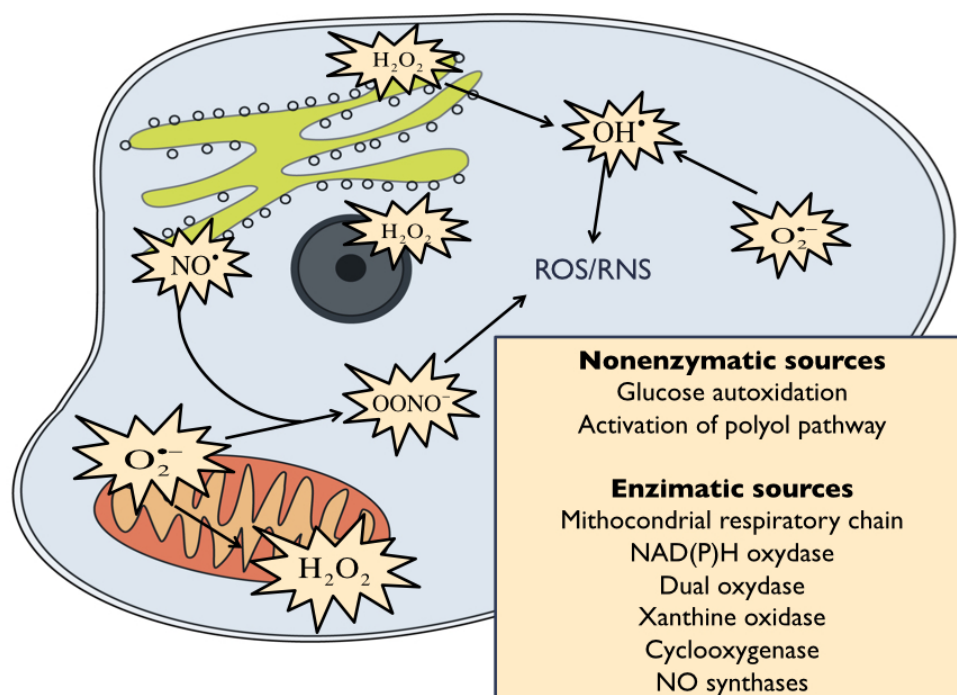


**Figure 2.1** Main pathways of ROS/RNS formation.

stress but rather by a decline in antioxidant defense and repair mechanisms, thus resulting in the accumulation of oxidative damage (Aarsland et al., 2004). For instance, the activities of SOD, catalase, glutathione peroxidase, and glutathione reductase are reduced in the affected brain regions of AD patients (Pappolla et al., 1992; Zemlan et al., 1989). The amount of

glutathione is also reduced in the substantia nigra of PD patients (Pearce et al., 1997). In addition, oxidative stress and other molecular mechanisms interact, which causes neurodegeneration such as protein misfolding.

Table 2.1 Main reactive oxygen and nitrogen species

<b>Reactive Oxygen Species (ROS)</b>			
<i>Radicals</i>		<i>Non radicals</i>	
Superoxide	$O_2^{\bullet -}$	Hydrogen Peroxide	$H_2O_2$
Hydroxyl	$HO^{\bullet}$	Singlet Oxygene	$O_2(^1\Delta_g)$
Peroxyl	$RO_2^{\bullet}$		
Alkoxyl	$RO^{\bullet}$		
Hydroperoxyl	$HO_2^{\bullet}$		
<b>Reactive Nitrogen Species (RNS)</b>			
<i>Radicals</i>		<i>Non radicals</i>	
Nitrogen monoxide	$NO^{\bullet}$	Nitrous acid	$HNO_2$
Nitrogen dioxide	$NO_2^{\bullet}$	Nitrosyl cation	$NO^+$
		Nitrosyl anion	$NO^-$
		Peroxynitrite	$ONOO^-$

### **Oxidative damage and protein conformational diseases**

AD, PD, Huntington's disease, ALS, and Friedreich's ataxia belong to a class of the protein conformational diseases that are characterized by the accumulation of disease-specific misfolded proteins in the central nervous system (Crunkhorn, 2012; Tabner et al., 2001; Zerovnik, 2010). Between 1906 and 1910, Alois Alzheimer and Gaetano Perusini first described a collection of dense deposits or plaques outside the neurons and bands of fibers or tangles within the autopsied brain cells of four people affected by an unknown type of dementia (Macchi et al., 1997). This disorder later became known as AD. The plaques were composed of amyloid beta peptides, and the tangles were tau/phosphorylated tau proteins.

Other examples of plaques and fibers include alpha-synuclein in Lewy body dementia (van Ham et al., 2008), and mutant huntingtin in Huntington's diseases (Scherzinger et al., 1997).

Under normal conditions, cells use mechanisms such as the unfolded protein response for general balancing of protein delivery to the endoplasmic reticulum (ER) and protein folding (Zhang & Kaufman, 2006). Furthermore, if proteins are misfolded, the cellular response is either to (i) break up abnormal protein aggregates and facilitating protein refolding, or (ii) deliver misfolded proteins to the proteasome for recycling if they cannot be rescued by refolding (Zhang & Kaufman, 2006). Disorders associated with abnormalities in protein conformations arise from the dysfunctional misfolding of proteins in non-native conformations. One consequence of the formation of these intracellular abnormal protein aggregates is ER dysfunction (stress) that leads to mitochondrial dysfunction, excessive production of ROS, and oxidative stress. The capacity of cells to combat elevated levels of ROS (and RNS) involves the activation of pro-survival pathways as well as the production of molecules endowed with antioxidant and anti-apoptotic actions (Calabrese et al., 2009).

Recent studies (de la Monte & Tong, 2014) have suggested that a localized, brain-specific, insulin/insulin-like growth factor resistance initiates a cascade driven by increased oxidative stress, neuroinflammation, impaired cell survival, mitochondrial dysfunction, dysregulated lipid metabolism, and ER stress. The cascade leads to neuronal dysfunction and death in AD. In this context, the molecular, biochemical, and degenerative features of AD correspond with the abnormalities that occur within the spectrum of systemic insulin resistance diseases.



**Table 2.2.2 Abridged list of the most common type of dementia-related disorders.** Modified from (Prince et al., 2014).

<b>Dementia subtype</b>	<b>Early characteristic symptoms</b>	<b>Neuropathology</b>	<b>Proportion of dementia cases</b>
Alzheimer's Disease (AD)	Impaired memory, apathy and depression  Gradual onset	Cortical amyloid plaques and neurofibrillary tangles	50-75%
Vascular Dementia (VaD)	Similar to AD, but memory less affected, and mood fluctuations more prominent  Physical frailty  Stepwise onset	Cerebrovascular disease Single infarcts in critical regions, or more diffuse multi-infarct disease	20-30%
Lewy Bodies Dementia (LBD)*	Marked fluctuation in cognitive ability  Visual hallucinations  Parkinsonism (tremor and rigidity)	Cortical Lewy bodies (alpha-synuclein)	<5%
Frontotemporal dementia	Personality changes  Mood changes  Disinhibition  Language difficulties	No single pathology – damage limited to frontal and temporal lobes	5-10%
Creutzfeldt-Jakob disease	Rapidly fatal disorder that impairs memory and coordination and causes behavior changes.	Prion proteins	<5%

\* Lewy body dementia (LBD) is not a single disorder but a spectrum of disorders including Parkinson's Disease Dementia (PDD) and Dementia with Lewy Bodies (DLB). Because DLB and PDD share many clinical and pathological characteristics, both are classified as forms of LBD.

## **Flavonoids as neuroprotectors**

### **Antioxidants**

The term *antioxidant* refers to any substance that, present at a low concentration compared with that of an oxidizable substrate, significantly delays or prevents the oxidation of that substrate (Halliwell, 1999). Antioxidants are thought to act against neurodegeneration by limiting the production of toxic substances and reducing damage by free radicals (Mao, 2013). There are relatively fewer antioxidant enzymes specifically focused on neuronal protection, suggesting that antioxidant nutrients may have a more prominent role in older and aging brains than in other organ systems (Olanow, 1990).

Numerous epidemiologic studies have shown an inverse correlation between dietary flavonoid consumption and age-dependent cognitive decline and dementia, including AD and PD (Commenges et al., 2000; de Rijk et al., 1997; Orgogozo et al., 1997). Emerging evidence suggests that dietary-derived flavonoids have the potential to improve human memory and neurocognitive performance via their capacity to protect vulnerable neurons, enhance existing neuronal function, and stimulate neuronal regeneration (Gutierrez-Merino et al., 2011; J. P. Spencer, 2009). A clinical study demonstrated that 12 weeks of dietary supplementation with grape juice may have neurocognitive benefits in older adults with early memory decline (R. Krikorian et al., 2010) and can improve memory functions in older adults with mild memory decline (Robert Krikorian et al., 2012). In addition, flavonoids have been shown to target the complex general mechanisms of neurodegenerative diseases in various cell cultures and animal models (Basli et al., 2012; Dajas et al., 2003; Echeverry et al., 2010; Zhu et al., 2007). However, clinical trials of flavonoid dietary supplementation or novel dosage forms based on red wine extract remain scarce (Albarracin et al., 2012).

The beneficial effects of these compounds have traditionally been attributed mainly to their antioxidant capacity in terms of radical scavenging properties of superoxide anions and hydroxyl and peroxy radicals (Nijveldt et al., 2001; Robak & Gryglewski, 1988). However, these actions seem to be mediated by the direct interactions of flavonoids and their metabolites with a number of cellular and molecular targets of crucial importance in controlling neuronal resistance to neurotoxins (Granzotto & Zatta, 2014; Zhu et al., 2007), ROS/RNS production (Calabrese et al., 2012), inflammatory mediators (Kao et al., 2010; Spilsbury et al., 2012), neuronal differentiation, long-term potentiation, and memory (J. P. E.

Spencer, 2008). Antioxidants stimulate endogenous antioxidant enzymes (Steffen et al., 2008) while inhibiting xanthine oxidase and nicotinamide adenine dinucleotide phosphate oxidase, two major enzymes that generate large amounts of ROS (Nijveldt et al., 2001; Steffen et al., 2008).

From a chemical point of view, flavonoids are C<sub>15</sub> compounds with C<sub>6</sub>–C<sub>3</sub>–C<sub>6</sub> carbon frameworks—i.e., two benzene rings (A and B rings) are linked together by a group of three carbons (C ring), as shown in Figure 2.1. The main classes of flavonoids differ in oxidation levels and substitution patterns on the C ring, whereas individual compounds within a class differ in their substitution patterns on the A and B rings (Crozier et al., 2009). In general, flavonoids are classified according to their chemical structures, as shown in Table 2.2: (i) flavonols, (ii) flavones, (iii) flavanones, (iv) flavan-3-ols, (v) anthocyanidins, and (vi) isoflavones.

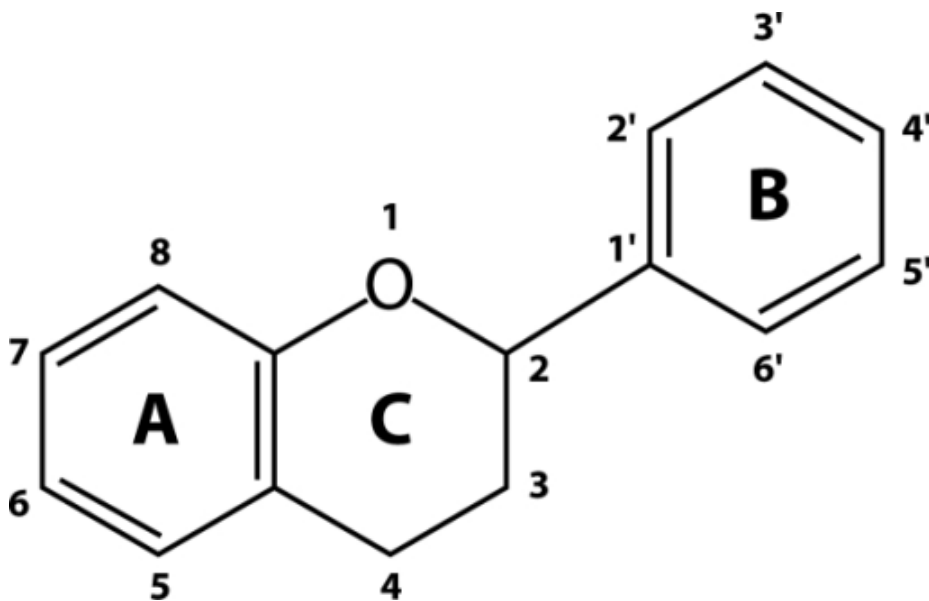
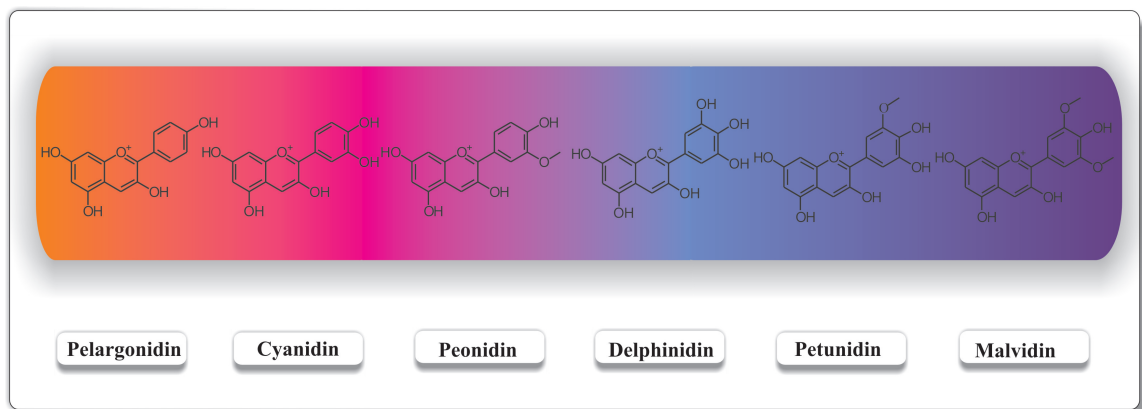


Figure 2.2 Basic structural formula of a flavonoid.

## Anthocyanins

Anthocyanins are glycosylated anthocyanidins, a subclass of flavonoids, that are found in plant tissue and display a great color diversity that touches nearly all visible spectra from orange and red to purple and blue (Del Rio et al., 2010; Kahkonen & Heinonen, 2003; Mazza, 1993; Waterhouse, 2002).



**Figure 2.3** Visible color range of common anthocyanidins (Ananga et al., 2013).

These compounds comprise one of the most widespread families of water-soluble pigments in the plant kingdom. As of 2013, the number of identified anthocyanins in nature was 702, and approximately 200 additional structures were proposed as tentative (Andersen & Jordheim, 2013). The six anthocyanidins commonly found in the edible parts of plants are cyanidin (50%), pelargonidin (12%), peonidin (12%), delphinidin (12%), petunidin (7%), and malvidin (7%) (Kong et al., 2003), and they are classified according to the number and position of hydroxyl and methoxyl groups on the flavan nucleus—i.e., depending on the chemical groups in R1 and R3 (Figure 2.2)

The anthocyanins consist of an aglycone (anthocyanidin), sugar(s), and in many cases, acyl group(s) and can thus be considered water-soluble glycosides of anthocyanidins. Anthocyanins are positively charged at acidic pH, and this equilibrium form is called flavylium cation (2-phenylbenzopyrylium). Although there are approximately 30 anthocyanidins, 90% of all anthocyanins are based on the six most common anthocyanidins listed above, which differ only in the hydroxylation and methoxylation patterns on their B rings (Figures 2.2 and 2.3).

The most common glycoside is 3-glycoside. If a second sugar is present, it is almost always a glucose residue at the 5-hydroxyl position. Such compounds are called 3,5-dimonosides. The most common sugar is glucose (90%), followed by rhamnose, galactose, xylose, and arabinose (Andersen & Markham, 2006). The anthocyanins can also be acylated; indeed, approximately 65% of reported anthocyanins with properly identified structures are acylated. The nature, number, and linkage positions of the acyl groups contribute substantially to anthocyanin diversity. Furthermore, the sugar units of anthocyanins may be acylated with aliphatic acyl groups, aromatic acyl groups, or both. The aromatic acyl groups include various hydroxycinnamic acids (*p*-coumaric, caffeic, ferulic, sinapic, and 3,5-dihydroxycinnamic acids) and two hydroxybenzoic acids (*p*-hydroxybenzoic and gallic acids). The aliphatic acyl group includes malonic acid (which is the most frequent aliphatic acyl group), and acetic, malic, succinic, tartaric, and oxalic acids (Andersen & Markham, 2006).

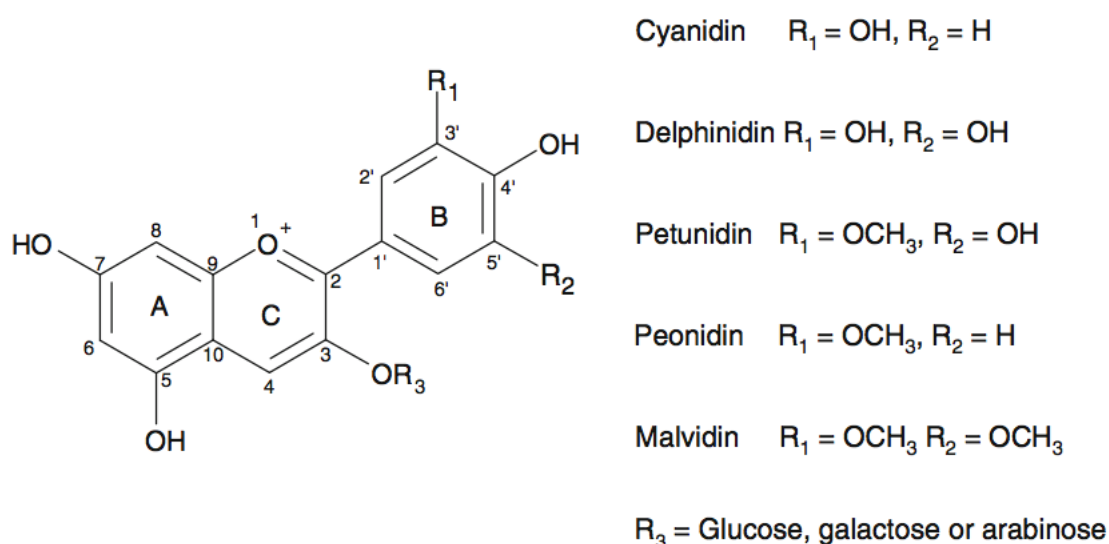
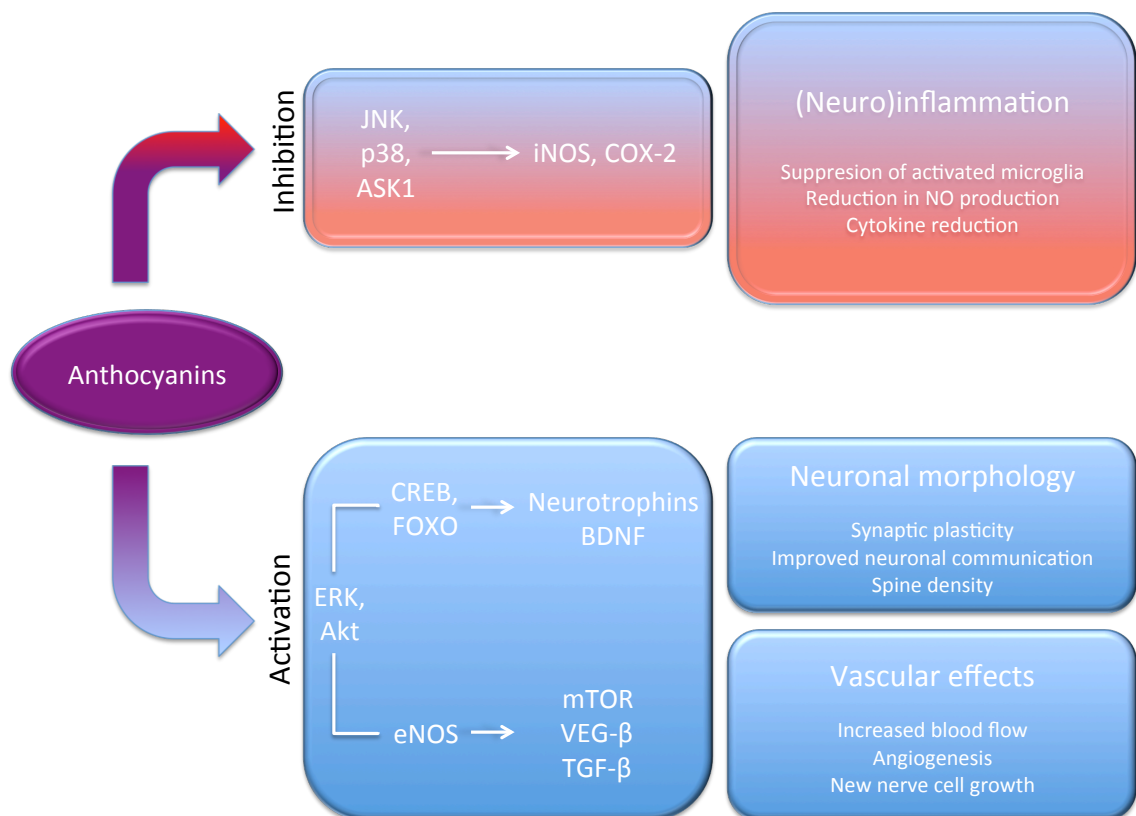


Figure 2.4 Structures of common anthocyanidins.

Cyanidin-3-O- $\beta$ -glucoside (C3G) has recently gained attention for its multifunctional neuroprotective effects, including protection against amyloid-beta-peptide-induced toxicity (Tarozzi et al., 2007; Tarozzi et al., 2010), antioxidant and cognitive promotion (Im et al., 2013; Shih et al., 2010), and anti-ischemic and anti-inflammatory activity (Di Giacomo et al., 2012; Kang et al., 2006). Indeed, chronic consumption of anthocyanins has been correlated with decreased incidence of age-associated cognitive decline and neurodegeneration (Gao et al., 2012; Robert Krikorian et al., 2012).

Another proposed mechanism of C3G neuroprotection involves effects on the vascular system—specifically, the capacity to increase brain blood flow and thus initiate neurogenesis in the hippocampus (Williams & Spencer, 2012). Recent *in vitro* studies have suggested that short-term C3G incubation (20 min) can activate signaling pathways related to neuroprotection—e.g., protection against ethanol-induced neuronal apoptosis in hippocampal neurons (Ali Shah et al., 2013). Importantly, C3G accumulates within brain endothelial cells (Milbury & Kalt, 2010) and has been shown to cross a blood–brain barrier cellular model in a time-dependent manner, in 1 hour (Faria et al., 2010).



**Figure 2.5 Signaling pathway involved in the cognitive benefit of anthocyanins.** Polyphenols activate eRK- cReB pathway and Akt- FOXO cascade leading to changes in synaptic strength and communication, and in angiogenesis through the activation of eNOS. On the other hand, anthocyanins are known to inhibit neuroinflammation through modulation of iNOS and COX-2, leading to a decrease in inflammatory markers. Altogether these effects enhance cognition and prevent neurodegeneration.

The biggest pharmacological concern of anthocyanins is their limited bioavailability, which results in very low plasma concentrations (0.1–1  $\mu\text{M}$ ) (Manach et al., 2005). These low concentrations are attributed to their poor absorption into the circulatory system from the small intestine and extensive cellular uptake into excretory organs (Vanzo et al., 2011) followed by fast and extensive metabolism. New insights into the complex metabolism of

anthocyanins have been obtained through recent feeding studies with human volunteers who ingested 0.5 g (1114  $\mu\text{mol}$ ) of  $^{13}\text{C}$ -labelled C3G. After 48 hours, the relative bioavailability of C3G was 12% of the dose, with 5.4% excreted in urine, 6.9% in breath, and fecal excretion accounting for an additional 32%. These results suggested that anthocyanins have greater bioavailability than that previously reported (Czank et al., 2013). The maximum concentration of anthocyanin-derived circulating metabolites varied between 11 nmol/L for 4-hydroxybenzoic acid-3-O-glucuronide (protocatechuic acid-3-O-glucuronide) and 1962 nmol/L for hippuric acid (de Ferrars et al., 2014). The accumulation of multiple metabolites might ultimately be responsible for the reported bioactivity of anthocyanins, with gut microflora apparently playing key roles in the biotransformation process.

Anthocyanins exhibit wide body distribution, as evidenced by their presence in various peripheral tissues. In particular, they are detected in the cortex and cerebellum of pigs fed a blueberry-supplemented diet for 4 weeks (Kalt et al., 2008). A similar study of oral administration in rats confirmed the presence of pelargonidin in the brain (el Mohsen et al., 2006). Moreover, an experiment in rats with ligated stomachs showed that anthocyanins were present in brain tissue after even a short incubation (10 min) in the stomach (Passamonti et al., 2005). The mechanisms remain to be elucidated, but the results of these studies suggest that anthocyanins accumulate in the central nervous system.

### **Bioavailability and Pharmacokinetic Issues**

Flavonoids are highly bioactive, and have low apparent toxicity, which makes their medicinal use very attractive. Low plasma concentrations are attributed to their poor absorption and extensive cellular uptake into excretory organs (Vanzo et al., 2011) followed by metabolism.

Tight regulation of flavonoid plasma concentration is accomplished by an additional mechanism, i.e. binding to serum albumin (Dufour & Dangles, 2005), which lowers plasma concentrations of unbound bioactive flavonoids, while offering a storing system for delayed release into the plasma. In addition, albumin-bound flavonoids are more stable against oxygen-dependent degradation (Kitson, 2004) so prolonging their biological availability and further extending their plasma half-life. These conditions would protect target tissues from a transient, spiking uptake of flavonoids, which might be trigger a toxic reaction of cells. Indeed, prolonged release of flavonoids from plasma proteins would determine a more constant rate of cellular uptake of flavonoids.

However, low bioavailability must not be correlated with low bioactivity. Recent studies suggest that also some of the flavonoid metabolites have potential to possess similar pharmacodynamics as the parent compound (Terao et al., 2011). Moreover, a given flavonoid with its metabolites could have opposite, additive, or synergistic effects; therefore, the observed bioactivity in *in vivo* settings depends on the particular phenolic profile. Synergistic bioactivity of multiple flavonoids, as found in food matrices, is also important. For instance, the antiproliferative activity in vascular smooth muscle cells of four red wine polyphenols, *i.e.* resveratrol, quercetin, ethyl gallate, and (+)-catechin, was stronger than predicted additive activity of each individual substance (Kurin et al., 2012). In addition, also in anti-cancer research, two flavonoids, diosmetin and luteolin, exert synergistic cytostatic effects (Androutsopoulos & Spandidos, 2013). Synergistic pharmacodynamics has been also observed for flavonoids and drugs, e.g. the antiviral actions of acyclovir were potentiated by the 4'-phenylflavone (Hayashi et al., 2012). In general, there are numerous other studies confirming the synergy potential of flavonoids. This suggests an explanation for some of the epidemiological observations related to the fact that dietary flavonoids, even if present in low concentrations (nM range) in plasma, display health-protective properties. On the other hand, this brings about problems for *in vitro* cell-based assays or *in situ* isolated organ studies, which must focus not only on using single molecules or mixture of molecules (plant extract), but importantly also on the mixture of all their metabolites, and in physiologically relevant concentration range (nM- $\mu$ M).

Another important pharmacological concept, *i.e.* hormesis, must be introduced at this point in order to further explain the paradox of *low bioavailability, but high bioactivity* of flavonoids. Hormetic dose response is characterized by a biphasic dose-response, e.g. low-dose stimulation and a high-dose inhibition, or vice versa, and can result from either a direct stimulation or through an overcompensation stimulatory response following disruption in homeostasis (Calabrese et al., 2011). Flavonoids also exhibit hormesis, what can be represented with an example of quercetin bioactivity on cell-based studies. Cancer preventive effects of quercetin are observed at low concentrations of approximately 1-40  $\mu$ M, and are likely to be mediated by quercetin's antioxidant properties, while pro-oxidant cytotoxic effects are present at concentrations of 40-100  $\mu$ M (Vargas & Burd, 2010). Flavonoids can be seen, in this context, as noxious molecules that reach subtoxic levels in human bodies, and thus induce mild cellular stress responses, which can involve activation of various kinases and

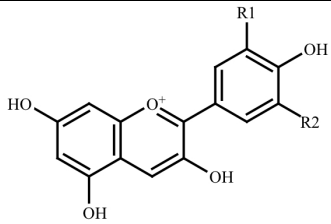
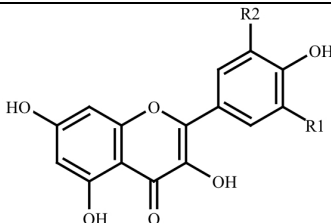
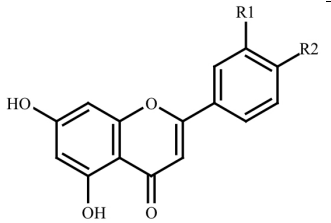
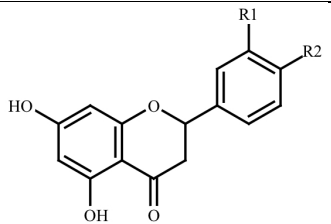


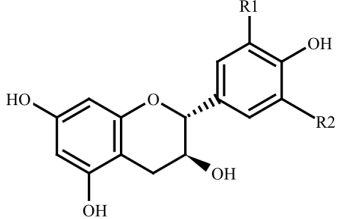
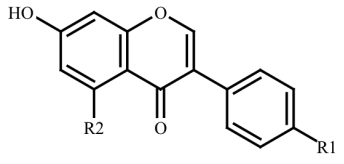
transcription factors that induce the expression of genes that encode antioxidant enzymes, protein chaperones, metabolic phase-II enzymes, neurotropic factors, and other cytoprotective proteins (Son et al., 2008).

Moreover, low concentrations of flavonoids (in physiological range) can affect the expression of genes involved in vascular aging. For instance, treatment of cultured human umbilical vein endothelial cells (HUVEC) with ferulic acid, quercetin or resveratrol (in 0.1  $\mu$ M concentration) resulted in down-regulation (>2-fold) of 363 genes and up-regulation (>2-fold) of 233 genes, out of 10,000 analyzed genes (Nicholson et al., 2008). Importantly, the mentioned compounds significantly increased the expression of the gene encoding endothelial NO synthase (eNOS), while decreased expression of the potent vasoconstrictor endothelin-1 (Nicholson et al., 2008). To further develop this concept, further research is needed to identify the cellular targets of flavonoids that account for cytoprotection (Mastaloudis & Wood, 2012), and not those who have *in vitro* antioxidant activity. For example, EGCG, via activation of Akt and ERK1/2 signaling pathway, upregulates heme oxygenase-1 expression in endothelial cells (Wu et al., 2006) what leads to protection against oxidative stress (Wu et al., 2006). However, future research must answer whether activation of signaling pathways is triggered by binding of flavonoids to the cell membrane receptors or by binding to the intracellular targets following trans-membrane transport.

To accurately translate observations from *in vitro* assays to *in vivo* studies, and even further to clinical studies, we must properly address the principal underlying mechanisms, which start by mechanistic interpretation of pharmacokinetic studies.

Table 2.2 Pharmacokinetic properties of different flavonoid subclasses, as reported in the literature on animal and human studies.

Flavonoid subclass	Structure	Pre-clinical pharmacokinetics Animal studies	Clinical pharmacokinetics Human studies
<b>Anthocyanidins</b>  (Note: <b>anthocyanins</b> (AC) are glycosylated form)		$c_{\max}$ (monomeric AC) = 0.18 $\mu\text{M}$ <sup>[1]</sup> - 0.84 $\mu\text{M}$ <sup>[2]</sup> $c_{\max}$ (mixture, total AC) = 0.1 $\mu\text{M}$ <sup>[3]</sup> - 3.8 $\mu\text{M}$ <sup>[4]</sup> $t_{\max}$ = 15 min <sup>[5]</sup> - 60 min <sup>[6]</sup> $t_{1/2}$ = NR <sup>a</sup> BA = 0.49 % <sup>[2]</sup> - 1.82 % <sup>[5]</sup>	$c_{\max}$ (monomeric AC) = 0.56 nM <sup>[7]</sup> - 5.8 nM <sup>[8]</sup> $c_{\max}$ (mixture, total AC) = 30 nM <sup>[6]</sup> - 0.5 $\mu\text{M}$ <sup>[9]</sup> $t_{\max}$ = 0.5 h <sup>[10]</sup> - 2.2 h <sup>[11]</sup> $t_{1/2}$ = 1.5 h <sup>[10]</sup> - 6.6 h <sup>[11]</sup>
<b>Flavonols</b>		$c_{\max}$ = 0.9 $\mu\text{M}$ <sup>[12]</sup> - 6.8 $\mu\text{M}$ <sup>[13]</sup> $t_{\max}$ = 30 min <sup>[14]</sup> - 2.9 h <sup>[15]</sup> $t_{1/2}$ = 14.8 h <sup>[15]</sup> - 65.4 h <sup>[15]</sup> BA = 0.5% <sup>[16]</sup> - 5.3 % <sup>[17]</sup>	$c_{\max}$ = 137 nM <sup>[18]</sup> - 7.64 $\mu\text{M}$ <sup>[19]</sup> $t_{\max}$ = 0.68 h <sup>[19]</sup> - 7.5 h <sup>[18]</sup> $t_{1/2}$ = 2.6 h <sup>[20]</sup> - 28.1 h <sup>[21]</sup>
<b>Flavones</b>		$C_{\max}$ = 134 nM <sup>[22]</sup> - 50 $\mu\text{M}$ <sup>[23]</sup> $t_{\max}$ = 15 min <sup>[24]</sup> - 3.9 h <sup>[23]</sup> $t_{1/2}$ = 0.8h <sup>[25]</sup> - 91.8 h <sup>[26]</sup> BA = 2.2 % <sup>[27]</sup>	$C_{\max}$ = 127 nM <sup>[28]</sup> - 300 nM <sup>[29]</sup> $t_{\max}$ = 0.5h <sup>[30]</sup> - 7.2h <sup>[28]</sup> $t_{1/2}$ = 3.1 h <sup>[29]</sup>
<b>Flavanones</b>		$C_{\max}$ = 21 nM <sup>[31]</sup> - 6 $\mu\text{M}$ <sup>[32]</sup> $t_{\max}$ = 20 <sup>[31]</sup> - 80 min <sup>[31]</sup> $t_{1/2}$ = 1.3 <sup>[32]</sup> - 2.2 h <sup>[32]</sup> BA = NR <sup>a</sup>	$C_{\max}$ = 60 nM <sup>[33]</sup> - 7.4 $\mu\text{M}$ <sup>[34]</sup> $t_{\max}$ = 2 h <sup>[35]</sup> - 5.8 h <sup>[33]</sup> $t_{1/2}$ = 1.3 h <sup>[32]</sup> - 3.1 h <sup>[34]</sup>

<b>Flavan-3-ols</b> (Synonym: catechins)		$C_{\max} = 0.3 \mu\text{M}^{[36]} - 2.7 \mu\text{M}^{[36]}$ $t_{\max} = 24\text{h}^{[37]}$ $t_{1/2} = 41 \text{ min}^{[38]} - 4.03 \text{ h}^{[36]}$ $\text{BA} = 0.1\%^{[38]} - 31.2\%^{[38]}$	$C_{\max} = 70 \text{ nM}^{[39]} - 7.35 \mu\text{M}^{[40]}$ $t_{\max} = 1.2\text{h}^{[39]} - 4.1\text{h}^{[41]}$ $t_{1/2} = 0.42 \text{ h}^{[42]} - 5.7 \text{ h}^{[43]}$
<b>Isoflavones</b> (Synonym: phytoestrogens)		$C_{\max} \text{ (rats)} = 2.2 \mu\text{M}^{[44]} - 20.9 \mu\text{M}^{[45]}$ $C_{\max} \text{ (cats)} = 5 \mu\text{M}^{[46]} - 15 \mu\text{M}^{[46]}$ $t_{\max} = 10 \text{ min}^{[45]} - 1.5\text{h}^{[46]}$ $t_{1/2} = 8.5 \text{ h}^{[44]} - 17 \text{ h}^{[47]}$ $\text{BA} = 1.4 \%^{[47]} - 30\%^{[47]}$	$C_{\max} = 0.17 \mu\text{M}^{[48]} - 25.4 \mu\text{M}^{[49]}$ $t_{\max} = 2.5\text{h}^{[49]} - 11\text{h}^{[49]}$ $t_{1/2} = 3.4\text{h}^{[50]} - 10.8\text{h}^{[51]}$

<sup>a</sup> BA, estimated oral bioavailability;  $c_{\max}$ , maximal plasma concentration (peak) after single dose oral ingestion;  $t_{\max}$ , time needed to reach  $c_{\max}$ ;  $t_{1/2}$ , elimination half-life; NR – not reported in the literature.

<sup>b</sup> detailed interactions between membrane transporters and specific flavonoids are presented in Table 1, with the corresponding references.

## Table References

- [1] Ichihyanagi, T.; Shida, Y.; Rahman, M. M.; Hatano, Y.; Matsumoto, H.; Hirayama, M.; Konishi, T., Metabolic pathway of cyanidin 3-O-beta-D-glucopyranoside in rats. *J Agric Food Chem* **2005**, *53*, (1), 145-50.
- [2] Matsumoto, H.; Ichihyanagi, T.; Iida, H.; Ito, K.; Tsuda, T.; Hirayama, M.; Konishi, T., Ingested delphinidin-3-rutinoside is primarily excreted to urine as the intact form and to bile as the methylated form in rats. *J Agric Food Chem* **2006**, *54*, (2), 578-82.
- [3] Wu, X.; Pittman, H. E., 3rd; McKay, S.; Prior, R. L., Aglycones and sugar moieties alter anthocyanin absorption and metabolism after berry consumption in weanling pigs. *J Nutr* **2005**, *135*, (10), 2417-24.
- [4] Miyazawa, T.; Nakagawa, K.; Kudo, M.; Muraishi, K.; Someya, K., Direct intestinal absorption of red fruit anthocyanins, cyanidin-3-glucoside and cyanidin-3,5-diglucoside, into rats and humans. *J Agric Food Chem* **1999**, *47*, (3), 1083-91.
- [5] Ichihyanagi, T.; Shida, Y.; Rahman, M. M.; Hatano, Y.; Konishi, T., Bioavailability and tissue distribution of anthocyanins in bilberry (*Vaccinium myrtillus* L.) extract in rats. *J Agric Food Chem* **2006**, *54*, (18), 6578-87.
- [6] Nielsen, I. L.; Dragsted, L. O.; Ravn-Haren, G.; Freese, R.; Rasmussen, S. E., Absorption and excretion of black currant anthocyanins in humans and watanabe heritable hyperlipidemic rabbits. *J Agric Food Chem* **2003**, *51*, (9), 2813-20.
- [7] Milbury, P. E.; Vita, J. A.; Blumberg, J. B., Anthocyanins are bioavailable in humans following an acute dose of cranberry juice. *J Nutr* **2010**, *140*, (6), 1099-104.
- [8] Kurilich, A. C.; Clevidence, B. A.; Britz, S. J.; Simon, P. W.; Novotny, J. A., Plasma and urine responses are lower for acylated vs nonacylated anthocyanins from raw and cooked purple carrots. *J Agric Food Chem* **2005**, *53*, (16), 6537-42.
- [9] Frank, T.; Janssen, M.; Netzet, G.; Christian, B.; Bitsch, I.; Netzel, M., Absorption and excretion of elderberry (*Sambucus nigra* L.) anthocyanins in healthy humans. *Methods Find Exp Clin Pharmacol* **2007**, *29*, (8), 525-33.
- [10] Frank, T.; Netzel, M.; Strass, G.; Bitsch, R.; Bitsch, I., Bioavailability of anthocyanidin-3-glucosides following consumption of red wine and red grape juice. *Can J Physiol Pharmacol* **2003**, *81*, (5), 423-35.
- [11] Mertens-Talcott, S. U.; Rios, J.; Jilma-Stohlawetz, P.; Pacheco-Palencia, L. A.; Meibohm, B.; Talcott, S. T.; Derendorf, H., Pharmacokinetics of anthocyanins and antioxidant effects after the consumption of anthocyanin-rich acai juice and pulp (*Euterpe oleracea* Mart.) in human healthy volunteers. *J Agric Food Chem* **2008**, *56*, (17), 7796-802.
- [12] Reinboth, M.; Wolfram, S.; Abraham, G.; Ungemach, F. R.; Cermak, R., Oral bioavailability of quercetin from different quercetin glycosides in dogs. *Br J Nutr* **2010**, *104*, (2), 198-203.
- [13] Zhao, G.; Zou, L.; Wang, Z.; Hu, H.; Hu, Y.; Peng, L., Pharmacokinetic profile of total quercetin after single oral dose of tartary buckwheat extracts in rats. *J Agric Food Chem* **2011**, *59*, (9), 4435-41.
- [14] Shimoi, K.; Yoshizumi, K.; Kido, T.; Usui, Y.; Yumoto, T., Absorption and urinary excretion of quercetin, rutin, and alphaG-rutin, a water soluble flavonoid, in rats. *J Agric Food Chem* **2003**, *51*, (9), 2785-9.
- [15] Lee, J.; Mitchell, A. E., Pharmacokinetics of quercetin absorption from apples and onions in healthy humans. *J Agric Food Chem* **2012**, *60*, (15), 3874-81.
- [16] Ader, P.; Wessmann, A.; Wolfram, S., Bioavailability and metabolism of the flavonol quercetin in the pig. *Free Radic Biol Med* **2000**, *28*, (7), 1056-67.
- [17] Chen, X.; Yin, O. Q.; Zuo, Z.; Chow, M. S., Pharmacokinetics and modeling of quercetin and metabolites. *Pharm Res* **2005**, *22*, (6), 892-901.
- [18] Erlund, I.; Kosonen, T.; Alftan, G.; Maenpaa, J.; Perttunen, K.; Kenraali, J.; Parantainen, J.; Aro, A., Pharmacokinetics of quercetin from quercetin aglycone and rutin in healthy volunteers. *Eur J Clin Pharmacol* **2000**, *56*, (8), 545-53.
- [19] Graefe, E. U.; Wittig, J.; Mueller, S.; Riethling, A. K.; Uehleke, B.; Drewelow, B.; Pforte, H.; Jacobasch, G.; Derendorf, H.; Veit, M., Pharmacokinetics and bioavailability of quercetin glycosides in humans. *J Clin Pharmacol* **2001**, *41*, (5), 492-9.
- [20] Schulz, H. U.; Schurer, M.; Bassler, D.; Weiser, D., Investigation of the bioavailability of hypericin, pseudohypericin, hyperforin and the flavonoids quercetin and isorhamnetin following single and multiple oral dosing of a hypericum extract containing tablet. *Arzneimittelforschung* **2005**, *55*, (1), 15-22.
- [21] Hollman, P. C.; Bijman, M. N.; van Gameren, Y.; Cnossen, E. P.; de Vries, J. H.; Katan, M. B., The sugar moiety is a major determinant of the absorption of dietary flavonoid glycosides in man. *Free Radic Res* **1999**, *31*, (6), 569-73.
- [22] Li, L.; Jiang, H.; Wu, H.; Zeng, S., Simultaneous determination of luteolin and apigenin in dog plasma by RP-HPLC. *J Pharm Biomed Anal* **2005**, *37*, (3), 615-20.
- [23] Chen, T.; Li, L. P.; Lu, X. Y.; Jiang, H. D.; Zeng, S., Absorption and excretion of luteolin and apigenin in rats after oral administration of *Chrysanthemum morifolium* extract. *J Agric Food Chem* **2007**, *55*, (2), 273-7.

- [24] Shimoi, K.; Okada, H.; Furugori, M.; Goda, T.; Takase, S.; Suzuki, M.; Hara, Y.; Yamamoto, H.; Kinae, N., Intestinal absorption of luteolin and luteolin 7-O-beta-glucoside in rats and humans. *FEBS Lett* **1998**, *438*, (3), 220-4.
- [25] Hao, X.; Cheng, G.; Sun, J.; Zou, M.; Yu, J.; Zhang, S.; Cui, F., Validation of an HPLC method for the determination of scutellarin in rat plasma and its pharmacokinetics. *J Pharm Biomed Anal* **2005**, *38*, (2), 360-3.
- [26] Gradolatto, A.; Basly, J. P.; Berges, R.; Teyssier, C.; Chagnon, M. C.; Siess, M. H.; Canivenc-Lavier, M. C., Pharmacokinetics and metabolism of apigenin in female and male rats after a single oral administration. *Drug Metab Dispos* **2005**, *33*, (1), 49-54.
- [27] Xing, J.; Chen, X.; Zhong, D., Absorption and enterohepatic circulation of baicalin in rats. *Life Sci* **2005**, *78*, (2), 140-6.
- [28] Meyer, H.; Bolarinwa, A.; Wolfram, G.; Linseisen, J., Bioavailability of apigenin from apiin-rich parsley in humans. *Ann Nutr Metab* **2006**, *50*, (3), 167-72.
- [29] Chen, X.; Cui, L.; Duan, X.; Ma, B.; Zhong, D., Pharmacokinetics and metabolism of the flavonoid scutellarin in humans after a single oral administration. *Drug Metab Dispos* **2006**, *34*, (8), 1345-52.
- [30] Wittemer, S. M.; Ploch, M.; Windeck, T.; Muller, S. C.; Drewelow, B.; Derendorf, H.; Veit, M., Bioavailability and pharmacokinetics of caffeoylquinic acids and flavonoids after oral administration of Artichoke leaf extracts in humans. *Phytomedicine* **2005**, *12*, (1-2), 28-38.
- [31] Mata-Bilbao Mde, L.; Andres-Lacueva, C.; Roura, E.; Jauregui, O.; Escribano, E.; Torre, C.; Lamuela-Raventos, R. M., Absorption and pharmacokinetics of grapefruit flavanones in beagles. *Br J Nutr* **2007**, *98*, (1), 86-92.
- [32] Erlund, I.; Meririnne, E.; Alfthan, G.; Aro, A., Plasma kinetics and urinary excretion of the flavanones naringenin and hesperetin in humans after ingestion of orange juice and grapefruit juice. *J Nutr* **2001**, *131*, (2), 235-41.
- [33] Manach, C.; Morand, C.; Gil-Izquierdo, A.; Bouteloup-Demange, C.; Remesy, C., Bioavailability in humans of the flavanones hesperidin and narirutin after the ingestion of two doses of orange juice. *Eur J Clin Nutr* **2003**, *57*, (2), 235-42.
- [34] Kanaze, F. I.; Bounartzi, M. I.; Georgarakis, M.; Niopas, I., Pharmacokinetics of the citrus flavanone aglycones hesperetin and naringenin after single oral administration in human subjects. *Eur J Clin Nutr* **2007**, *61*, (4), 472-7.
- [35] Bugianesi, R.; Catasta, G.; Spigno, P.; D'Uva, A.; Maiani, G., Naringenin from cooked tomato paste is bioavailable in men. *J Nutr* **2002**, *132*, (11), 3349-52.
- [36] Takizawa, Y.; Morota, T.; Takeda, S.; Aburada, M., Pharmacokinetics of (-)-epicatechin-3-O-gallate, an active component of Onpi-to, in rats. *Biol Pharm Bull* **2003**, *26*, (5), 608-12.
- [37] Kohri, T.; Matsumoto, N.; Yamakawa, M.; Suzuki, M.; Nanjo, F.; Hara, Y.; Oku, N., Metabolic fate of (-)-[4-(3)H]epigallocatechin gallate in rats after oral administration. *J Agric Food Chem* **2001**, *49*, (8), 4102-12.
- [38] Chen, L.; Lee, M. J.; Li, H.; Yang, C. S., Absorption, distribution, elimination of tea polyphenols in rats. *Drug Metab Dispos* **1997**, *25*, (9), 1045-50.
- [39] Henning, S. M.; Niu, Y.; Lee, N. H.; Thames, G. D.; Minutti, R. R.; Wang, H.; Go, V. L.; Heber, D., Bioavailability and antioxidant activity of tea flavanols after consumption of green tea, black tea, or a green tea extract supplement. *Am J Clin Nutr* **2004**, *80*, (6), 1558-64.
- [40] Chow, H. H.; Hakim, I. A.; Vining, D. R.; Crowell, J. A.; Ranger-Moore, J.; Chew, W. M.; Celaya, C. A.; Rodney, S. R.; Hara, Y.; Alberts, D. S., Effects of dosing condition on the oral bioavailability of green tea catechins after single-dose administration of Polyphenon E in healthy individuals. *Clin Cancer Res* **2005**, *11*, (12), 4627-33.
- [41] Chow, H. H.; Cai, Y.; Hakim, I. A.; Crowell, J. A.; Shahi, F.; Brooks, C. A.; Dorr, R. T.; Hara, Y.; Alberts, D. S., Pharmacokinetics and safety of green tea polyphenols after multiple-dose administration of epigallocatechin gallate and polyphenon E in healthy individuals. *Clin Cancer Res* **2003**, *9*, (9), 3312-9.
- [42] Lee, M. J.; Lambert, J. D.; Prabhu, S.; Meng, X.; Lu, H.; Maliakal, P.; Ho, C. T.; Yang, C. S., Delivery of tea polyphenols to the oral cavity by green tea leaves and black tea extract. *Cancer Epidemiol Biomarkers Prev* **2004**, *13*, (1), 132-7.
- [43] Kimura, M.; Umegaki, K.; Kasuya, Y.; Sugisawa, A.; Higuchi, M., The relation between single/double or repeated tea catechin ingestions and plasma antioxidant activity in humans. *Eur J Clin Nutr* **2002**, *56*, (12), 1186-93.
- [44] Coldham, N. G.; Sauer, M. J., Pharmacokinetics of [(14)C]Genistein in the rat: gender-related differences, potential mechanisms of biological action, and implications for human health. *Toxicol Appl Pharmacol* **2000**, *164*, (2), 206-15.
- [45] Piskula, M. K., Soy isoflavone conjugation differs in fed and food-deprived rats. *J Nutr* **2000**, *130*, (7), 1766-71.
- [46] Bell, K. M.; Pearce, P. D.; Ugarte, C. E.; Hendriks, W. H., Preliminary investigation into the absorption of genistein and daidzein by domestic cats (*Felis catus*). *J Nutr* **2006**, *136*, (7 Suppl), 2004S-2006S.

- [47] Cave, N. J.; Backus, R. C.; Marks, S. L.; Klasing, K. C., The bioavailability and disposition kinetics of genistein in cats. *J Vet Pharmacol Ther* **2007**, 30, (4), 327-35.
- [48] Izumi, T.; Piskula, M. K.; Osawa, S.; Obata, A.; Tobe, K.; Saito, M.; Kataoka, S.; Kubota, Y.; Kikuchi, M., Soy isoflavone aglycones are absorbed faster and in higher amounts than their glucosides in humans. *J Nutr* **2000**, 130, (7), 1695-9.
- [49] Bloedon, L. T.; Jeffcoat, A. R.; Lopaczynski, W.; Schell, M. J.; Black, T. M.; Dix, K. J.; Thomas, B. F.; Albright, C.; Busby, M. G.; Crowell, J. A.; Zeisel, S. H., Safety and pharmacokinetics of purified soy isoflavones: single-dose administration to postmenopausal women. *Am J Clin Nutr* **2002**, 76, (5), 1126-37.
- [50] Shelnut, S. R.; Cimino, C. O.; Wiggins, P. A.; Ronis, M. J.; Badger, T. M., Pharmacokinetics of the glucuronide and sulfate conjugates of genistein and daidzein in men and women after consumption of a soy beverage. *Am J Clin Nutr* **2002**, 76, (3), 588-94.
- [51] Setchell, K. D.; Brown, N. M.; Desai, P. B.; Zimmer-Nechimias, L.; Wolfe, B.; Jakate, A. S.; Creutzinger, V.; Heubi, J. E., Bioavailability, disposition, and dose-response effects of soy isoflavones when consumed by healthy women at physiologically typical dietary intakes. *J Nutr* **2003**, 133, (4), 1027-35.

## Bibliographic references

- Aarsland, D., Andersen, K., Larsen, J. P., Perry, R., Wentzel-Larsen, T., Lolk, A., & Kragh-Sorensen, P. (2004). The rate of cognitive decline in Parkinson disease. *Arch Neurol*, *61*(12), 1906-1911. doi: 10.1001/archneur.61.12.1906
- Aguiar, C. C., Almeida, A. B., Araujo, P. V., de Abreu, R. N., Chaves, E. M., do Vale, O. C., . . . Vasconcelos, S. M. (2012). Oxidative stress and epilepsy: literature review. *Oxid Med Cell Longev*, *2012*, 795259. doi: 10.1155/2012/795259
- Ahdab-Barmada, M., Moossy, J., Nemoto, E. M., & Lin, M. R. (1986). Hyperoxia produces neuronal necrosis in the rat. *J Neuropathol Exp Neurol*, *45*(3), 233-246.
- Albarracin, S. L., Stab, B., Casas, Z., Sutachan, J. J., Samudio, I., Gonzalez, J., . . . Barreto, G. E. (2012). Effects of natural antioxidants in neurodegenerative disease. *Nutr Neurosci*, *15*(1), 1-9. doi: 10.1179/1476830511Y.0000000028
- Ali Shah, S., Ullah, I., Lee, H. Y., & Kim, M. O. (2013). Anthocyanins protect against ethanol-induced neuronal apoptosis via GABAB1 receptors intracellular signaling in prenatal rat hippocampal neurons. *Molecular Neurobiology*, *48*(1), 257-269. doi: 10.1007/s12035-013-8458-y
- Andersen, Ø. M., & Jordheim, M. (2013). Basic Anthocyanin Chemistry and Dietary Sources *Anthocyanins in Health and Disease* (pp. 13-90): CRC Press.
- Andersen, Ø. M., & Markham, K. R. (Eds.). (2006). *Flavonoids: chemistry, biochemistry, and applications*: CRC Press.
- Androusoyopoulos, V. P., & Spandidos, D. A. (2013). The flavonoids diosmetin and luteolin exert synergistic cytostatic effects in human hepatoma HepG2 cells via CYP1A-catalyzed metabolism, activation of JNK and ERK and P53/P21 up-regulation. *J Nutr Biochem*, *24*(2), 496-504. doi: 10.1016/j.jnutbio.2012.01.012
- Basli, A., Soulet, S., Chaher, N., Mérillon, J.-M., Chibane, M., Monti, J.-P., & Richard, T. (2012). Wine Polyphenols: Potential Agents in Neuroprotection. *Oxidative Medicine and Cellular Longevity*, *2012*(2), 1-14. doi: 10.1021/jf0735073
- Blennow, K., de Leon, M. J., & Zetterberg, H. (2006). Alzheimer's disease. *Lancet*, *368*(9533), 387-403. doi: 10.1016/S0140-6736(06)69113-7
- Boveris, A., Oshino, N., & Chance, B. (1972). The cellular production of hydrogen peroxide. *Biochem J*, *128*(3), 617-630.
- Calabrese, V., Cornelius, C., Dinkova-Kostova, A. T., Iavicoli, I., Di Paola, R., Koverech, A., . . . Calabrese, E. J. (2011). Cellular stress responses, hormetic phytochemicals and vitagenes in aging and longevity. *Biochimica et biophysica acta*. doi: 10.1016/j.bbadis.2011.11.002
- Calabrese, V., Cornelius, C., Dinkova-Kostova, A. T. A., Iavicoli, I. I., Di Paola, R. R., Koverech, A. A., . . . Calabrese, E. J. (2012). Cellular stress responses, hormetic phytochemicals and vitagenes in aging and longevity. [Review]. *Biochimica et Biophysica Acta (BBA) - Bioenergetics*, *1822*(5), 753-783. doi: 10.1016/j.bbadis.2011.11.002
- Calabrese, V., Cornelius, C., & Mancuso, C. (2009). *Redox Homeostasis and Cellular Stress Response in Aging and Neurodegeneration*: Humana Press.
- Chen, H., Yoshioka, H., Kim, G. S., Jung, J. E., Okami, N., Sakata, H., . . . Chan, P. H. (2011). Oxidative stress in ischemic brain damage: mechanisms of cell death and potential molecular targets for neuroprotection. *Antioxid Redox Signal*, *14*(8), 1505-1517. doi: 10.1089/ars.2010.3576

- Commenges, D., Scotet, V., Renaud, S., Jacqmin-Gadda, H., Barberger-Gateau, P., & Dartigues, J. F. (2000). Intake of flavonoids and risk of dementia. *Eur J Epidemiol*, *16*(4), 357-363.
- Crozier, A., Jaganath, I. B., & Clifford, M. N. (2009). Dietary phenolics: chemistry, bioavailability and effects on health. *Nat Prod Rep*, *26*(8), 1001-1043. doi: 10.1039/b802662a
- Crunkhorn, S. (2012). Protein conformational diseases: Rescuing protein homeostasis. *Nat Rev Drug Discov*, *11*(2), 105. doi: 10.1038/nrd3662
- Czank, C., Cassidy, A., Zhang, Q., Morrison, D. J., Preston, T., & Botting, N. P. (2013). Human metabolism and elimination of the anthocyanin, cyanidin-3-glucoside: a <sup>13</sup>C-tracer study.
- Dajas, F., Rivera, F., Blasina, F., Arredondo, F., Echeverry, C., Lafon, L., . . . Heizen, H. (2003). Cell culture protection and in vivo neuroprotective capacity of flavonoids. *Neurotox Res*, *5*(6), 425-432.
- Danilov, C. A., & Fiskum, G. (2008). Hyperoxia promotes astrocyte cell death after oxygen and glucose deprivation. *Glia*, *56*(7), 801-808. doi: 10.1002/glia.20655
- de Ferrars, R. M., Czank, C., Zhang, Q., Botting, N. P., Kroon, P. A., Cassidy, A., & Kay, C. D. (2014). The pharmacokinetics of anthocyanins and their metabolites in humans. *Br J Pharmacol*, *171*(13), 3268-3282. doi: 10.1111/bph.12676
- de la Monte, S. M., & Tong, M. (2014). Brain metabolic dysfunction at the core of Alzheimer's disease. [10.1016/j.bcp.2013.12.012]. *Biochem Pharmacol*, *88*(4), 548-559. doi: papers3://publication/doi/10.1016/j.bcp.2013.12.012
- de Rijk, M. C., Breteler, M. M., den Breeijen, J. H., Launer, L. J., Grobbee, D. E., van der Meche, F. G., & Hofman, A. (1997). Dietary antioxidants and Parkinson disease. The Rotterdam Study. *Arch Neurol*, *54*(6), 762-765.
- Del Rio, D., Borges, G., & Crozier, A. (2010). Berry flavonoids and phenolics: bioavailability and evidence of protective effects. *Br J Nutr*, *104 Suppl 3*, S67-90. doi: 10.1017/S0007114510003958
- Di Giacomo, C., Acquaviva, R., Santangelo, R., Sorrenti, V., Vanella, L., Li Volti, G., . . . Galvano, F. (2012). Effect of Treatment with Cyanidin-3-O-β-D-Glucoside on Rat Ischemic/Reperfusion Brain Damage. [Research article]. *Evidence-based complementary and alternative medicine : eCAM*, *2012*, 285750. doi: 10.1155/2012/285750
- Droge, W. (2002). Free radicals in the physiological control of cell function. *Physiol Rev*, *82*(1), 47-95. doi: 10.1152/physrev.00018.2001
- Dufour, C., & Dangles, O. (2005). Flavonoid-serum albumin complexation: determination of binding constants and binding sites by fluorescence spectroscopy. *Biochim Biophys Acta*, *1721*(1-3), 164-173. doi: 10.1016/j.bbagen.2004.10.013
- Echeverry, C., Arredondo, F., Abin-Carriquiry, J. A., Midiwo, J. O., Ochieng, C., Kerubo, L., & Dajas, F. (2010). Pretreatment with natural flavones and neuronal cell survival after oxidative stress: a structure-activity relationship study. *J Agric Food Chem*, *58*(4), 2111-2115. doi: 10.1021/jf902951v
- el Mohsen, M., Marks, J., Kuhnle, G., Moore, K., Debnam, E., Kaila Srail, S., . . . Spencer, J. (2006). Absorption, tissue distribution and excretion of pelargonidin and its metabolites following oral administration to rats. *The British journal of nutrition*, *95*(1), 51-58.
- Faria, A., Pestana, D., Teixeira, D., Azevedo, J., De Freitas, V., Mateus, N., & Calhau, C. (2010). Flavonoid transport across RBE4 cells: A blood-brain barrier model. *Cell Mol Biol Lett*, *15*(2), 234-241. doi: 10.2478/s11658-010-0006-4



- Farina, M., Avila, D. S., da Rocha, J. B. T., & Aschner, M. (2013). Metals, oxidative stress and neurodegeneration: A focus on iron, manganese and mercury. *Neurochemistry international*, *62*(5), 575-594. doi: 10.1016/j.neuint.2012.12.006
- Folbergrova, J., Otahal, J., & Druga, R. (2012). Brain superoxide anion formation in immature rats during seizures: protection by selected compounds. *Exp Neurol*, *233*(1), 421-429. doi: 10.1016/j.expneurol.2011.11.009
- Frisoni, G. B., Bocchetta, M., Chetelat, G., Rabinovici, G. D., de Leon, M. J., Kaye, J., . . . Area, I. S. s. N. P. I. (2013). Imaging markers for Alzheimer disease: which vs how. *Neurology*, *81*(5), 487-500. doi: 10.1212/WNL.0b013e31829d86e8
- Gandhi, S., & Abramov, A. Y. (2012). Mechanism of Oxidative Stress in Neurodegeneration. *Oxidative Medicine and Cellular Longevity*, *2012*(3), 1-11. doi: 10.1515/BC.2003.059
- Gandy, S., & DeKosky, S. T. (2013). Toward the treatment and prevention of Alzheimer's disease: rational strategies and recent progress. *Annu Rev Med*, *64*, 367-383. doi: 10.1146/annurev-med-092611-084441
- Gao, X., Cassidy, A., Schwarzschild, M. A., Rimm, E. B., & Ascherio, A. (2012). Habitual intake of dietary flavonoids and risk of Parkinson disease. *Neurology*, *78*(15), 1138-1145. doi: WNL.0b013e31824f7fc4 [pii] 10.1212/WNL.0b013e31824f7fc4
- Gillette Guyonnet, S., Abellan Van Kan, G., Andrieu, S., Barberger Gateau, P., Berr, C., Bonnefoy, M., . . . Vellas, B. (2007). IANA task force on nutrition and cognitive decline with aging. *J Nutr Health Aging*, *11*(2), 132-152.
- Granzotto, A., & Zatta, P. (2014). Resveratrol and Alzheimer's disease: message in a bottle on red wine and cognition. *Front Aging Neurosci*, *6*, 95. doi: 10.3389/fnagi.2014.00095
- Gutierrez-Merino, C., Lopez-Sanchez, C., Lagoa, R., Samhan-Arias, A. K., Bueno, C., & Garcia-Martinez, V. (2011). Neuroprotective actions of flavonoids. *Curr Med Chem*, *18*(8), 1195-1212. doi: BSP/CMC/E-Pub/2011/ 072 [pii]
- Halliwell, B. (1999). Antioxidant defence mechanisms: from the beginning to the end (of the beginning). *Free Radic Res*, *31*(4), 261-272.
- Halliwell, B. (2006). Proteasomal dysfunction: a common feature of neurodegenerative diseases? Implications for the environmental origins of neurodegeneration. *Antioxid Redox Signal*, *8*(11-12), 2007-2019. doi: 10.1089/ars.2006.8.2007
- Hayashi, K., Inuma, M., Sasaki, K., & Hayashi, T. (2012). In vitro and in vivo evaluation of a novel antiherpetic flavonoid, 4'-phenylflavone, and its synergistic actions with acyclovir. *Arch Virol*, *157*(8), 1489-1498. doi: 10.1007/s00705-012-1335-6
- Higgins, G. C., Beart, P. M., Shin, Y. S., Chen, M. J., Cheung, N. S., & Nagley, P. (2010). Oxidative stress: emerging mitochondrial and cellular themes and variations in neuronal injury. *J Alzheimers Dis*, *20 Suppl 2*, S453-473. doi: 10.3233/JAD-2010-100321
- Hinkelbein, J., Feldmann, R. E., Jr., & Kalenka, A. (2010). Time-dependent alterations of cerebral proteins following short-term normobaric hyperoxia. *Mol Cell Biochem*, *339*(1-2), 9-21. doi: 10.1007/s11010-009-0365-1
- Im, S.-E., Nam, T.-G., Lee, H., Han, M.-W., Heo, H. J., Koo, S. I., . . . Kim, D.-O. (2013). Anthocyanins in the ripe fruits of *Rubus coreanus* Miquel and their protective effect on neuronal PC-12 cells. *Food Chemistry*, *139*(1-4), 604-610. doi: 10.1016/j.foodchem.2012.12.057
- Kahkonen, M. P., & Heinonen, M. (2003). Antioxidant activity of anthocyanins and their aglycons. *J Agric Food Chem*, *51*(3), 628-633.
- Kalt, W., Blumberg, J. B., McDonald, J. E., Vinqvist-Tymchuk, M. R., Fillmore, S. A., Graf, B. A., . . . Milbury, P. E. (2008). Identification of anthocyanins in the liver, eye, and brain of blueberry-fed pigs. *J Agric Food Chem*, *56*(3), 705-712. doi: 10.1021/jf071998l

- Kang, T. H., Hur, J. Y., Kim, H. B., Ryu, J. H., & Kim, S. Y. (2006). Neuroprotective effects of the cyanidin-3-O-beta-d-glucopyranoside isolated from mulberry fruit against cerebral ischemia. *Neurosci Lett*, *391*(3), 122-126.
- Kao, T.-K., Ou, Y.-C., Raung, S.-L., Lai, C.-Y., Liao, S.-L., & Chen, C.-J. (2010). Inhibition of nitric oxide production by quercetin in endotoxin/cytokine-stimulated microglia. [Comparative Study]. *Life Sciences*, *86*(9-10), 315-321. doi: 10.1016/j.lfs.2009.12.014
- Kitson, T. M. (2004). Spectrophotometric and kinetic studies on the binding of the bioflavonoid quercetin to bovine serum albumin. *Biosci Biotechnol Biochem*, *68*(10), 2165-2170. doi: JST.JSTAGE/bbb/68.2165 [pii]
- Kong, J.-M., Chia, L.-S., Goh, N.-K., Chia, T.-F., & Brouillard, R. (2003). Analysis and biological activities of anthocyanins. *Phytochemistry*, *64*(5), 923-933. doi: 10.1016/s0031-9422(03)00438-2
- Krikorian, R., Boespflug, E. L., Fleck, D. E., Stein, A. L., Wightman, J. D., Shidler, M. D., & Sadat-Hossieny, S. (2012). Concord Grape Juice Supplementation and Neurocognitive Function in Human Aging. *J Agric Food Chem*. doi: 10.1021/jf300277g
- Krikorian, R., Shidler, M. D., Nash, T. A., Kalt, W., Vinqvist-Tymchuk, M. R., Shukitt-Hale, B., & Joseph, J. A. (2010). Blueberry supplementation improves memory in older adults. *J Agric Food Chem*, *58*(7), 3996-4000. doi: 10.1021/jf9029332
- Kurin, E., Atanasov, A. G., Donath, O., Heiss, E. H., Dirsch, V. M., & Nagy, M. (2012). Synergy study of the inhibitory potential of red wine polyphenols on vascular smooth muscle cell proliferation. *Planta Med*, *78*(8), 772-778. doi: 10.1055/s-0031-1298440
- Langa, K. M., Foster, N. L., & Larson, E. B. (2004). Mixed dementia: emerging concepts and therapeutic implications. *JAMA*, *292*(23), 2901-2908. doi: 10.1001/jama.292.23.2901
- Luchsinger, J. A., & Mayeux, R. (2004). Dietary factors and Alzheimer's disease. *Lancet Neurol*, *3*(10), 579-587. doi: 10.1016/S1474-4422(04)00878-6
- Macchi, G., Brahe, C., & Pomponi, M. (1997). Alois Alzheimer and Gaetano Perusini: should man divide what fate united? [10.3233/BEN-1997-10401]. *Behavioural neurology*, *10*(4), 105-108. doi: papers3://publication/doi/10.3233/BEN-1997-10401
- Manach, C., Williamson, G., Morand, C., Scalbert, A., & Remesy, C. (2005). Bioavailability and bioefficacy of polyphenols in humans. I. Review of 97 bioavailability studies. *Am J Clin Nutr*, *81*(1), 230S-242S.
- Mao, P. (2013). Oxidative Stress and Its Clinical Applications in Dementia. *Journal of Neurodegenerative Diseases*, *2013*, 15. doi: 10.1155/2013/319898
- Mastaloudis, A., & Wood, S. M. (2012). Age-related changes in cellular protection, purification, and inflammation-related gene expression: role of dietary phytonutrients. *Ann N Y Acad Sci*, *1259*, 112-120. doi: 10.1111/j.1749-6632.2012.06610.x
- Mazza, G., Miniati, E. (1993). Anthocyanins in fruits, vegetables and grains (pp. 379). Boca Raton, Florida: CRC Press.
- McDowell, I., Xi, G., Lindsay, J., & Tierney, M. (2007). Mapping the connections between education and dementia. *J Clin Exp Neuropsychol*, *29*(2), 127-141. doi: 10.1080/13803390600582420
- Mhatre, M., Floyd, R. A., & Hensley, K. (2004). Oxidative stress and neuroinflammation in Alzheimer's disease and amyotrophic lateral sclerosis: Common links and potential therapeutic targets. *J Alzheimers Dis*, *6*(2), 147-157.
- Milbury, P. E., & Kalt, W. (2010). Xenobiotic Metabolism and Berry Flavonoid Transport across the Blood-Brain Barrier. *J Agric Food Chem*, *58*(7), 3950-3956. doi: 10.1021/jf903529m
- Moreira, P. I., Carvalho, C., Zhu, X., Smith, M. A., & Perry, G. (2010). Mitochondrial dysfunction is a trigger of Alzheimer's disease pathophysiology. *Biochim Biophys Acta*, *1802*(1), 2-10. doi: 10.1016/j.bbadis.2009.10.006

- Mortimer, J. A. (1997). Brain reserve and the clinical expression of Alzheimer's disease. *Geriatrics*, 52 Suppl 2, S50-53.
- Nagley, P., Higgins, G. C., Atkin, J. D., & Beart, P. M. (2010). Multifaceted deaths orchestrated by mitochondria in neurones. *Biochim Biophys Acta*, 1802(1), 167-185. doi: 10.1016/j.bbadis.2009.09.004
- Neuropathology Group. Medical Research Council Cognitive, F., & Aging, S. (2001). Pathological correlates of late-onset dementia in a multicentre, community-based population in England and Wales. Neuropathology Group of the Medical Research Council Cognitive Function and Ageing Study (MRC CFAS). *Lancet*, 357(9251), 169-175.
- Nicholson, S. K., Tucker, G. A., & Brameld, J. M. (2008). Effects of dietary polyphenols on gene expression in human vascular endothelial cells. *Proc Nutr Soc*, 67(1), 42-47. doi: 10.1017/S0029665108006009
- Nijveldt, R. J., van Nood, E., van Hoorn, D. E., Boelens, P. G., van Norren, K., & van Leeuwen, P. A. (2001). Flavonoids: a review of probable mechanisms of action and potential applications. *Am J Clin Nutr*, 74(4), 418-425.
- Olanow, C. W. (1990). Oxidation reactions in Parkinson's disease. *Neurology*, 40(10 Suppl 3), suppl 32-37; discussion 37-39.
- Orgogozo, J. M., Dartigues, J. F., Lafont, S., Letenneur, L., Commenges, D., Salamon, R., . . . Breteler, M. B. (1997). Wine consumption and dementia in the elderly: a prospective community study in the Bordeaux area. *Rev Neurol (Paris)*, 153(3), 185-192.
- Pappolla, M. A., Omar, R. A., Kim, K. S., & Robakis, N. K. (1992). Immunohistochemical evidence of oxidative [corrected] stress in Alzheimer's disease. *Am J Pathol*, 140(3), 621-628.
- Passamonti, S., Vrhovsek, U., Vanzo, A., & Mattivi, F. (2005). Fast access of some grape pigments to the brain. *J Agric Food Chem*, 53(18), 7029-7034. doi: 10.1021/jf050565k
- Pearce, R. K., Owen, A., Daniel, S., Jenner, P., & Marsden, C. D. (1997). Alterations in the distribution of glutathione in the substantia nigra in Parkinson's disease. *J Neural Transm*, 104(6-7), 661-677.
- Prince, M., Albanese, E., Guerchet, M., & Prina, M. (2014). *World Alzheimer Report 2014 Dementia and Risk Reduction an Analysis of Protective and Modifiable Factors*: Londres: Alzheimers Disease . . .
- Robak, J., & Gryglewski, R. J. (1988). Flavonoids are scavengers of superoxide anions. *Biochem Pharmacol*, 37(5), 837-841.
- Savva, G. M., Wharton, S. B., Ince, P. G., Forster, G., Matthews, F. E., Brayne, C., . . . Aging, S. (2009). Age, neuropathology, and dementia. *N Engl J Med*, 360(22), 2302-2309. doi: 10.1056/NEJMoa0806142
- Scherzinger, E., Lurz, R., Turmaine, M., Mangiarini, L., Hollenbach, B., Hasenbank, R., . . . Wanker, E. E. (1997). Huntingtin-encoded polyglutamine expansions form amyloid-like protein aggregates in vitro and in vivo. *Cell*, 90(3), 549-558.
- Schneider, J. A., Arvanitakis, Z., Bang, W., & Bennett, D. A. (2007). Mixed brain pathologies account for most dementia cases in community-dwelling older persons. *Neurology*, 69(24), 2197-2204. doi: 10.1212/01.wnl.0000271090.28148.24
- Shih, P.-H., Chan, Y.-C., Liao, J.-W., Wang, M.-F., & Yen, G.-C. (2010). Antioxidant and cognitive promotion effects of anthocyanin-rich mulberry (*Morus atropurpurea* L.) on senescence-accelerated mice and prevention of Alzheimer's disease. *The Journal of nutritional biochemistry*, 21(7), 598-605. doi: 10.1016/j.jnutbio.2009.03.008

- Shin, E. J., Jeong, J. H., Chung, Y. H., Kim, W. K., Ko, K. H., Bach, J. H., . . . Kim, H. C. (2011). Role of oxidative stress in epileptic seizures. *Neurochem Int*, *59*(2), 122-137. doi: 10.1016/j.neuint.2011.03.025
- Shobab, L. A., Hsiung, G. Y., & Feldman, H. H. (2005). Cholesterol in Alzheimer's disease. *Lancet Neurol*, *4*(12), 841-852. doi: 10.1016/S1474-4422(05)70248-9
- Sims, N. R., & Muyderman, H. (2010). Mitochondria, oxidative metabolism and cell death in stroke. *Biochim Biophys Acta*, *1802*(1), 80-91. doi: 10.1016/j.bbadis.2009.09.003
- Skowronska, M., & Albrecht, J. (2013). Oxidative and nitrosative stress in ammonia neurotoxicity. *Neurochem Int*, *62*(5), 731-737. doi: 10.1016/j.neuint.2012.10.013
- Son, T. G., Camandola, S., & Mattson, M. P. (2008). Hormetic dietary phytochemicals. *Neuromolecular Med*, *10*(4), 236-246. doi: 10.1007/s12017-008-8037-y
- Spencer, J. P. (2009). Flavonoids and brain health: multiple effects underpinned by common mechanisms. *Genes Nutr*, *4*(4), 243-250. doi: 10.1007/s12263-009-0136-3
- Spencer, J. P. E. (2008). Food for thought: the role of dietary flavonoids in enhancing human memory, learning and neuro-cognitive performance. *Proc Nutr Soc*, *67*(2), 238-252. doi: 10.1017/S0029665108007088
- Spilsbury, A., Vauzour, D., Spencer, J. P. E., & Rattray, M. (2012). Regulation of NF- $\kappa$ B activity in astrocytes: effects of flavonoids at dietary-relevant concentrations. *Biochemical and biophysical research communications*, *418*(3), 578-583. doi: 10.1016/j.bbrc.2012.01.081
- Standridge, J. B. (2004). Pharmacotherapeutic approaches to the prevention of Alzheimer's disease. *Am J Geriatr Pharmacother*, *2*(2), 119-132.
- Steffen, Y., Gruber, C., Schewe, T., & Sies, H. (2008). Mono-O-methylated flavanols and other flavonoids as inhibitors of endothelial NADPH oxidase. *Arch Biochem Biophys*, *469*(2), 209-219.
- Tabner, B. J., Turnbull, S., El-Agnaf, O., & Allsop, D. (2001). Production of reactive oxygen species from aggregating proteins implicated in Alzheimer's disease, Parkinson's disease and other neurodegenerative diseases. *Curr Top Med Chem*, *1*(6), 507-517.
- Tarozzi, A., Morroni, F., Hrelia, S., Angeloni, C., Marchesi, A., Cantelli-Forti, G., & Hrelia, P. (2007). Neuroprotective effects of anthocyanins and their in vivo metabolites in SH-SY5Y cells. *Neurosci Lett*, *424*(1), 36-40. doi: 10.1016/j.neulet.2007.07.017
- Tarozzi, A., Morroni, F., Merlicco, A., Bolondi, C., Teti, G., Falconi, M., . . . Hrelia, P. (2010). Neuroprotective effects of cyanidin 3-O-glucoopyranoside on amyloid beta (25-35) oligomer-induced toxicity. *Neuroscience Letters*, *473*(2), 72-76. doi: 10.1016/j.neulet.2010.02.006
- Terao, J., Murota, K., & Kawai, Y. (2011). Conjugated quercetin glucuronides as bioactive metabolites and precursors of aglycone in vivo. *Food Funct*, *2*(1), 11-17. doi: 10.1039/c0fo00106f
- Ubhi, K., Peng, K., Lessig, S., Estrella, J., Adame, A., Galasko, D., . . . Masliah, E. (2010). Neuropathology of dementia with Lewy bodies in advanced age: a comparison with Alzheimer disease. *Neurosci Lett*, *485*(3), 222-227. doi: 10.1016/j.neulet.2010.09.016
- Valko, M., Leibfritz, D., Moncol, J., Cronin, M. T. D., Mazur, M., & Telser, J. (2007). Free radicals and antioxidants in normal physiological functions and human disease. [Review]. *The international journal of biochemistry & cell biology*, *39*(1), 44-84. doi: 10.1016/j.biocel.2006.07.001
- van Ham, T. J., Thijssen, K. L., Breitling, R., Hofstra, R. M., Plasterk, R. H., & Nollen, E. A. (2008). *C. elegans* model identifies genetic modifiers of alpha-synuclein inclusion formation during aging. *PLoS Genet*, *4*(3), e1000027. doi: 10.1371/journal.pgen.1000027

- Vanzo, A., Vrhovsek, U., Tramer, F., Mattivi, F., & Passamonti, S. (2011). Exceptionally Fast Uptake and Metabolism of Cyanidin 3-Glucoside by Rat Kidneys and Liver. *Journal of natural products*. doi: 10.1021/np100948a
- Vargas, A. J., & Burd, R. (2010). Hormesis and synergy: pathways and mechanisms of quercetin in cancer prevention and management. *Nutr Rev*, 68(7), 418-428.
- Wang, S., Li, N., Pan, W., & Tang, B. (2012). Advances in functional fluorescent and luminescent probes for imaging intracellular small-molecule reactive species. *TrAC Trends in Analytical Chemistry*, 39, 3-37. doi: 10.1016/j.trac.2012.07.010
- Waterhouse, A. L. (2002). Wine phenolics. *Ann N Y Acad Sci*, 957, 21-36.
- Williams, R. J., & Spencer, J. P. (2012). Flavonoids, cognition, and dementia: actions, mechanisms, and potential therapeutic utility for Alzheimer disease. *Free Radic Biol Med*, 52(1), 35-45. doi: 10.1016/j.freeradbiomed.2011.09.010
- Wu, C. C., Hsu, M. C., Hsieh, C. W., Lin, J. B., Lai, P. H., & Wung, B. S. (2006). Upregulation of heme oxygenase-1 by Epigallocatechin-3-gallate via the phosphatidylinositol 3-kinase/Akt and ERK pathways. *Life Sci*, 78(25), 2889-2897.
- Zemlan, F. P., Thienhaus, O. J., & Bosmann, H. B. (1989). Superoxide dismutase activity in Alzheimer's disease: possible mechanism for paired helical filament formation. *Brain Res*, 476(1), 160-162.
- Zerovnik, E. (2010). Protein conformational pathology in Alzheimer's and other neurodegenerative diseases; new targets for therapy. *Curr Alzheimer Res*, 7(1), 74-83.
- Zhang, K., & Kaufman, R. J. (2006). The unfolded protein response: a stress signaling pathway critical for health and disease. *Neurology*, 66(2 Suppl 1), S102-109. doi: 10.1212/01.wnl.0000192306.98198.ec
- Zhu, J. T. T., Choi, R. C. Y., Chu, G. K. Y., Cheung, A. W. H., Gao, Q. T., Li, J., . . . Tsim, K. W. K. (2007). Flavonoids possess neuroprotective effects on cultured pheochromocytoma PC12 cells: a comparison of different flavonoids in activating estrogenic effect and in preventing beta-amyloid-induced cell death. *J Agric Food Chem*, 55(6), 2438-2445. doi: 10.1021/jf063299z

# **Chapter 3. Review of Analytical Techniques**

Nanotechnology, which is the creation of functional materials, devices, and systems through the control of nanoscale materials (Wang, 2005), has recently become one of the most influential fields at the forefront of systems biology, in which it plays a critical role in the discovery and validation of biomarkers by providing access to a wealth of information delivered by omics technologies (Sakamoto et al., 2010).

In systems biology, omics technology components have the potential to be used for early detection of disease, to predict patient response to therapy, and to identify biomarkers (Kell, 2006). This field is still evolving, but strong evidence in the scientific literature supports the role of nanotechnology as an empowering contributor that provides access to previously inaccessible data with excellent proficiency and resolution.

## **Metabolomics**

Within the last decade, metabolomics has attracted great interest primarily in the search for disease biomarkers. Small molecules in a biological system can provide a wealth of information about overall functionality and perturbations within pathways and cycles of whole biological systems or selected cells, tissue, or organs (Fiehn, 2002).

The term *metabonomics* was first formulated by the Nicholson group in 1999 to describe “the multiparametric, quantitative study of dynamic metabolome responses in living systems to physiological and pathophysiological stimulation or genetic modification” (Nicholson et al., 1999). In 2001, a competing term, *metabolomics*, was proposed and generally defined as the “comprehensive and quantitative analysis of all metabolites” (Fiehn, 2002). Because the two terms are increasingly used interchangeably, this thesis uses *metabolomics* to encompass the definition of both words.

The metabolome is the complete set of an organism’s metabolites. It represents a vast number of components that belong to a wide variety of classes. Metabolites are small intra- and extracellular molecules (smaller than 1.5 kDa) that act as carriers, substrates, or intermediate products in cellular biochemical pathways and reflect the upstream activities of genes and proteins. Common examples of metabolites are amino acids, lipids, organic acids, nucleotides, and vitamins, although inorganic and reactive species are also studied (Kell, 2007; Lahner et al., 2003). These compounds differ in their physical and chemical properties and occur in wide concentration ranges. Metabolites occur further down the line from genes or proteins to

functions (the end products of cellular regulatory processes), and are therefore most closely related (compared with genes and proteins) to the activities of biological systems at the functional level. Therefore, metabolites are sensitive probes for homeostasis and its regulation (Goodacre, 2004, 2005).

Metabolites are also modulated by several factors unrelated to the genome and reflect, for example, interactions with commensal microorganisms and modifications caused by nutrition or exposure to drugs and pollutants. Diseases, toxic insults, and other pathophysiological stimuli are expected to interfere with metabolism, consequently causing biochemical changes that can be captured as metabolic profiles or signatures.

In contrast to transcriptional analysis, metabolomics does not necessitate a sequenced genome, and results are readily transferable from one species to another because metabolic detoxification pathways remain relatively well conserved. Another strength of metabolomics approaches is the possibility of collecting and integrating data from different compartments of the same organism—for example, biofluids such as urine or blood and tissues from specific organs. For these reasons, metabolomics has been increasingly recognized as a valuable tool in fields ranging from toxicology to plant physiology to biomedical research.

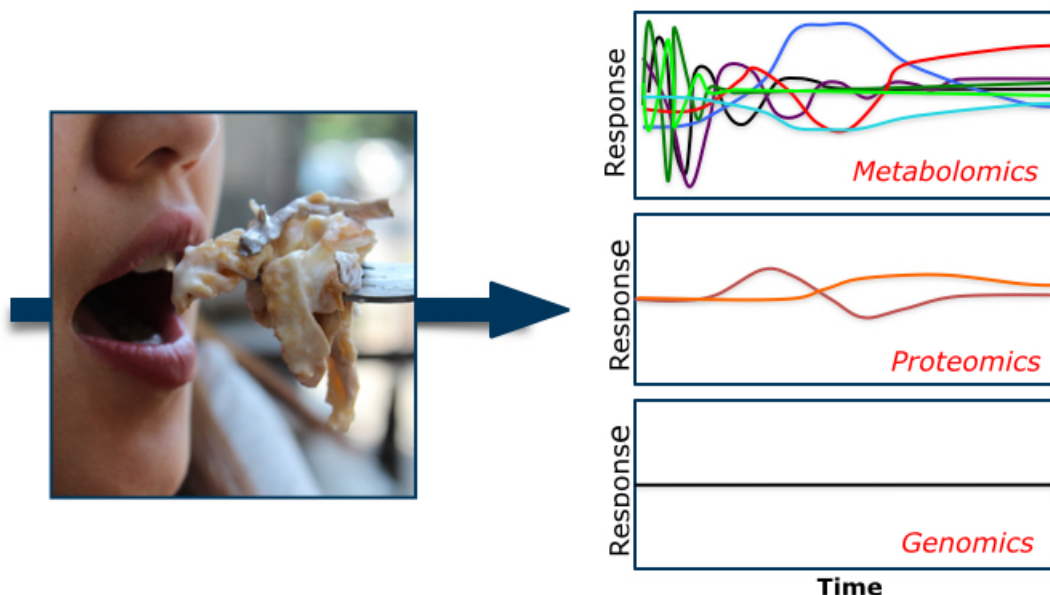


Figure 3.1 Metabolomics is more time sensitive than other “omics”.



Metabolomics is not without its challenges, however. Currently, no single analytical technique provides a comprehensive view of all of the metabolites present in a sample (Dettmer et al., 2007; Schiavo et al., 2008). Nevertheless, a number of integrated approaches have been developed to overcome the limitations of current technologies (Crockford et al., 2006; Lenz & Wilson, 2007).

### **Types of analyses**

Metabolomics analyses consist of a sequence of steps that include sample preparation, metabolite extraction, derivatization, metabolite separation, detection, and data treatment. In general, metabolomics analyses have been classified as targeted or untargeted.

**Targeted metabolomics** is commonly driven by a specific biochemical question or hypothesis that motivates the investigation of a specific group of intended metabolites or one or more related metabolic pathways (Pereira et al., 2010; Ramautar et al., 2008). Targeted or metabolite-specific methods include the following:

- **Metabolite profiling**

Metabolic profiling is the analysis of a group of metabolites related to either a specific metabolic pathway or a class of compounds. Some metabolites have been so widely studied that new nomenclatures have recently appeared—in lipidomics, for example, which assesses qualitative and quantitative information about the constitution of the cellular lipidome (a subcompartment of the metabolome comprising lipid classes, subclasses, and signaling molecules) and provides insights into the biochemical mechanisms of lipid metabolism and lipid–lipid and lipid–protein interactions (Griffiths & Wang, 2009). Metabolite profiling uses hyphenated techniques such as gas chromatography–mass spectrometry, liquid chromatography–mass spectrometry (LC/MS), and capillary electrophoresis–mass spectrometry. These techniques provide detailed chromatographic profiles of samples and measurements of the relative or absolute amounts of the components therein.

- **Target metabolite analysis**

A more direct approach, target metabolite analysis measures selected analytes, such as biomarkers of disease or toxicant exposure or substrates and products of enzymatic

reactions (Fiehn, 2002). Based on the aim of a study, metabolites are selected for analysis and specific analytical methods are developed for their determination (Dettmer et al., 2007). The analysis of C3G and its methylated derivatives with high-performance liquid chromatography (HPLC)–mass spectrometry and pharmacokinetic characterization presented in Chapter 4 is an example of target metabolite analysis.

- **Metabolic fingerprinting**

Metabolic fingerprinting techniques involve the collection of spectra of unpurified solvent extracts under standardized conditions. These approaches initially ignore the assignment of individual peaks, which are frequently overlapping. Multivariate statistical methods such as principal component analysis (PCA) are used to compare sets of spectra to identify clusters of similarity or difference on which to draw conclusions about the classification of individual samples. The identities of metabolites responsible for differences between classes can be investigated from loading plots generated with PCA and related techniques (Ward et al., 2007). As such, only peaks that differ between samples are analyzed, thereby avoiding the time-consuming task of identifying all peaks. Nuclear magnetic resonance spectroscopy, Raman spectroscopy, and Fourier-transform infrared spectroscopy are referred to as “fingerprinting” methods. They are more rapid, general screening methods that can be configured for high throughput and are suitable for determining differences and classifying samples (Halket et al., 2005). An example can be found in the development of a new method based on surface-enhanced Raman spectroscopy (SERS) presented in Chapter 7.

These targeted approaches and practical aspects of quantitative metabolomics are discussed in detail elsewhere (Xu et al., 2009).

By comparison, **untargeted metabolomics** approaches are global in scope, usually hypothesis free, and focus on the detection, identification, and quantitation of as many metabolites as analytically possible in biological samples. These approaches search for variations that can be used to obtain patterns or fingerprints that discriminate comparative samples (Monton & Soga, 2007). Because untargeted metabolomics requires no prior knowledge, it can be used to identify novel metabolic biomarkers of disease and drug efficacy. In the case of samples obtained from rats treated with or without C3G (see Chapter

5), the aim was to identify treatment-related differences in one or more of the numerous endogenous metabolites found in the brain.

Computational and mathematical models are then used to facilitate data processing and comparative analysis of metabolomics data subsets either for signature validation or biomarker identification.

## Metabolomics Workflow

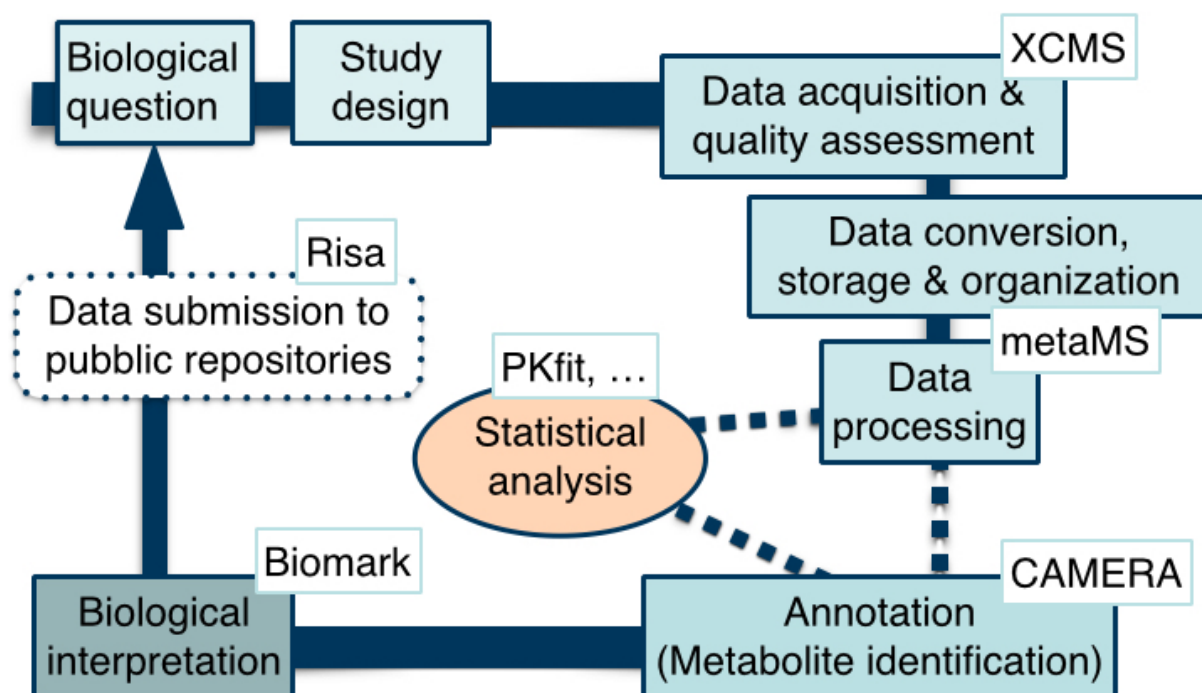


Figure 3.2 Metabolomic workflow.

Figure 3.2 graphically represents the *metabolomics workflow* that starts with a biological question, including the design of experiments and data collection and analysis, and ends with the biological interpretation of results. Figure 3.1 also includes examples of the actions and tools used in this thesis. In this chapter, we describe strategies and methodology for data processing and statistical analysis, which are key factors in the metabolomics workflow.

## **Statistical analyses**

Several data analyses and pattern-recognition algorithms are used to interpret the complex metabolic information obtained from experimental measurements and connect it to distinct biological phenomena. Statistical data analysis methods may include univariate/multivariate and unsupervised/supervised methods (Goodacre, 2005).

## **Univariate methods**

Univariate methods are central to metabolomics. Typically, statistical hypothesis tests, such as a *t*-test or analysis of variance (ANOVA), are used to confirm significant differences between means. A key issue in statistical hypothesis testing is the increased risk of committing a type I error (incorrectly rejecting a null hypothesis): when comparing a large number of samples with hundreds of features, a significance threshold of  $p < 0.05$  is insufficient (Broadhurst & Kell, 2006). There is a high probability that features identified as significant at  $p < 0.05$  are not truly significant. A simple Bonferroni (Broadhurst & Kell, 2006) or the alternative and less stringent false discovery rate (FDR) (Benjamini & Hochberg, 1995) can be used to reduce the possibility of false discoveries. An FDR-adjusted  $p$  value (also called the  $q$  value) of 0.05 implies that 5% of significant tests will result in false positives.

## **Multivariate methods**

The term *chemometrics* was coined by Svante Wold and Bruce R. Kowalski in the early 1970s and is defined as the application of mathematical, statistical, graphical, or symbolic methods to extract information from complex biological and chemical systems for the selection of optimal experimental procedures and data treatments for analysis (Eriksson et al., 2004; Wold, 1991) Since its introduction, chemometrics has grown into a well-established data analysis tool applied to various fields of chemistry, especially analytical chemistry, in areas such as multivariate calibration, quantitative structure–activity modeling, pattern recognition, and multivariate statistical process monitoring and control (Trygg et al., 2007).

Metabolomics studies generate large and complex multivariate datasets. Therefore, chemometrics has become an integral part of global profiling and fingerprinting because it provides interpretable models for complex intercorrelated data and tools for making good use of measured data and devising quantitative models and visual representations of information. However, metabolomic datasets require several data preprocessing steps before multivariate

analysis to achieve optimal characterization of the samples and generate reliable, interpretable models using multivariate analysis techniques.

### **Preprocessing**

During preprocessing, data variables are centered and scaled with methods that are chosen based on the instrumental technique used (van den Berg et al., 2006). Normalization methods reduce the variance between samples through normalization to a constant sum, constant feature (e.g., an internal standard), or reference sample. Autoscaling (subtraction of the mean from each value within columns and dividing by the standard deviation) and Pareto scaling (the same process as autoscaling but dividing by the square root of the standard deviation) are common scaling methods used to reduce variance between the variables in metabolomics datasets. However, many other approaches, such as logarithmic or exponential scaling, are available (Broadhurst & Kell, 2006; Hendriks et al., 2011; van den Berg et al., 2006). Some of the most common methods are listed in Table 3.1.

After preprocessing, the use of multivariate statistical methods is critical for identifying statistically significant differences within large sets of information-rich chemical and biological data. The most common of these methods are listed in Table 3.2. Two general types of pattern recognition algorithms are used in multivariate statistical analyses: unsupervised and supervised (Worley & Powers, 2013).

**Table 3.1 List of most commonly used data scaling methods in multivariate analyses.**

Method	Equation	Goal	Advantage	Disadvantage
Centering	$\tilde{x}_{ik} = x_{ik} - \bar{x}_k$	Focus on differences, not similarities	Removes offset from the data	Unsuitable for heteroscedastic data
Auto scaling	$\tilde{x}_{ik} = \frac{x_{ik} - \bar{x}_k}{s_k}$	Compare metabolites based on correlation	All metabolites equally important	Inflation of measurement errors
Range scaling	$\tilde{x}_{ik} = \frac{x_{ik} - \bar{x}_k}{x_{k,\max} - x_{k,\min}}$	Compare metabolites relative to biological response range	All metabolites equally important. Biologically related scaling	Inflation of measurement errors, sensitive to outliers
Pareto scaling	$\tilde{x}_{ik} = \frac{x_{ik} - \bar{x}_k}{\sqrt{s_k}}$	Reduce relative importance of large values, partially preserve data structure	Stays closer to original measurement than UV	Sensitive to large fold changes
Vast scaling	$\tilde{x}_{ik} = \frac{x_{ik} - \bar{x}_k}{s_k} \cdot \frac{\bar{x}_k}{s_k}$	Focus on small fluctuations	Aims for robustness, uses prior group knowledge	Not suited for large induced variation without group structure
Level scaling	$\tilde{x}_{ik} = \frac{x_{ik} - \bar{x}_k}{\bar{x}_k}$	Focus on relative response	Suited for biomarker identification	Inflation of measurements errors
Log scaling	$\tilde{x}_{ik} = \log(x_{ik})$ $x'_{ik} = \tilde{x}_{ik} - \bar{x}_k$	Correct for heteroscedasticity, pseudo scaling. Make multiplicative models additive	Reduce heteroscedasticity, multiplicative effects become additive	Difficulties with values with large relative standard deviation and zeros

$\mathbf{X}$  is a data matrix; the mean of the  $k$ -th variable in  $\mathbf{X}$  is represented by  $\bar{x}_k$  and its deviation represented by  $s_k$ , the sample standard deviation.  $\tilde{x}_{ik}$  and  $x'_{ik}$  represent the data after different pretreatment steps. Modified from (van den Berg et al., 2006).

## **Unsupervised analysis**

In unsupervised analyses, all variables are unlabeled and no prior information is used. The most common unsupervised method in metabolomics multivariate data analysis, PCA, is typically used first even if complex algorithms with supervised analyses are later implemented (van den Berg et al., 2006). PCA is a mathematical transformation that provides a low-dimension view of multidimensional data by transforming a large number of intercorrelated variables into a smaller set of uncorrelated variables called principal components (PCs) while maintaining the variation of the dataset. Coordinate scores represent the original samples in a new space in which dimensions are linear combinations of the original variables, called loadings (Begam & Kumar, 2014). The first PC explains the maximum variance, and subsequent PCs capture the remaining variance in decreasing order. PCA can be used to provide a quick overview of the data, possible groupings, and outliers. Therefore it is a first choice in a metabolomics experiment to check whether the variance in the data reflects true biological difference.

## **Supervised analysis**

In supervised analyses, prior information is used to build a matrix of predictors and a matrix (or a vector) of responses. The aim is to test how predictor data determine the behavior of response variables. Regression is an example of a supervised approach. Another main supervised method is classification. Importantly, regression and classification are closely related because most regression methods can be used as classification approaches. A wide variety of algorithms are available, the most common being projection to latent structures and orthogonal projection to latent structures, which are often combined with discriminant analysis to establish an optimal position with which to trace a discriminant surface that best separates classes. Further details about these methods can be found elsewhere (Eriksson et al., 2004; Trygg et al., 2007).

**Table 3.2 Common statistical techniques in metabolomics.** Modified from (Hendriks et al., 2011).

Technique		Use
Artificial Neural Networks	ANN	Machine-learning technique, relating inputs to an output through non-linear functions, mimicking neural networks of the brain
ANOVA-Simultaneous Component Analysis	ASCA	Finding underlying structure when the data are collected according to an experimental design
Discriminant Analysis	DA	Methods relating explanatory variables to a categorical response (e.g., controls versus diseased subjects)
Multi-level data	ML	Data with a multi-level structure (e.g., time series measured for different subjects)
Multi-level Partial Least Squares Discriminant Analysis	ML-PLS-DA	Multi-level version of PLS-DA
Multi-level SCA	MSCA	SCA method for multi-level data
Multi-way data	N-way data	Data that can be meaningfully arranged in a cube or higher-way array
N-way Partial Least Squares Discriminant Analysis	N-PLS-DA	Generalization of PLS-DA to N-way data
Orthogonal Partial Least Squares Discriminant Analysis	OPLS-DA	Version of PLS-DA with a simplified interpretation
Parallel Factor Analysis	PARAFAC	Generalization of PCA for N-way data
Parallel Factor Analysis ANOVA-Simultaneous Component Analysis	PARAFASCA	Combination of PARAFAC and ASCA for N-way data with an underlying experimental design
Principal Component Analysis	PCA	Exploratory analysis method reducing multivariate data to a few underlying (principal) components
Partial Least Squares	PLS	Regression method suitable for high-dimensional collinear data
Partial Least Squares Discriminant Analysis	PLS-DA	Discriminant analysis method based on PLS
Principal Component Discriminant Analysis	PCDA	Discriminant analysis method based on PCA
Regression		Methods relating explanatory variables to continuous responses
Random Forests	RF	Method relating explanatory variables to categorical or continuous responses using averaging over an ensemble of simple models
Simultaneous Component Analysis	SCA	Generalization of PCA for simultaneous analysis of several data sets
Support Vector Machines	SVM	Discriminant analysis method based on hyperplanes separating groups



### **Analytical platforms**

Liquid chromatography coupled to mass spectrometry (LC/MS) and Surface-enhanced Raman spectroscopy (SERS) are the two analytical platform employed in this thesis for metabolite identification and metabolic fingerprinting.

### **LC/MS**

In LC/MS, a prior chromatographic separation of a complex mixture sample is followed by analyte identification with MS. Currently, HPLC and ultra-performance liquid chromatography (UPLC) are used more frequently than any other separation technique for metabolic studies. Nano HPLC/UPLC is a relatively new development in chromatography driven by recent advances in proteomics that require decreasing inner diameters of liquid chromatography columns to accommodate smaller sample amounts and increased sensitivity (Murad et al., 2011; Petriz et al., 2015; Weinhold et al., 2015). Nano HPLC/UPLC provides minimal sample loss, higher sensitivity, higher peak capacity, superior separation efficiency, and superior coupling to MS (Sangaraju et al., 2012). The flow rate ranges from nanoliters to microliters per minute, and capillary columns are used instead of normal HPLC columns.

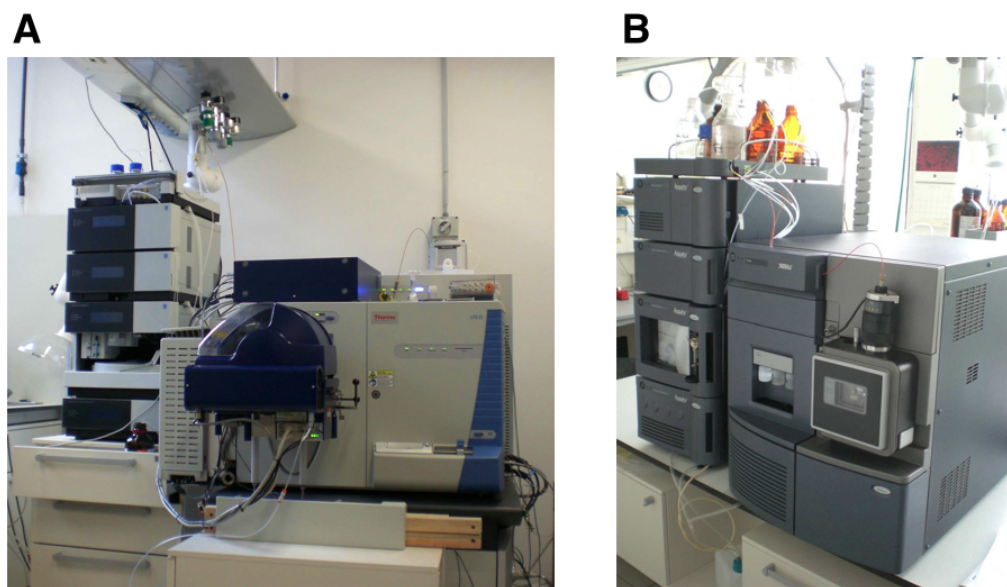


**Figure 3.3 A Nano HPLC (Dionex)- Orbitrap FTMS (ThermoScientific); B UPLC-MS/MS Xevo (Waters).**

Coupled with MS, HPLC and UPLC are powerful tools for separating and characterizing the majority of metabolites and yielding accurate quantitative data.

Coupled with MS, they become powerful tools that allow the separation and characterization of the majority of metabolites, yielding accurate quantitative data.

## SERS

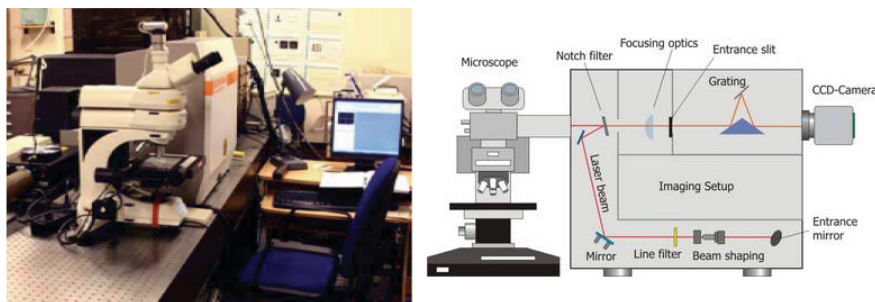


**Figure 3.4 InVia Raman system (Renishaw)**

SERS is a nondestructive analytical technique based on the inelastic scattering of a monochromatic light (usually provided by a laser source) by vibrating molecules. The applicability of Raman spectroscopy to metabolomics is limited due to the low efficiency of the Raman scattering process, but Raman intensity can be increased by amplifying the electromagnetic fields generated by the excitation of localized surface plasmons (see Figure 3.5) if an analyte is adsorbed onto a specific metal surface or in very close proximity to it (typically 10 nm maximum) (Aroca, 2006; Lis & Cecchet, 2014).

SERS exploits this arrangement and provides structure-specific vibrational spectra of adsorbates with extremely high sensitivity. The technique also ensures high selectivity because only adsorbed species can be detected. The technique facilitates investigations of small populations of molecules down to the single-molecule level (Bonifacio et al., 2014). These advantageous characteristics have made SERS a valuable tool for the nondestructive investigation of small-molecule populations that meets the requirements for micro and trace analytics, metabolomics, and biomedical and pharmaceutical studies (Vicario et al., 2015). From a metabolomics perspective, one of the more recent and exciting applications of SERS is the molecular imaging of living cells, in which silver or gold nanoparticles in suspension provide the necessary SERS enhancements to enable mapping molecular distributions in living cells and visualization of specific cellular pathways. (Palonpon et al., 2013).

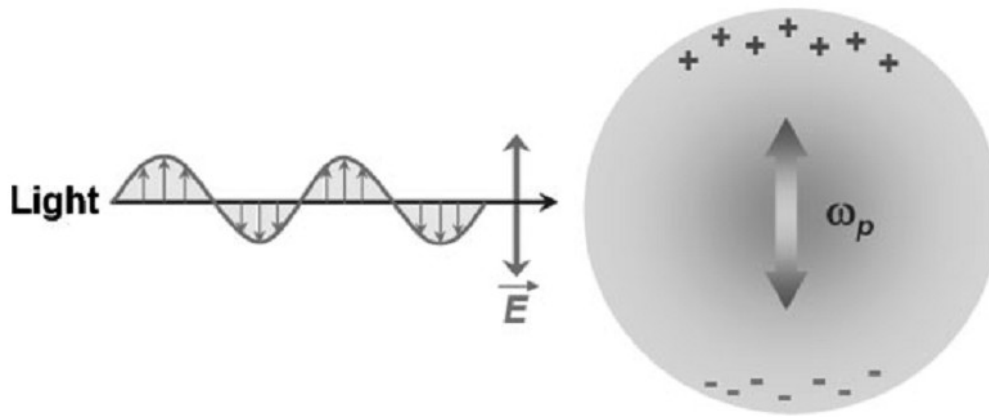


**Figure 3.5 Schematic image of plasmon oscillation for a metal nanoparticle.** Metals can be considered a plasma composed of polarizable free electron, and positive ion core. The laser light excites the collective oscillations of the surface conduction electrons in a metal (surface plasmons) and the free electron coherently oscillate at the plasmon frequencies ( $\omega_p$ ). This excitation results in the enhancement of the local electromagnetic field intensity experienced by a molecule adsorbed or in close proximity to the metal surface. The field induced at the surface of the nanoparticles is given by:

$$E_{induced} = \left\{ \frac{[\varepsilon_1(\omega) - \varepsilon_2]}{[\varepsilon_1(\omega) + 2\varepsilon_2]} \right\} E_{incident}$$

where  $\varepsilon_1(\omega)$  is the complex dielectric function of the metal structure and  $\varepsilon_2$  is the relative permittivity of the surrounding medium. As a consequence of the presence of this secondary electromagnetic field, the intensity of the Raman scattered light is enhanced. The increased electromagnetic field results in enhanced Raman scattered light (ER) is given by  $E_R = \alpha_R g E_0$  where  $\alpha_R$  is the fraction of the photons undergoing inelastic scattering under normal conditions and  $g$  is the average field enhancement over the particle surface (Ko et al., 2008).

## Bibliographic references

- Aroca, R. (2006). Surface-Enhanced Raman Scattering *Surface-Enhanced Vibrational Spectroscopy* (pp. 73-106): John Wiley & Sons, Ltd.
- Begam, B. F., & Kumar, J. S. (2014). Visualization of Chemical Space Using Principal Component Analysis. [10.5829/idosi.wasj.2014.29.dmsct.10]. *World Applied Sciences Journal*. doi: papers3://publication/doi/10.5829/idosi.wasj.2014.29.dmsct.10
- Benjamini, Y., & Hochberg, Y. (1995). Controlling the false discovery rate: a practical and powerful approach to multiple testing. *Journal of the Royal Statistical Society. Series B (Methodological)*, 289-300.
- Bonifacio, A., Dalla Marta, S., Spizzo, R., Cervo, S., Steffan, A., Colombatti, A., & Sergio, V. (2014). Surface-enhanced Raman spectroscopy of blood plasma and serum using Ag and Au nanoparticles: a systematic study. *Anal Bioanal Chem*, 406(9-10), 2355-2365. doi: 10.1007/s00216-014-7622-1
- Broadhurst, D. I., & Kell, D. B. (2006). Statistical strategies for avoiding false discoveries in metabolomics and related experiments. [10.1007/s11306-006-0037-z]. *Metabolomics*, 2(4), 171-196. doi: papers3://publication/doi/10.1007/s11306-006-0037-z
- Crockford, D. J., Holmes, E., Lindon, J. C., Plumb, R. S., Zira, S., Bruce, S. J., . . . Nicholson, J. K. (2006). Statistical heterospectroscopy, an approach to the integrated analysis of NMR and UPLC-MS data sets: application in metabonomic toxicology studies. *Anal Chem*, 78(2), 363-371. doi: 10.1021/ac051444m
- Dettmer, K., Aronov, P. A., & Hammock, B. D. (2007). Mass spectrometry-based metabolomics. *Mass Spectrometry Reviews*(26), 51-78.
- Eriksson, L., Antti, H., Gottfries, J., Holmes, E., Johansson, E., Lindgren, F., . . . Wold, S. (2004). Using chemometrics for navigating in the large data sets of genomics, proteomics, and metabonomics (gpm). *Anal Bioanal Chem*, 380(3), 419-429. doi: 10.1007/s00216-004-2783-y
- Fiehn, O. (2002). Metabolomics--the link between genotypes and phenotypes. *Plant Mol Biol*, 48(1-2), 155-171.
- Goodacre, R. (2004). Metabolic profiling: pathways in discovery. *Drug Discov Today*, 9(6), 260-261. doi: 10.1016/S1359-6446(04)03027-2
- Goodacre, R. (2005). Making sense of the metabolome using evolutionary computation: seeing the wood with the trees. *J Exp Bot*, 56(410), 245-254. doi: 10.1093/jxb/eri043
- Griffiths, W. J., & Wang, Y. (2009). Mass spectrometry: from proteomics to metabolomics and lipidomics. *Chem Soc Rev*, 38(7), 1882-1896. doi: 10.1039/b618553n
- Halket, J. M., Waterman, D., Przyborowska, A. M., Patel, R. K., Fraser, P. D., & Bramley, P. M. (2005). Chemical derivatization and mass spectral libraries in metabolic profiling by GC/MS and LC/MS/MS. *J Exp Bot*, 56(410), 219-243. doi: 10.1093/jxb/eri069
- Hendriks, M. M. W. B., van Eeuwijk, F. A., Jellema, R. H., Westerhuis, J. A., Reijmers, T. H., Hoefsloot, H. C. J., & Smilde, A. K. (2011). Data-processing strategies for metabolomics studies. [10.1016/j.trac.2011.04.019]. *Trends in Analytical Chemistry*, 30(10), 1685-1698. doi: papers3://publication/doi/10.1016/j.trac.2011.04.019

- Kell, D. B. (2006). Theodor Bucher Lecture. Metabolomics, modelling and machine learning in systems biology - towards an understanding of the languages of cells. Delivered on 3 July 2005 at the 30th FEBS Congress and the 9th IUBMB conference in Budapest. *FEBS J*, 273(5), 873-894. doi: 10.1111/j.1742-4658.2006.05136.x
- Kell, D. B. (2007). Metabolomic biomarkers: search, discovery and validation. *Expert Rev Mol Diagn*, 7(4), 329-333. doi: 10.1586/14737159.7.4.329
- Lahner, B., Gong, J., Mahmoudian, M., Smith, E. L., Abid, K. B., Rogers, E. E., . . . Salt, D. E. (2003). Genomic scale profiling of nutrient and trace elements in *Arabidopsis thaliana*. *Nat Biotechnol*, 21(10), 1215-1221. doi: 10.1038/nbt865
- Lenz, E. M., & Wilson, I. D. (2007). Analytical strategies in metabolomics. *J Proteome Res*, 6(2), 443-458. doi: 10.1021/pr0605217
- Lis, D., & Cecchet, F. (2014). Localized surface plasmon resonances in nanostructures to enhance nonlinear vibrational spectroscopies: towards an astonishing molecular sensitivity. *Beilstein J Nanotechnol*, 5, 2275-2292. doi: 10.3762/bjnano.5.237
- Monton, M. R., & Soga, T. (2007). Metabolome analysis by capillary electrophoresis-mass spectrometry. *J Chromatogr A*, 1168(1-2), 237-246; discussion 236. doi: 10.1016/j.chroma.2007.02.065
- Murad, A. M., Souza, G. H., Garcia, J. S., & Rech, E. L. (2011). Detection and expression analysis of recombinant proteins in plant-derived complex mixtures using nanoUPLC-MS(E). *J Sep Sci*, 34(19), 2618-2630. doi: 10.1002/jssc.201100238
- Nicholson, J. K., Lindon, J. C., & Holmes, E. (1999). 'Metabonomics': understanding the metabolic responses of living systems to pathophysiological stimuli via multivariate statistical analysis of biological NMR spectroscopic data. *Xenobiotica*, 29(11), 1181-1189. doi: 10.1080/004982599238047
- Palonpon, A. F., Ando, J., Yamakoshi, H., Dodo, K., Sodeoka, M., Kawata, S., & Fujita, K. (2013). Raman and SERS microscopy for molecular imaging of live cells. *Nat Protoc*, 8(4), 677-692. doi: 10.1038/nprot.2013.030
- Pereira, D. M., Valentão, P., Ferreres, F., & Andrade, P. B. (2010). Metabolomic Analysis of Natural Products. In C. K. Zacharis & P. D. Tzanavaras (Eds.), *Reviews in Pharmaceutical and Biomedical Analysis* (pp. 1-19): Bentham Science Publishers Ltd.
- Petritz, B. A., Almeida, J. A., Gomes, C. P., Pereira, R. W., Murad, A. M., & Franco, O. L. (2015). NanoUPLC/MS(E) proteomic analysis reveals modulation on left ventricle proteome from hypertensive rats after exercise training. *J Proteomics*, 113, 351-365. doi: 10.1016/j.jprot.2014.10.010
- Ramautar, R., Mayboroda, O. A., Derks, R. J., van Nieuwkoop, C., van Dissel, J. T., Somsen, G. W., . . . de Jong, G. J. (2008). Capillary electrophoresis-time of flight-mass spectrometry using noncovalently bilayer-coated capillaries for the analysis of amino acids in human urine. *Electrophoresis*, 29(12), 2714-2722. doi: 10.1002/elps.200700929
- Sakamoto, J. H., van de Ven, A. L., Godin, B., Blanco, E., Serda, R. E., Grattoni, A., . . . Ferrari, M. (2010). Enabling individualized therapy through nanotechnology. [10.1016/j.phrs.2009.12.011]. *Pharmacol Res*, 62(2), 57-89. doi: papers3://publication/doi/10.1016/j.phrs.2009.12.011
- Sangaraju, D., Goggin, M., Walker, V., Swenberg, J., & Tretyakova, N. (2012). NanoHPLC-nanoESI(+)-MS/MS quantitation of bis-N7-guanine DNA-DNA cross-links in tissues

- of B6C3F1 mice exposed to subppm levels of 1,3-butadiene. *Anal Chem*, 84(3), 1732-1739. doi: 10.1021/ac203079c
- Schiavo, S., Ebbel, E., Sharma, S., Matson, W., Kristal, B. S., Hersch, S., & Vouros, P. (2008). Metabolite identification using a nanoelectrospray LC-EC-array-MS integrated system. *Anal Chem*, 80(15), 5912-5923. doi: 10.1021/ac800507y
- Trygg, J., Holmes, E., & Lundstedt, T. (2007). Chemometrics in metabonomics. *J Proteome Res*, 6(2), 469-479. doi: 10.1021/pr060594q
- van den Berg, R. A., Hoefsloot, H. C., Westerhuis, J. A., Smilde, A. K., & van der Werf, M. J. (2006). Centering, scaling, and transformations: improving the biological information content of metabolomics data. *BMC Genomics*, 7, 142. doi: 10.1186/1471-2164-7-142
- Vicario, A., Sergo, V., Toffoli, G., & Bonifacio, A. (2015). Surface-enhanced Raman spectroscopy of the anti-cancer drug irinotecan in presence of human serum albumin. *Colloids Surf B Biointerfaces*, 127C, 41-46. doi: 10.1016/j.colsurfb.2015.01.023
- Wang, J. (2005). Nanomaterial-based electrochemical biosensors. [10.1039/B414248A]. *Analyt*, 130(4), 421-426. doi: 10.1039/B414248A
- Ward, J. L., Baker, J. M., & Beale, M. H. (2007). Recent applications of NMR spectroscopy in plant metabolomics. *FEBS J*, 274(5), 1126-1131. doi: 10.1111/j.1742-4658.2007.05675.x
- Weinhold, A., Wielsch, N., Svato, A., & Baldwin, I. T. (2015). Label-free nanoUPLC-MS E based quantification of antimicrobial peptides from the leaf apoplast of *Nicotiana attenuata*. *BMC Plant Biol*, 15(1), 18. doi: 10.1186/s12870-014-0398-9
- Wold, S. (1991). Chemometrics, why, what and where to next? *J Pharm Biomed Anal*, 9(8), 589-596.
- Worley, B., & Powers, R. (2013). Multivariate analysis in metabolomics. *Current Metabolomics*, 1(1), 92-107.
- Xu, E. Y., Schaefer, W. H., & Xu, Q. (2009). Metabolomics in pharmaceutical research and development: metabolites, mechanisms and pathways. *Curr Opin Drug Discov Devel*, 12(1), 40-52.

**Section II - A metabolomic and  
pharmacokinetic study on Cyanidin-3-  
glucoside**

# **Chapter 4. Short-term pharmacokinetic of Cyanidin-3-glucoside (C3G)**

## **Chapter Overview**

Chapter 4 presents the relationship between plasma C3G values and C3G amounts in the rat brain in the very early phase (i.e. 0-20 min) after C3G administration. We also studied fast-forming derivatives of C3G to better describe the short-term changes. From the kinetic perspective, we showed that C3G is rapidly distributed into the brain. Since both metabolism and excretion of C3G and its derivatives affect the brain pharmacokinetics, the liver and kidney extracts were analyzed in a similar manner. The study design enabled us to calculate a set of Mean Time (MT) parameters that are useful indicators of the retention properties of C3G in peripheral tissues.



## Experimental section

### Materials

All the chromatographic solvents were HPLC grade or LC-MS grade for the MS experiments. Acetonitrile, acetone, methanol p-cumaric acid and formic acid were purchased from Sigma Aldrich (Milan, Italy). Isotopically labelled compounds, rosmarinic acid-d7 and cinnamic acid-d5, were purchased from C/D/N Isotopes Inc. (Quebec, Canada). Pure anthocyanins were obtained from Polyphenol Laboratories AS (Sandnes, Norway) and Heparin from Schwarz Pharma (Milan, Italy). All chemicals were used without further purification. Ultra pure Milli-Q water (Merck Millipore, Billerica, MA, USA) was used for the preparation of all solutions. Phosphate buffered saline (PBS) was prepared as following: 6.03 mM  $\text{Na}_2\text{HPO}_4$ , 3.91 mM  $\text{NaH}_2\text{PO}_4$  and 139 mM NaCl (Carlo Erba, Milan, Italy) were dissolved in MilliQ water (Millipore) and pH was adjusted to 7.4 with HCl.

### Study design and protocol

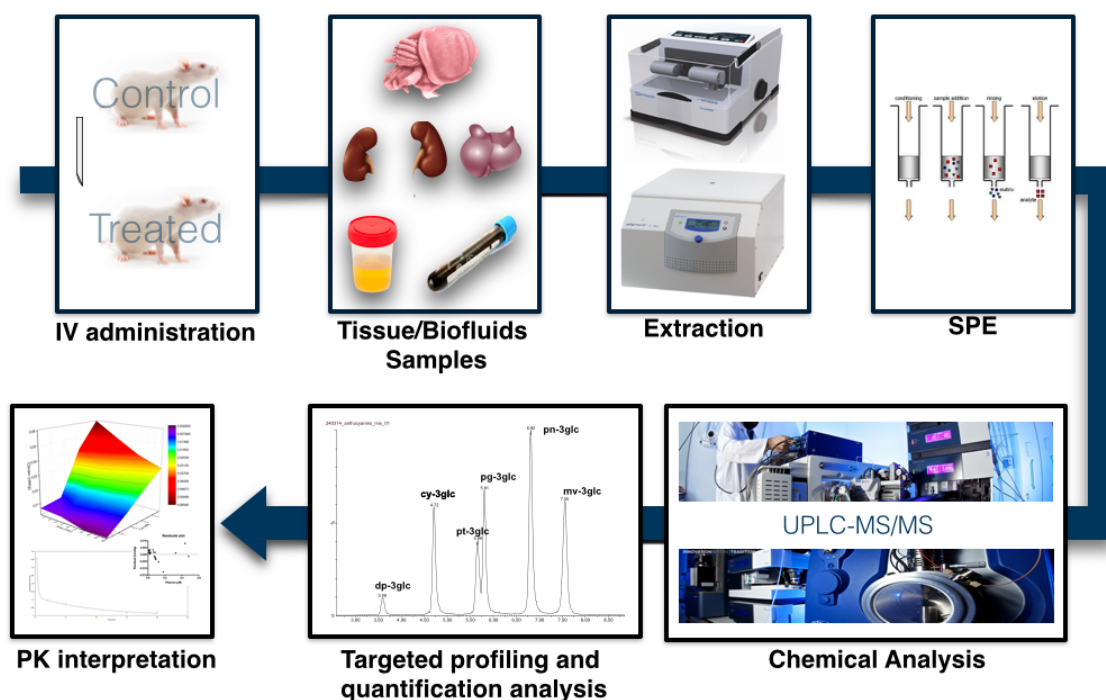


Figure 4.1 Experimental design and targeted analytical workflow.

The experiment was designed as a one-component pharmacokinetic study with quantitative analysis of the target metabolites in selected organs (liver, kidney and brain) and biofluids (plasma and urine), (see Figure 4.1). The principal aim of this study was to characterize the presence of C3G in the anaesthetized rat brain. The three main questions posed were: i) is there any relationship between [C3G] in the blood and in the brain?; ii) what is the time needed for C3G to distribute in the brain?; iii) for how long is biologically meaningful C3G concentration maintained in the brain? To address these questions, C3G was administered intravenously, so as to prevent inter-individual variability in gastrointestinal absorption.

Twenty-two male Wistar rats (*Rattus Norvegicus*, Harlan Italy S.r.l.), of same age (15 weeks), 293-390 g of body weight, were used. The rats were randomly divided into 5 groups, according to the time that elapsed after intravenous administration of the test compound, and one control group. Each time point was represented by four biological replicates. All animals were allowed to acclimate to the animal facility of the University of Trieste for at least 2 week before studies were initiated. The experimental design was vetted and approved by the bioethical committee of the University of Trieste (internal code 140PAS14), according to the provisions of the European Community Council Directive (*Directive 2010/63/EU of the European Parliament and of the Council of 22 September 2010 on the protection of animals used for scientific purposes*, 2010). The animals (n=22) were maintained in cages in a room at  $23 \pm 2^{\circ}\text{C}$ , 50-60% humidity with a 12-hour light-dark cycle. The night before the experiment, food was withdrawn from the cages but water was given *ad libitum*. On the day of the experiment, the rats were anesthetized with intra-peritoneal administration of tiletamine/zolazepam (1:1, 25 mg/kg body weight) and xylazine (10 mg/kg body weight). During anesthesia (10 min in all cases), the heart and ventilation rate were monitored. The rats were placed on their backs, with the ventral side up and with the legs spread separately on a thermo-isolated support. The penis was extruded by sliding the prepuce downwards. The dorsal penis vein was then seen along both sides of the penis and exactly 10 min after anesthesia 0.2 mL PBS without (control group) or with (treated group) 668 nmol cyanidin 3-glucoside (C3G) in PBS was injected using a 24-G hypodermic needle. Then the injection site was pressed with a swab for a few seconds, and the glans was encouraged to retract to prevent further bleeding (Waynforth & Flecknell, 1992). One min before sacrificing the rats, sodium heparin (0.1 ml, 500 IU) was injected again into the dorsal penis vein, exposed in the same way. Exactly 10 min after anesthesia and the corresponding time point after I.V. administration (0.25, 5, 10, 15, 20 min), the rats were sacrificed by decapitation. Blood

draining and excision of the organs were carried out according to the literature (Andreja Vanzo et al., 2011). Urine was collected through the urinary bladder with a syringe. Kidneys, liver and brain were washed with mQ water, immediately frozen in liquid nitrogen and stored at -80 °C.

### **Organ collection and extract preparation**

Immediately after sampling, 5 mL of blood were transferred into ice-cold (-20 °C), deoxygenated aqueous 95 % methanol in a ratio 1:9 (v/v). The urine was weighted and transferred into ice-cold, deoxygenated aqueous 95 % methanol at a ratio of 1:9 (w/v). Frozen kidneys, liver and brain were grounded under cryogenic conditions (-196° C) to 5 µm particles in a CryoMill (Retsch, Germany), using a single 25 mm i. d. steel ball (30 seconds, 25/sec frequency). The pulverized tissue was rapidly transferred (without thawing) into ice-cold, deoxygenated aqueous 95 % methanol at a ratio of 1:9 (w/v). Cinnamic acid-d<sub>5</sub>, as internal standard, was dissolved in the aqueous methanol at concentration of 0.1 mg/L for the monitoring of the extraction protocol in biofluids and tissues.

All samples were extracted with an orbital shaker for 10 min at room temperature. The methanol extracts were then centrifuged for 5 min at 3600 rpm at 4 °C, decanted under a stream of nitrogen in 50 mL dark glass vessels and stored at -80 °C.

Clean-up of extracted samples in methanol was performed by solid phase extraction (SPE), as previously described (Passamonti et al., 2003). Briefly, 5 mL of extracted samples were evaporated on a rotary evaporator and reconstituted in 10 mL of acidified water. Anthocyanins were extracted by solid-phase adsorption onto a hydrophobic matrix (Sep-Pak C18, 0.35 g, Waters, Milford, MA). Anthocyanins were eluted with methanol, evaporated to dryness and immediately dissolved with 500 µL of methanol:water (50:50). Rosmarinic acid, as internal standard at 1 mg/L, was added in the aqueous methanol for allowing the adjustment of quantitative recovery after sample reconstitution. Samples were filtered through a 0.22 µm PVDF filter (Millipore, Bedford, MA) into HPLC vials for the subsequent quantitative analysis.

### **Quantitative analysis**

C3G and its derivatives were quantitatively analyzed by an ultra performance LC (UPLC)

system coupled to a triple quadrupole (TQ) mass spectrometer.

The UPLC-MS/MS method was chosen to take advantage of the selectivity and sensitivity combined to wide dynamic range of MRM detection in tandem spectrometry, thus allowing the simultaneous quantitation of the main expected metabolites throughout the experiment. A Waters Acquity UPLC (Waters, Manchester, UK) controlled by MassLynx 4.1 was used. Separation of the target metabolites and 2 deuterated internal standards was performed on a reversed phase (RP) ACQUITY UPLC 1.8  $\mu\text{m}$  2.1 x 100 mm HSS T3 column (Waters) protected with an Acquity UPLC BEH HSS T3 1.8  $\mu\text{m}$ , 2.1 x 5 mm precolumn (Waters), at 40° C and under a mobile phase flow rate of 0.28 mL/min. Mobile phases of 0.1% formic acid in Milli-Q water (A) and 0.1% formic acid in acetonitrile (B) were used. Chromatographic separation was performed using a multistep linear gradient as follows: 0 min, 5% B; 0-3 min, 5%-20% B; 3-4.30 min; 20% B; 4.30-9 min, 20%-45% B, 9-11 min, 45%-100% B, 11-14 min, 100%; and 14.01-17 min, 5% as equilibration time. Injection volume was 10  $\mu\text{L}$ , and the samples were kept at 4 1/4C throughout the analysis.

The TQ mass spectrometer used was a Waters Xevo TQ (Milford, Massachusetts, USA) coupled with an electrospray interface. Quantification and confirmation of the anthocyanins were performed using two MRM (multiple reaction monitoring) transition for each compound, using the conditions previously reported (Andreja Vanzo et al., 2011). The first transition, corresponding to the most abundant fragment, was used as quantifier ion, and the second as qualifier ion. For calibration, standard anthocyanins were serially diluted in aqueous methanol (50:50), in a concentration range 0.01  $\mu\text{g/L}$  - 100 mg/L. The range of calibration curves was obtained on the basis of the linearity of the responses. Acceptable linearity was achieved when the coefficient of calibration curves ( $R^2$ ) was at least 0.99. Quantitative data were processed with Targetlynx software (Masslynx, Waters). C3G and its derivatives were quantified with the appropriated standard reference with the exception of isoPN3G, expressed as equivalent of PN3G.

### **Recovery and residual blood correction**

According to the published method (Andreja Vanzo et al., 2011), the amounts in each matrix were calculated by taking into consideration the appropriate recovery, and by assuming that rat plasma volume is 3.375  $\mu\text{L/g}$  of rat weight (International Life Sciences Institute, 1994). The correction for the residual blood in the brain was performed as proposed in (Fridén et al.,

2010), by subtracting the estimated amount of C3G, PNG and PT3G in the effective plasma space.

### **Pharmacokinetics analysis**

Pharmacokinetic parameters of I.V. administration of C3G in rats were determined from the mean (n=4) plasma concentration–time data by both non-compartmental and compartmental analysis as implemented in PK-Solver (version 2.0) (Zhang et al., 2010). The statistical and graphical analyses were accomplished using the software package Prism version 6.0 (GraphPad Software Inc., San Diego, Calif., USA) and Origin 2015 (OriginLab).

### **Non-compartmental analysis (NCA)**

Non-compartmental analysis (NCA) is a standard technique of PK analysis. NCA is easier to apply and relies on fewer assumptions than compartmental modeling. Standard NCA assumes linear PK, i.e. all transport processes are assumed to follow first-order kinetics (P Veng-Pedersen, 2001), and does not provide a mechanistic description.

For NCA, the area under the concentration-time (AUC) curve was calculated using log/linear trapezoidal method from time 0 to the last sampling point 20 min after administration. This means that linear interpolation is used for ascending parts of the curve and logarithmic interpolation is used for descending parts of the curve. Plasma concentrations are assumed to decline mono-exponentially between two measured concentrations for the descending part of the curve. The PK parameters determined were the concentration at time 0 ( $C_0$ ), the terminal elimination rate constant ( $\lambda_z$ ), the terminal elimination half-life ( $t_{1/2}$ ), the apparent volume of distribution at terminal phase ( $V_z$ ), the relative volume of distribution at steady state ( $V_{ss}$ ), and the total body clearance (CL).

The mean time (MT) parameters dealing with the tissue distribution of C3G were calculated from the moments of the concentration-time curve in plasma and specific target tissues, as described (McNamara et al., 1987; P. Veng-Pedersen, 1989). Briefly, Mean residence time (MRT) is the time that a molecule stays in the body, excluding the gastrointestinal tract. MRT was calculated as the ratio of the area under the first moment concentration time curve (AUMC) divided by the area under the zero moment curve (AUC). The terminal elimination half-life ( $t_{1/2}$ ) and AUC respective to C3G derivatives were also calculated to determine exposure to any derivatives compared with the parent compound. Maximum plasma

concentrations ( $C_{MAX}$ ), and their times of maximal occurrence ( $T_{MAX}$ ) were taken directly from the observed data.

### Two-Compartment Model Analysis (TCMA)

Mean concentrations of C3G in plasma versus time were further analyzed by a two-compartment, mammillary open, IV bolus model, with first order elimination (Figure 2).

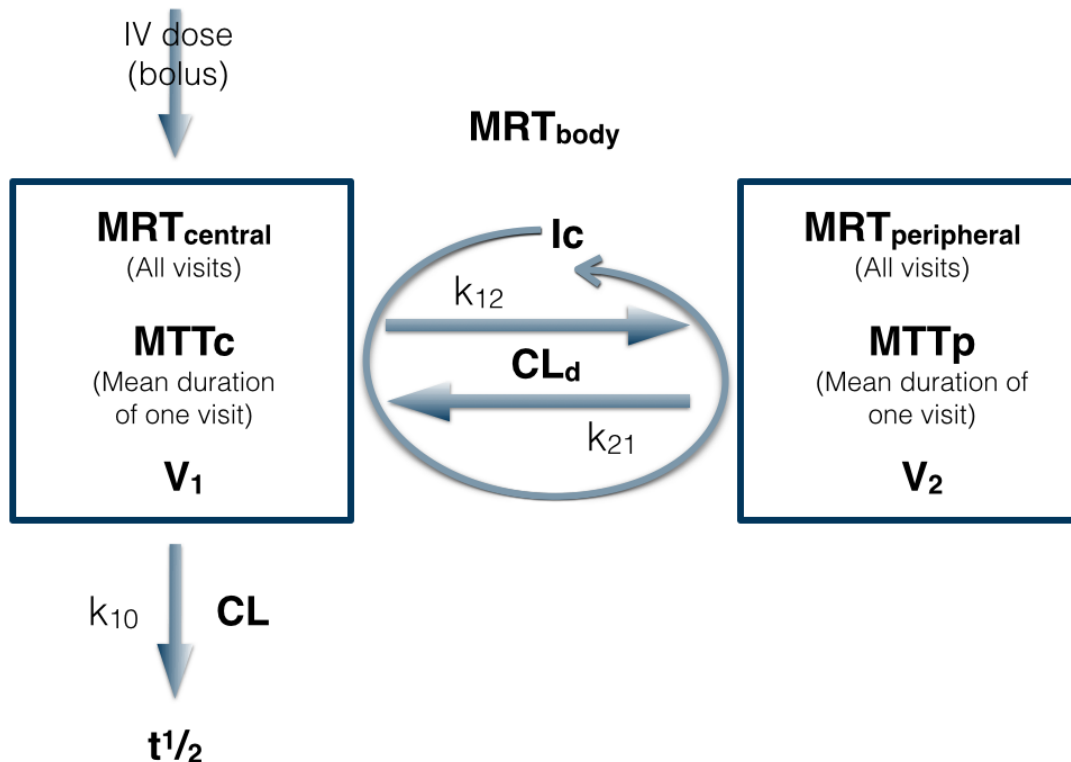


**Figure 4.2 Hybrid 2 compartment model.** The information contained in the plasma concentration versus time profile can be used to describe the disposition of the drug in the body, in terms of mean times spent in the different compartments ( $MRT_{central}$  and  $MRT_{peripheral}$ ), number of visits ( $I_c$ ) in these compartments and mean duration of one visit ( $MTT$ ).

Here, the two-compartment model is envisioned with a central compartment, which includes the plasma vascular space (circulation), and a peripheral compartment, which corresponds to some extravascular "tissue" space. Total body clearance ( $CL$ ) accounts for irreversible removal of drug from the plasma or central compartment (volume  $V_1$ ), while distribution clearance ( $CL_D$ ) effects C3G uptake and removal from the peripheral compartment ( $V_2$ ) by flow/permeability mechanisms. Under these conditions, the representative equations for the

drug concentrations in blood or plasma ( $C_p$ ) and in peripheral space ( $C_t$ ) after an IV bolus dose into the central compartment are:

$$C_{p(t)} = Ae^{-\alpha t} + Be^{-\beta t}$$

and

$$C_{t(t)} = C(e^{-\alpha t} - e^{-\beta t})$$

where  $C_{p(t)}$  and  $C_{t(t)}$  are the concentrations of C3G in the two compartments at time  $t$ ;  $\alpha$  and  $\beta$  are the Eigen values, macro-constants characterized by the first-order rate constants for C3G transfer out of and into the central compartment,  $k_{12}$  and  $k_{21}$ , respectively, and the first-order rate constant for drug elimination from the central compartment,  $k_{10}$ .

$$\alpha = \frac{(k_{10} + k_{12} + k_{21}) + \{(k_{10} + k_{12} + k_{21})^2 - 4k_{10} \cdot k_{21}\}^{\frac{1}{2}}}{2}$$

$$\beta = \frac{(k_{10} + k_{12} + k_{21}) - \{(k_{10} + k_{12} + k_{21})^2 - 4k_{10} \cdot k_{21}\}^{\frac{1}{2}}}{2}$$

and  $A$ ,  $B$  and  $C$  are pre-exponential factors defined in terms of the dose ( $D$ ),  $V_1$ , and  $k_{21}$ ,

$$A = \frac{D}{V_1} \cdot \frac{(k_{21} - \alpha)}{(\beta - \alpha)}$$

$$B = \frac{D}{V_1} \cdot \frac{(k_{21} - \beta)}{(\alpha - \beta)}$$

$$C = \frac{D}{V_1} \cdot \frac{k_{21}}{(\alpha - \beta)}$$

Since plasma concentrations often span a wide range, it is useful to employ a weighting procedure for the raw data that allows to fit low concentrations and high concentrations simultaneously. Data for model fitting were iteratively reweighted by modulating the reciprocal of the squared predicted concentrations ( $1/C_{pre}^2$ ). The goodness-of-fit was assessed by visual inspection of the residual plots, parameter estimation precision, correlation ( $R^2$ ) between the observed and predicted concentration values, weighted sum of squared residuals (WSS), Akaike's information criterion (AIC), and Schwarz criteria (SC). The lower the WSS, AIC, and SC, the more appropriate is the selected model (Figure 3).

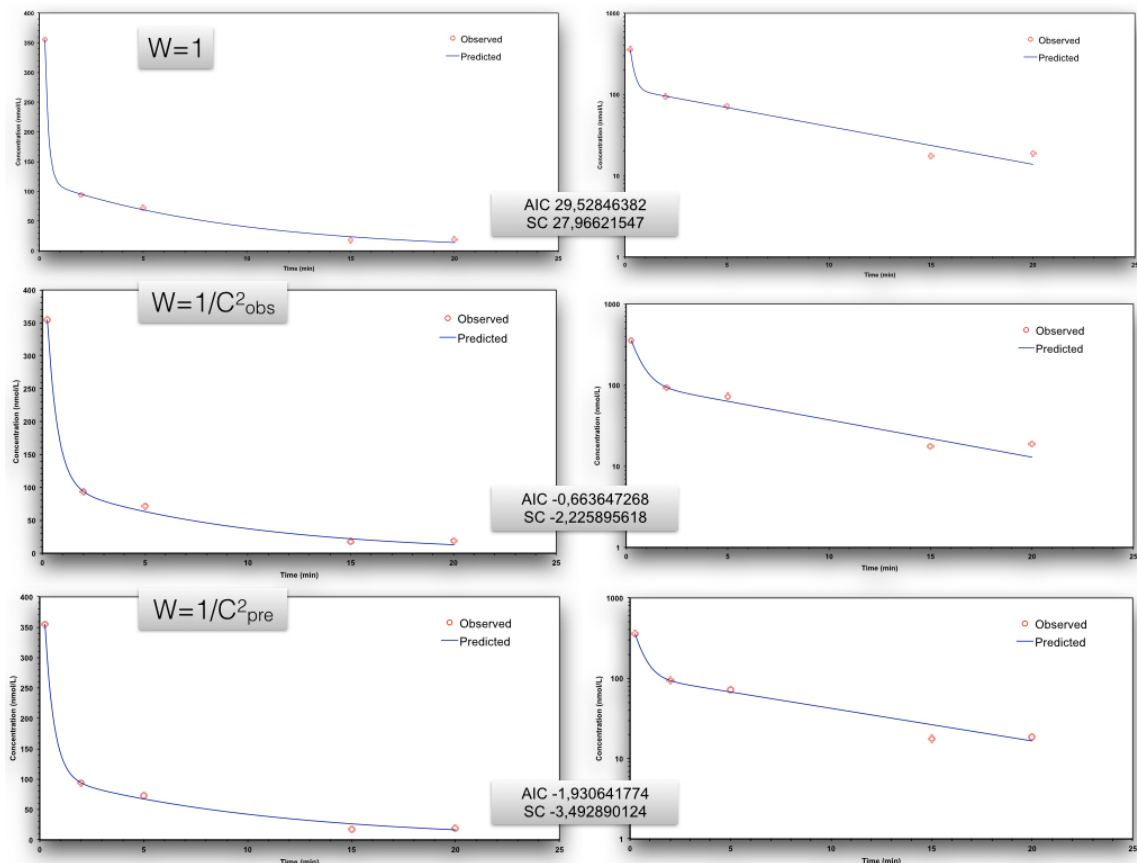


**Figure 4.3 Comparison between different weightings schemes.**

In addition, the information contained in the plasma concentration versus time profile were used to describe the disposition of the drug in the body, in terms of mean times spent in the different compartments (MRT<sub>central</sub> and MRT<sub>peripheral</sub>), number of visits (I<sub>c</sub>) in these compartments and mean duration of one visit (MTTC), according to the methods proposed by Kong and Jusko (Kong & Jusko, 1988).



## Results and discussion

Table 1 reports the concentrations of C3G and other anthocyanins measured in plasma of anaesthetized rats over a period of 0-20 min after I.V. administration of 668 nmol C3G. In accordance with previous PK studies, the elimination of C3G from plasma appeared to follow a first-order kinetics. The disappearance of C3G was very fast, its biotransformation was rapid and substantial, allowing for the quick appearance of some derivatives in the circulation. D3G appeared transiently in plasma only at 2 min. PT3G was detected in plasma only in trace amounts within the first 5 min. No aglycones or conjugated derivatives were detected.

Table 2 reports the concentrations of C3G and other anthocyanins measured in the brain, the liver and the kidneys. C3G distribution and methylation to PN3G were very rapid in these tissues, where PT3G was also found. The amounts recovered in the urine are reported in Table 3. Rat urine showed relatively high amounts of C3G and major metabolites. As much as 15% of the injected dose was recovered 5 min after the injection.

A noteworthy feature is the high rate of C3G disappearance following I.V. administration, thereby making it an analytical challenge to detect plasma C3G at sufficient amounts for its PK parameters to be determined.

**Table 4.1 Mean plasma concentrations (nM) of C3G and its derivatives in Wistar rats following intravenous administration of 668 nmol of C3G. Results are expressed as mean  $\pm$  SEM (n=4).**

Time (min)	C3G	PN3G	PT3G	D3G	M3G	PG3G	TOT
0.25	354.84 $\pm$ 54.19	33.68 $\pm$ 5.51	2.20 $\pm$ 1.05	nd	9.13 $\pm$ 3.46	4.50 $\pm$ 0.62	404.34 $\pm$ 64.83
2	93.80 $\pm$ 9.01	13.05 $\pm$ 2.35	4.95 $\pm$ 3.16	12.81 $\pm$ 10.46	95.83 $\pm$ 61.71	1.89 $\pm$ 0.17	222.33 $\pm$ 86.86
5	72.19 $\pm$ 5.47	12.31 $\pm$ 1.37	1.71 $\pm$ 1.39	nd	16.45 $\pm$ 13.08	2.01 $\pm$ 0.28	104.67 $\pm$ 21.58
15	17.50 $\pm$ 2.04	3.73 $\pm$ 0.94	nd	nd	3.67 $\pm$ 0.14	1.90 $\pm$ 0.19	26.80 $\pm$ 3.31
20	18.78 $\pm$ 4.06	3.40 $\pm$ 0.22	nd	nd	8.60 $\pm$ 3.88	1.55 $\pm$ 0.13	32.33 $\pm$ 8.29
<b>AUC<sub>0-20</sub></b> (nM min)	1165.23	174.77	nsd	nsd	343.45	40.41	1825.57
<b>Half life</b> (min)	6.90	8.16	nsd	nsd	5.29	44.67	5.36

<sup>nd</sup> Not detected; <sup>nsd</sup> data not sufficient to estimate the terminal slope; AUC<sub>0-20</sub>, Area Under the Curve from 0 to 20 min; t<sub>1/2</sub>, Half-life; C3G, cyanidin-3-O-glucoside; D3G, delphinidin-3-O-glucoside; PN3G, peonidin-3-O-glucoside; PT3G, Petunidin-3-O-glucoside; M3G, malvidin-3-O-glucoside; PG3G, Pelargonidin-3-O-glucoside.

**Table 4.2. Mean concentrations of C3G and its derivatives in liver, kidneys and brain of Wistar rats following intravenous administration of 668 nmol of C3G. Concentrations are expressed as mean  $\pm$  SEM (n=4).**

	<b>Time</b> (min)	<b>C3G</b> (pmol/g)	<b>PN3G</b> (pmol/g)	<b>PT3G</b> (pmol/g)	<b>isoPN3G</b> (pmol/g)
<b>Liver</b>	0.25	56.61 $\pm$ 11.79	539.38 $\pm$ 71.33	1.23 $\pm$ 0.59	13.86 $\pm$ 4.32
	2	19.22 $\pm$ 1.99	317.61 $\pm$ 35.86	2.42 $\pm$ 0.08	6.19 $\pm$ 2.09
	5	20.91 $\pm$ 2.61	364.74 $\pm$ 44.85	1.09 $\pm$ 0.52	15.85 $\pm$ 1.82
	15	11.02 $\pm$ 2.24	216.10 $\pm$ 36.06	1.60 $\pm$ 0.44	1.39 $\pm$ 1.14
	20	5.54 $\pm$ 0.33	100.84 $\pm$ 6.33	3.06 $\pm$ 0.19	0.64 $\pm$ 0.25
	<b>AUC<sub>0-t</sub></b> (pmol/g min)		345.29	5610.12	33.85
<b>Half-life</b> (min)		8.15	9.99	nsd	3.18
<b>MTT<sub>L</sub></b> (min)		1.43	3.93	nsd	N/A
	<b>Time</b> (min)	<b>C3G</b> (nmol/g)	<b>PN3G</b> (nmol/g)	<b>PT3G</b> (pmol/g)	
<b>Kidney</b>	0.25	1.69 $\pm$ 0.47	1.99 $\pm$ 0.55	2.04 $\pm$ 0.59	
	2	1.40 $\pm$ 0.16	1.56 $\pm$ 0.18	2.82 $\pm$ 0.28	
	5	0.58 $\pm$ 0.08	0.85 $\pm$ 0.08	2.40 $\pm$ 0.13	
	15	0.57 $\pm$ 0.17	0.89 $\pm$ 0.22	2.29 $\pm$ 0.07	
	20	0.44 $\pm$ 0.04	0.90 $\pm$ 0.14	2.53 $\pm$ 0.26	
	<b>AUC<sub>0-t</sub></b> (nmol/g min)		14.32	20.36	48.13*
<b>Half-life</b> (min)		11.66	20.80	135.08	
<b>MTT<sub>K</sub></b> (min)		8.54	23.11	187.44	
	<b>Time</b> (min)	<b>C3G</b> (pmol/g)	<b>PN3G</b> (pmol/g)	<b>PT3G</b> (pmol/g)	
<b>Brain</b>	0.25	40.46 $\pm$ 9.67	nd	nd	
	2	7.48 $\pm$ 0.79	2.07 $\pm$ 1.18	1.15 $\pm$ 0.62	
	5	7.05 $\pm$ 0.55	0.70 $\pm$ 0.30	1.01 $\pm$ 0.46	
	15	2.18 $\pm$ 0.58	0.40 $\pm$ 0.38	2.45 $\pm$ 0.22	
	20	2.21 $\pm$ 0.44	0.37 $\pm$ 0.13	1.90 $\pm$ 0.60	
	<b>AUC<sub>0-t</sub></b> (pmol/g min)		119.89	17.10	32.42
<b>Half-life</b> (min)		8.80	15.57	nsd	
<b>MTT<sub>B</sub></b> (min)		0.43	8.61	nsd	

\* pmol min g<sup>-1</sup> L<sup>-1</sup>; N/A Not applicable; nd, not detected; nsd data not sufficient to estimate the terminal slope; AUC<sub>0-inf</sub>, Area under curve; MTT<sub>B</sub>, Mean Transit Time in the brain; MTT<sub>K</sub>, Mean Transit time in kidneys; MTT<sub>L</sub>, Mean Transit Time in the liver.

### **Plasma Pharmacokinetics of C3G**

The plasma PK parameters, calculated by both non-compartmental and two compartment model analysis, are reported in Table 4. Notably, half-life ( $t^{1/2}$ ), volume of distribution at steady state ( $V_{ss}$ ) and total body clearance (CL) were similar if calculated by either method. The plasma concentrations of C3G at time zero ( $C_0$ ) were 550 or 429 nM, if calculated by either compartmental or non-compartmental analysis, respectively. The results allow several novel insights into C3G distribution and metabolism, and they also corroborate findings previously made in the same (Andreja Vanzo et al., 2011) or in other rodent species (Marczylo et al., 2009).

The mean half-life of C3G was less than 8 min, meaning that ca. 10% of the residual amount of C3G was eliminated per min. Accordingly, we can estimate that the time window needed to accurately describe complete elimination is no more than 1 hour (considering the general rule of a thumb for a complete elimination in 5-6 half-lives, which is in our case 40-50 min).

At the steady state, the volume of distribution of C3G was 4.58 L, which is much greater than total body water (Brown et al., 1997), suggesting that C3G is extensively distributed in tissues. As a consequence, the plasma concentration cannot be used as a proxy for predicting the concentration in tissues, with the possible exception of brain, as discussed below.

It is noteworthy that the total body clearance of C3G was 0.49 L/min, a figure that is significantly higher than the cardiac output (0.10 L/min). Therefore, blood-flow independent elimination can be assumed, e.g. by rapid degradation to undetectable products or by direct metabolism occurring in the blood (plasma, red blood cells, and/or endothelial surface). Indeed, anthocyanins can undergo both spontaneous and enzyme-catalyzed decomposition to a phenolic acid and the unstable phloroglucinol aldehyde (2,4,6-trihydroxybenzaldehyde), (Fleschhut et al., 2006).

### **Non-Compartmental Analysis**

According to NCA, the calculated maximum plasma concentration of C3G ( $C_0$ ) was 429 nM at time 0, the terminal elimination rate constant  $\lambda_z$  was  $0.1 \text{ min}^{-1}$  and the terminal elimination half-life ( $t^{1/2}$ ) was 6.9 min. The mean residence time (MRT) was 8.72 min, the apparent volume of distribution at terminal phase ( $V_z$ ) was 4.92 L, the relative volume of distribution at steady state ( $V_{ss}$ ) was 4.31 L, and the total body clearance (CL) was 0.49 L/min.

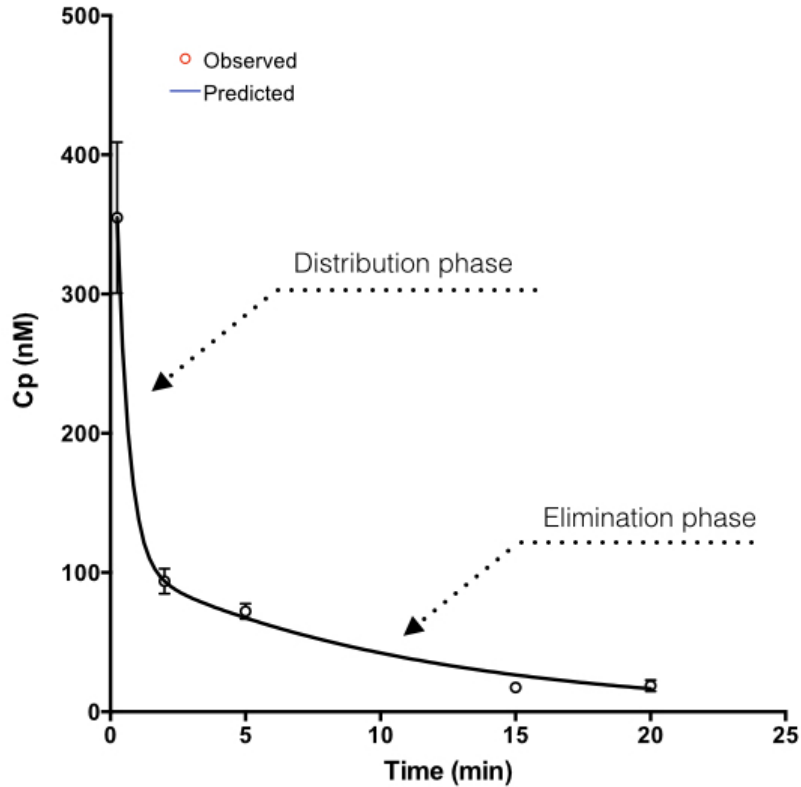


Figure 4.4 Two-compartment model fitting to the C3G plasma concentration-time profile in Wistar rats following intravenous administration of 668 nmol of C3G ( $R^2 = 0.9992$ ; WSS = 0.14; AIC = -1.93; SC = -3.49). Concentrations are expressed as mean  $\pm$  SEM (n=4).

### Two-compartment model analysis

The disappearance of C3G from plasma could be also fitted to a two-compartment, mammillary open model, with first order elimination ( $R^2 = 0.9992$ ; WSS = 0.14; AIC = -1.93; SC = -3.49), as shown in Figure 4: a very rapid decline in the first 2 min (distribution phase) that was followed by a slower declining phase (elimination phase).

The physiological parameters resulting from this model were: i) the volume in the central compartment ( $V_1$ , 1.21 L) ii) the volume in the peripheral compartment ( $V_2$ , 3.36 L, suggesting that the major fraction resided in the peripheral compartment), iii) the distribution half-life ( $t^{1/2}_d$ , 0.30 min, suggesting that after 18 s, half of the compound had been already cleared from the plasma. In other words, it takes ca. 8 seconds for distribution to go to 50% completion and between 25 to 42 seconds for distribution to go to completion), iii) the elimination half-life ( $t^{1/2}_e$ , 7.41 min, so that during the terminal phase of elimination ca. 10% of the residual amount of C3G is eliminated per min), iv) the total body clearance (CL, 0.49 L/min), v) the distribution clearance ( $CL_d$ , 1.76 L/min) and vi) the volume of distribution at steady state ( $V_{ss}$ , 4.58 L).

When distribution equilibrium is achieved, 0.24% of C3G is present in plasma and 99.76% is distributed outside plasma. A diagram of this model is shown in Figure 5.

**Table 4.3. Pharmacokinetic parameters of intravenous administration of 668 nmol of C3G in Wistar rats.**

Non-compartmental analysis		Two-compartment model analysis			
Parameter	Value	Parameter	Value	Parameter	Value
$\lambda_z$ (min <sup>-1</sup> )	0.10	a (nM)	442.79	b (nM)	107.68
T <sub>max</sub> (min)	0.25	$\alpha$ (min <sup>-1</sup> )	2.29	$\beta$ (min <sup>-1</sup> )	0.09
C <sub>max</sub> (nM)	354.84				
C <sub>0</sub> (nM)	429.12	k <sub>10</sub> (min <sup>-1</sup> )	0.41	Cl <sub>d</sub> (L/min)	1.76
AUC <sub>0-inf</sub> (nM*min)	1352.14	k <sub>12</sub> (min <sup>-1</sup> )	1.45	Cl <sub>d</sub> (L/min kg)	5.18
AUMC (nM*min <sup>2</sup> )	11789.96	k <sub>21</sub> (min <sup>-1</sup> )	0.52	CL (L/min)	0.49
MRT (min)	8.72	t <sup>1</sup> / <sub>2d</sub> (min)	0.30	CL (L/min/kg)	1.46
V <sub>z</sub> (L)	4.92	t <sup>1</sup> / <sub>2e</sub> (min)	7.41	AUC <sub>0-inf</sub> (nM*min)	1334.49
CL (L/min)	0.49	C <sub>0</sub> (nM)	550.47	AUMC (nM*min <sup>2</sup> )	12394.67
t <sup>1</sup> / <sub>2</sub> (min)	6.90	V <sub>1</sub> (L)	1.21	MRT (min)	9.22
V <sub>ss</sub> (L)	4.31	V <sub>2</sub> (L)	3.36	MRT <sub>C</sub> (min)	2.44
		V <sub>1</sub> (L/kg)	3.57	MRT <sub>P</sub> (min)	6.78
		V <sub>2</sub> (L/kg)	9.90	MTT (min)	0.54
		V <sub>2</sub> /V <sub>1</sub>	2.77	MTT <sub>P</sub> (min)	1.91
		V <sub>ss</sub> (L)	4.58	I <sub>C</sub>	3.55
		V <sub>ss</sub> (L/kg)	12.62	K <sub>p</sub>	2.77

a, T<sub>0</sub> intercept of distribution kinetics;  $\alpha$ , Exponent of the polyexponential equation (slope factor); AUC<sub>0-inf</sub>, Area under curve out to infinity; AUMC, Area Under the first Moment Curve from time 0 to infinity;  $\beta$ , Exponent of the polyexponential equation (slope factor); b, T<sub>0</sub> intercept of elimination phase; C<sub>0</sub>, back-extrapolated drug concentration following rapid bolus iv administration; CL<sub>d</sub>, Distribution clearance; CL, Total body clearance; C<sub>max</sub>, Maximum observed concentration; I<sub>C</sub>, number of circulations; k<sub>10</sub>, rate constant for elimination of drug from central compartment to outside body; k<sub>12</sub>, rate constant for distribution of drug from central compartment to peripheral compartment; k<sub>21</sub>, rate constant for redistribution of drug from peripheral to central compartment; MRT, Mean residence time; MRT<sub>C</sub>, Mean residence time in the central compartment; MRT<sub>P</sub>, Mean residence time in the peripheral space; MTT, Mean transit time; MTT<sub>P</sub>, Mean Transit Time in the peripheral space; t<sub>max</sub>, Time of occurrence of C<sub>max</sub>; t<sup>1</sup>/<sub>2</sub>, Terminal elimination half-life; t<sup>1</sup>/<sub>2d</sub>, Distribution half-life; t<sup>1</sup>/<sub>2e</sub>, Elimination half-life; V<sub>1</sub>, Volume of central compartment; V<sub>2</sub>, Volume of peripheral compartment; K<sub>p</sub>, partition coefficient over the two compartments; V<sub>ss</sub>, Volume of distribution at steady state;  $\lambda_z$ , First order terminal elimination rate constant.

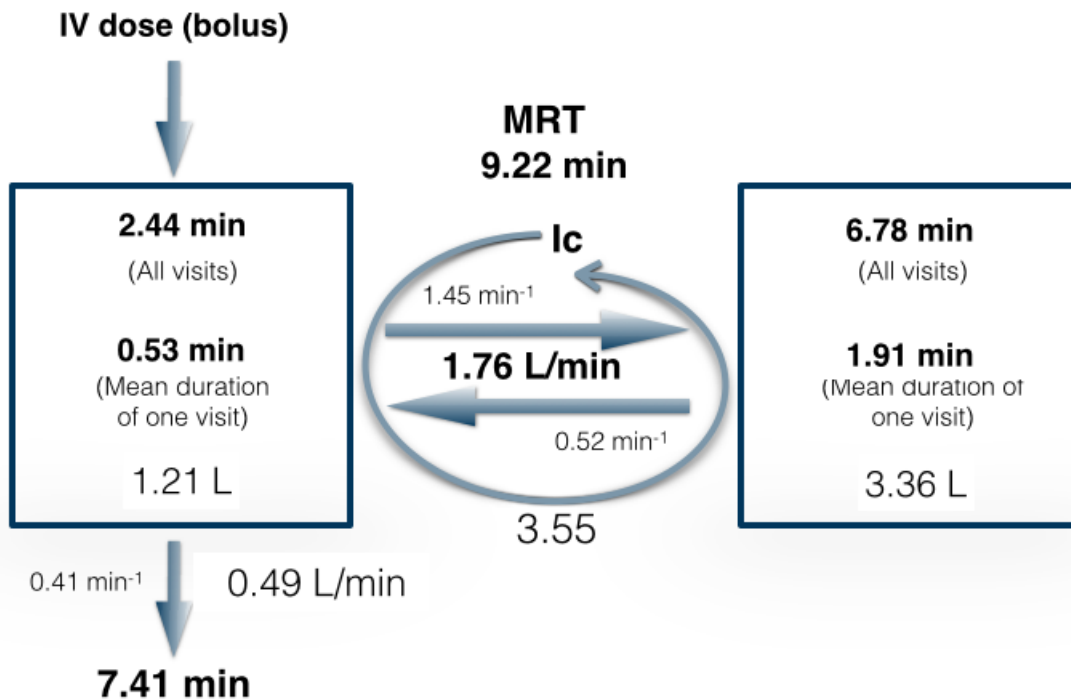


**Figure 4.5 Hybrid 2 compartment model.**

### **Peripheral Bioavailability**

The so-called "*peripheral bioavailability*" of C3G may be evaluated by examining the various mean time (MT) parameters in terms of the tendency of the C3G molecules to distribute into and remain in the peripheral space.

The MT parameters indicate that C3G molecules tend to spend a longer time (73.51 % of its MRT) in the peripheral space than in the central compartment. This speaks in favor of an accumulation pattern for C3G molecules. The mean residence time of C3G in the body (MRT, 9.21 min) is the sum of the mean residence time in the peripheral space (MRT<sub>P</sub>, 6.77 min) and the mean residence time in the central compartment or circulation (MRT<sub>C</sub>, 2.44 min); the partition coefficient between the peripheral and central spaces (K<sub>p</sub>, calculated as MRT<sub>P</sub>/MRT<sub>C</sub>) was 2.77; iii) the mean transient time of C3G molecules in the peripheral space (MTT<sub>P</sub> 0.14 min), which is defined as the mean time needed for C3G molecules to return to the general systemic circulation (central compartment) subsequent to entering the peripheral space; and iv) the number of circulations made by a molecule on average before being eliminated (I<sub>C</sub>, calculated as MRT<sub>P</sub>/ MTT<sub>P</sub>) was 3.56. In other words, while seven molecules are being distributed from the central to peripheral space, two molecules are being eliminated.

### Tissue pharmacokinetics of C3G and its metabolites

The concentrations-time courses of C3G in selected tissues are shown in Figure 6. C3G, PN3G and PT3G could be detected in liver, kidneys and brain (Figure 6 and Table 2).

The amounts of C3G found in tissues were in descending order of kidney (0.44 – 1.69 nmol/g), liver (5.64 – 58.61 pmol/g) and brain (2.41 – 44.11 pmol/g). The AUC values of C3G in the brain and in the liver were similar (345.3 and 119.9 pmol/g min, respectively) and both figures were different from the value of the kidneys (14.3 nmol/g min), as reported in Table 2.

Since this experiment was focused on the distributive phase of the concentration-time profile in both the sampled tissues and plasma, the data enabled us to estimate the Mean Transit Time in each specific tissue (MTTi). Under these experimental conditions, this value is a good descriptor of tissue distribution differences (McNamara et al., 1987). Distribution of C3G

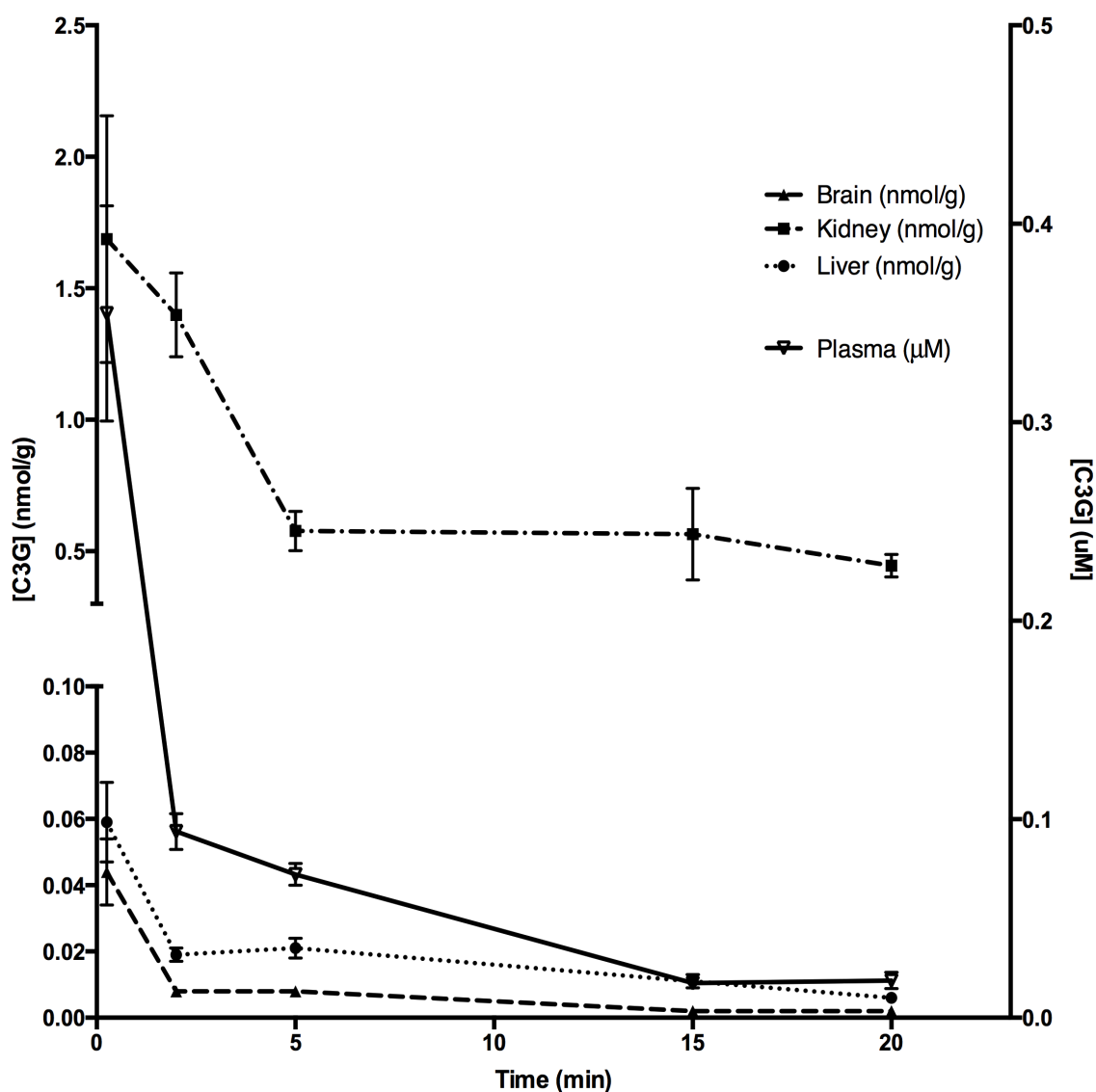


Figure 4.6 Concentrations-time courses of C3G in selected tissues.

occurred most quickly in the brain ( $MTT_b$ , 0.43 min), followed by the liver ( $MTT_l$ , 1.43 min) and then the kidney ( $MTT_k$ , 8.54 min).

The amounts of PN3G recovered in tissues were in descending order of kidney (0.90 – 1.99 nmol/g), liver (100.84 – 539.38 pmol/g) and brain (0.37 – 2.07 pmol/g). The 4' positional isomer isoPN3G was detected here as an expected metabolite, based on a critical re-assessment (Pojer et al., 2013) of previous data obtained by our group. It was here confirmed to be a minor peak, around 2.59% of PN3G, only in the liver. The AUC of PN3G in the kidneys and in the liver was 116.5 times and 32.10 times higher than in plasma, respectively, indicating strong metabolic capacity. For comparison, the AUC in the brain was only 9.78% of that in plasma.

The presence of PN3G in the sampled tissues ( $MTT_l$ , 3.93 min;  $MTT_k$ , 23.11 min;  $MTT_b$ , 8.61 min) was significantly longer than C3G.

### **Significance of C3G in the brain**

At 15 sec after the intravenous administration, C3G concentration in plasma was in the same physiological range, as observed in the post-absorption phase (Tsuda et al., 1999). Under these conditions, the C3G levels reached in the brain were approximately 50 nM (The amounts found in the brain were 2.41 – 44.11 pmol/g.), i.e. a value at which it could interact with biological targets eliciting biological responses.

Shortly after, plasma C3G levels rapidly declined, probably due to the rapid disposition of the injected bolus. However, under conditions that simulate the normal peroral consumption, absorption from the gastro-intestinal compartment lasts longer, so it can be speculated that plasma C3G concentration remains elevated for a longer time, as previously shown (Passamonti et al., 2003; A. Vanzo et al., 2008).

Importantly, the parallel decline of C3G concentrations in the brain and those measured in plasma, as well as the  $MTT_B$  (0.43 min), also suggests no excessive retention of the compound in the brain tissue. Such an extensive distribution of C3G, also in the brain, despite the unfavorable chemical properties of the molecule (hydrophilic molecule) in terms of cell membrane passage, is probably a result of the action of a specific transport mechanism (Kell, 2013). Indeed, C3G has been shown to pass the endothelial cell membrane in a short time frame (<1 min) (Ziberna et al., 2012).



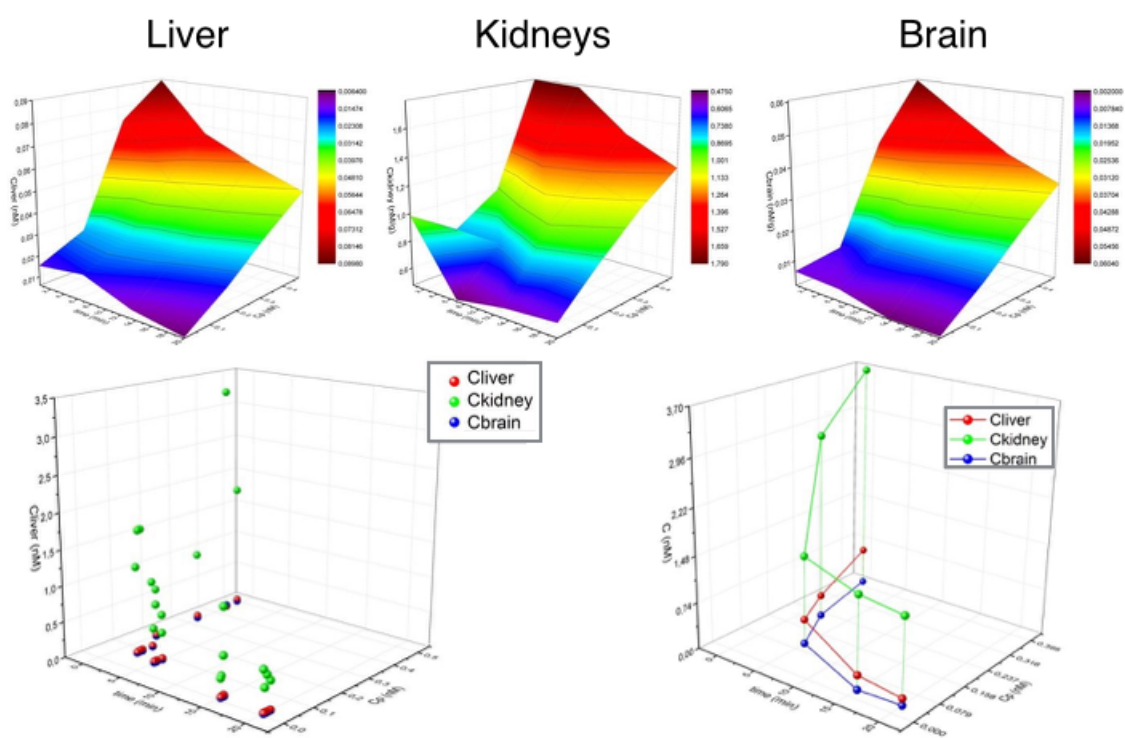


Figure 4.7 The ratio between the total anthocyanins concentration in the studied tissues and the total anthocyanin concentration in plasma, at each time point.

As a result, the levels of C3G in the brain linearly correlated with the plasma values, thus providing a measure of the capacity to maintain brain C3G in equilibrium with C3G in the circulation. Furthermore, our data suggest a relatively low inter-individual variability of the blood-brain barrier permeability with respect to C3G under the chosen experimental conditions. Therefore, it can be suggested that the plasma C3G concentrations are a good indicator of the C3G levels in the brain. This implies that further pharmacokinetic studies might be designed accordingly, e.g. by increasing the number of blood samples taken from a single animal, following C3G administration. In the case of oral administration, notably entailing large inter-individual variability of C3G levels in the circulation, any inter-individual variability in plasma levels of C3G should be accompanied by a corresponding variability in C3G brain levels.

To demonstrate the intactness of the blood-brain barrier under the chosen experimental conditions, we showed that the anthocyanin's profile in the brain (with AUC C3G >PT3G>PN3G, Table 2) was clearly different from that observed in plasma (with AUC

C3G>M3G>PN3G>PG3G, Table 1).

C3G uptake from plasma into the studied organs was also estimated as the sum of anthocyanins detected in tissues versus plasma. We found that this ratio increased over time in all tissues, except in the brain (Figure 7). Indeed, the brain was the only organ in which no substantial metabolism was detected, and a linear correlation between plasma and brain C3G levels was observed (Figure 8) over a physiologically relevant range of C3G plasma concentration (18.78 – 354.84 nM). No correlation could be observed with the other metabolites, once more suggesting the selectivity of the blood-brain barrier.

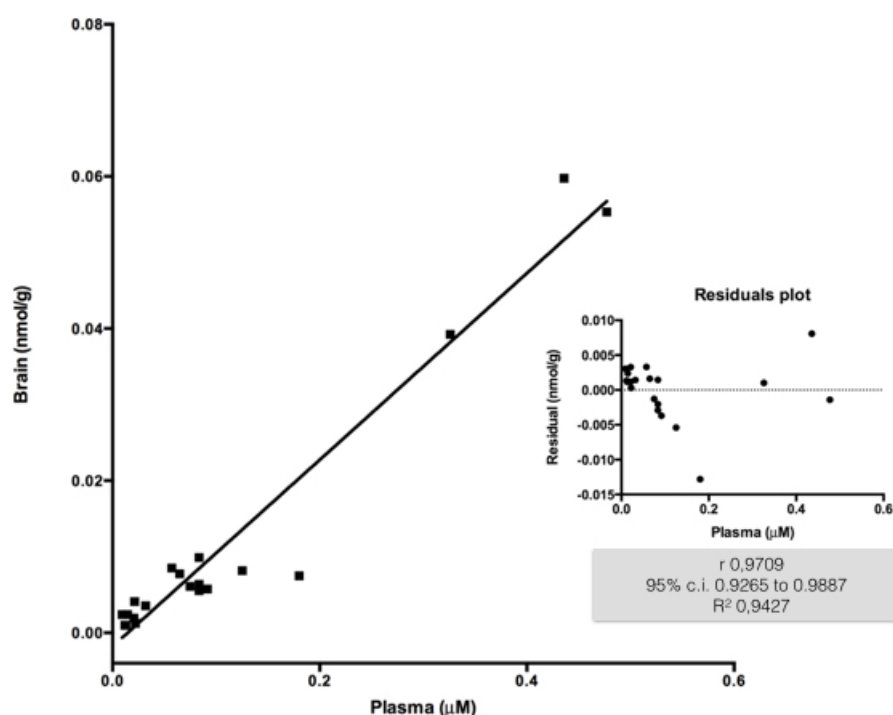


Figure 4.8 Positive linear correlation ( $R^2$ , 0.9427) between plasma and brain C3G concentrations in individual rats.

### Urinary excretion

Urine concentrations of C3G and methylated derivatives in Wistar rats following intravenous administration of C3G were determined over a period of 0 – 20 minutes. Urine concentration-time data are listed in Table 5. We detected the urinary excretion after 2 min, which represents the time needed for C3G to undergo uptake, metabolism and excretion in the kidneys. Rat urine showed relatively high amounts of C3G and major metabolites. Moreover, 15% of the injected dose was recovered in 5 min after the injection.

**Table 4.4.** Urine concentrations of C3G and its derivatives in Wistar rats following intravenous administration of 668 nmol of C3G.

<b>Time (min)</b>	<b>C3G (nmol/g)</b>	<b>PN3G (nmol/g)</b>	<b>PT3G (pmol/g)</b>	<b>D3G (nmol/g)</b>	<b>M3G (pmol/g)</b>	<b>PG3G (pmol/g)</b>	<b>TOT (nmol/g)</b>
0.25	0.02 ± 0.01	0.01 ± 0.00	4.58 ± 2.84	0.02 ± 0.01	28.35 ± 17.87	1.57 ± 0.40	0.09 ± 0.05
2	2.69 ± 0.82	1.48 ± 0.41	3.30 ± 1.59	0.03 ± 0.00	9.57 ± 4.52	7.92 ± 2.59	4.23 ± 1.24
5	20.20 ± 2.61	6.54 ± 0.33	nd	0.05 ± 0.01	5.15 ± 1.88	47.09 ± 4.16	26.84 ± 2.96
15	11.95 ± 6.53	5.67 ± 2.24	nd	0.02 ± 0.01	3.17 ± 1.64	33.22 ± 16.09	17.68 ± 8.81
20	5.66 ± 1.31	5.16 ± 1.11	nd	0.03 ± 0.01	0.00 ± 0.00	20.98 ± 5.61	10.87 ± 2.44

nd, Not detected.

## Conclusions

Our study provides long-needed quantitative data about C3G distribution in rat biofluids and organs, including the brain. Moreover, the obtained results are now available for designing and interpreting the intervention trials in animals and humans, which are aiming at establishing the link between intake of anthocyanin-rich food or supplements and the protection against age-related cognitive dysfunctions.

However, our study has several important limitations. Our study was done on a small number of animals, and shall be repeated in a larger trial to confirm our novel findings related to the identification of C3G in the brain. However, these pioneering experiments (first documented trial of C3G in short-term pharmacokinetics, i.e. we sacrificed 3 animals at time point 15 sec) are in agreement with the 3R principles for animal research that warrants the reduction of animals for risky hypotheses-based experiments.

Another issue is that in general the total recoveries from anthocyanin extraction procedures, similar to those used in the current study, are low (38.6-57.7% from plasma, and 21.4-46.4% from tissues in (Andreja Vanzo et al., 2011)). Hence it is possible that the apparently poor total recovery of the dose can be assigned to the incomplete extraction and detection. Indeed, the poor recovery may be hypothesized to be due to the very strong binding of anthocyanins with proteins in the sample (Tang et al., 2014; Wiese et al., 2009).

Anthocyanins can also be metabolized into yet unidentified C3G derivatives, or covalently bound to proteins in plasma or inside cells, or to other polymers during the extraction and analysis methods.

## Bibliographic References

- Brown, R. P., Delp, M. D., Lindstedt, S. L., Rhomberg, L. R., & Beliles, R. P. (1997). Physiological Parameter Values for Physiologically Based Pharmacokinetic Models. *Toxicology and Industrial Health*, 13(4), 407-484. doi: 10.1177/074823379701300401
- Directive 2010/63/EU of the European Parliament and of the Council of 22 September 2010 on the protection of animals used for scientific purposes. (2010). Official J Eur Union Retrieved from <http://eur-lex.europa.eu/LexUriServ/LexUriServ.do?uri=OJ:L:2010:276:0033:0079:en:PDF>.
- Fleschhut, J., Kratzer, F., Rechkemmer, G., & Kulling, S. E. (2006). Stability and biotransformation of various dietary anthocyanins in vitro. *European Journal of Nutrition*, 45(1), 7-18. doi: Doi 10.1007/S00394-005-0557-8
- Fridén, M., Ljungqvist, H., Middleton, B., Bredberg, U., & Hammarlund-Udenaes, M. (2010). Improved measurement of drug exposure in the brain using drug-specific correction for residual blood. *J Cereb Blood Flow Metab*, 30(1), 150-161. doi: 10.1038/jcbfm.2009.200
- International Life Sciences Institute. (1994). Physiological Parameter Values for PBPK Models (R. S. Institute, Trans.): International Life Sciences Institute.
- Kell, D. B. (2013). Finding novel pharmaceuticals in the systems biology era using multiple effective drug targets, phenotypic screening, and knowledge of transporters: where drug discovery went wrong and how to fix it. *The FEBS journal*. doi: 10.1111/febs.12268
- Kong, A. N., & Jusko, W. J. (1988). Definitions and applications of mean transit and residence times in reference to the two-compartment mammillary plasma clearance model. *J Pharm Sci*, 77(2), 157-165.
- Marczylo, T. H., Cooke, D., Brown, K., Steward, W. P., & Gescher, A. J. (2009). Pharmacokinetics and metabolism of the putative cancer chemopreventive agent cyanidin-3-glucoside in mice. *Cancer Chemotherapy and Pharmacology*, 64(6), 1261-1268. doi: 10.1007/s00280-009-0996-7
- McNamara, P. J., Fleishaker, J. C., & Hayden, T. L. (1987). Mean residence time in peripheral tissue. *Journal of pharmacokinetics and biopharmaceutics*, 15(4), 439-450.
- Passamonti, S., Vrhovsek, U., & Vanzo, A. (2003). The stomach as a site for anthocyanins absorption from food. *FEBS Lett*, 544(1-3), 210-213.
- Pojer, E., Mattivi, F., Johnson, D., & Stockley, C. S. (2013). The Case for Anthocyanin Consumption to Promote Human Health: A Review. *Comprehensive Reviews in Food Science and Food Safety*, 12(5), 483-508.
- Tang, L., Zhang, D., Xu, S., Zuo, H., Zuo, C., & Li, Y. (2014). Different spectroscopic and molecular modeling studies on the interaction between cyanidin - 3 - O - glucoside and bovine serum albumin. [10.1002/bio.2524]. *Luminescence*, 29(2), 168-175. doi: papers3://publication/doi/10.1002/bio.2524

- Tsuda, T., Horio, F., & Osawa, T. (1999). Absorption and metabolism of cyanidin 3-O-beta-D-glucoside in rats. *FEBS Lett*, 449(2-3), 179-182.
- Vanzo, A., Terdoslavich, M., Brandoni, A., Torres, A. M., Vrhovsek, U., & Passamonti, S. (2008). Uptake of grape anthocyanins into the rat kidney and the involvement of bilitranslocase. *Mol Nutr Food Res*, 52(10), 1106-1116. doi: 10.1002/mnfr.200700505
- Vanzo, A., Vrhovsek, U., Tramer, F., Mattivi, F., & Passamonti, S. (2011). Exceptionally fast uptake and metabolism of cyanidin 3-glucoside by rat kidneys and liver. *Journal of natural products*, 74(5), 1049-1054. doi: 10.1021/np100948a
- Veng-Pedersen, P. (1989). Mean time parameters dealing with the tissue distribution of drugs: limitations and extensions. *J Pharm Sci*, 78(3), 264-266.
- Veng-Pedersen, P. (2001). Noncompartmentally-based pharmacokinetic modeling. *Advanced drug delivery reviews*, 48(2-3), 265-300. doi: 10.1016/S0169-409X(01)00119-3
- Waynforth, H. B., & Flecknell, P. A. (1992). *Experimental and surgical technique in the rat* (2nd ed. ed.): Academic.
- Wiese, S., Gärtner, S., Rawel, H. M., Winterhalter, P., & Kulling, S. E. (2009). Protein interactions with cyanidin - 3 - glucoside and its influence on  $\alpha$  - amylase activity. [10.1002/jsfa.3407]. *J. Sci. Food Agric.*, 89(1), 33-40. doi: papers3://publication/doi/10.1002/jsfa.3407
- Zhang, Y., Huo, M., Zhou, J., & Xie, S. (2010). PKSolver: An add-in program for pharmacokinetic and pharmacodynamic data analysis in Microsoft Excel. *Comput Methods Programs Biomed*, 99(3), 306-314. doi: 10.1016/j.cmpb.2010.01.007
- Ziberna, L., Tramer, F., Moze, Š., Vrhovsek, U., & Passamonti, S. (2012). Transport and bioactivity of cyanidin 3-glucoside into the vascular endothelium. *Free Radic Biol Med*. doi: 10.1016/j.freeradbiomed.2012.02.027

# **Chapter 5. A data analysis pipeline for an untargeted metabolomic workflow**

## **Chapter Overview**

Chapter 5 presents the development of a validation framework and accuracy measures applied to an untargeted metabolomic workflow. The experiment deals with the analysis of hundreds of samples, characterized by several thousands of metabolic features, that is impossible to analyze manually. Thus, we discuss the key elements of the workflow, such as multivariate and machine learning data analysis and data visualization tools, to provide an integrated hypothesis building analysis pipeline for the selection of biomarker candidates.

## Experimental section

### Materials

All the chromatographic solvents were HPLC grade or LC-MS grade for the MS experiments. Acetonitrile, acetone, methanol p-cumaric acid and formic acid were purchased from Sigma Aldrich (Milan, Italy). Isotopically labelled compounds, rosmarinic acid-d7 were purchased from C/D/N Isotopes Inc. (Quebec, Canada). Pure anthocyanins were obtained from Polyphenol Laboratories AS (Sandnes, Norway) and Heparin from Schwarz Pharma (Milan, Italy). All chemicals were used without further purification.

Ultra pure Milli-Q water (Merck Millipore, Billerica, MA, USA) was used for the preparation of all solutions. Phosphate buffered saline (PBS) was prepared as following: 6.03 mM  $\text{Na}_2\text{HPO}_4$ , 3.91 mM  $\text{NaH}_2\text{PO}_4$  and 139 mM NaCl (Carlo Erba, Milan, Italy) were dissolved in MilliQ water and pH was adjusted to 7.4 with HCl.

### Study design and protocol

The experiment was designed as a one-component pharmacokinetic study with untargeted profiling of brain, plasma and urine (see Figure 5.1). The experimental design was vetted and approved by the bioethical committee of the University of Trieste (internal code 140PAS14), according to the provisions of the European Community Council Directive (*Directive 2010/63/EU of the European Parliament and of the Council of 22 September 2010 on the protection of animals used for scientific purposes*, 2010). More details about surgery procedures and animals handling can be found in chapter four. Briefly, Twenty-two male Wistar rats (*Rattus Norvegicus*, Harlan Italy S.r.l.), of same age (15 weeks), 293-390 g of body weight, were randomly divided into 5 groups, according to the time that elapsed after intravenous administration of the test compound, and one control group. The rats were anesthetized with intra-peritoneal administration of tiletamine/zolazepam (1:1, 25 mg/kg body weight) and xylazine (10 mg/kg body weight). They received i.v. administration of 0.2 mL PBS, with (test) or without (control) 668 nmol cyanidin 3-glucoside. According to a previous study, the same dose of cyanidin 3-glucoside made it possible to observe a peak plasma concentration of about 1.5  $\mu\text{M}$  cyanidin 3-glucoside 1 min after i.v. administration (Vanzo et al. 2011). One min before sacrificing the rats, sodium heparin (0.1 mL, 500 IU) was injected.

10 min after anesthesia and the corresponding time point after i.v. administration (0.25, 5, 10, 15, 20 min), the rats were sacrificed by decapitation. Urine was collected through the urinary bladder with a syringe. The brain was washed with mQ water, immediately frozen in liquid nitrogen and stored at -80 °C.

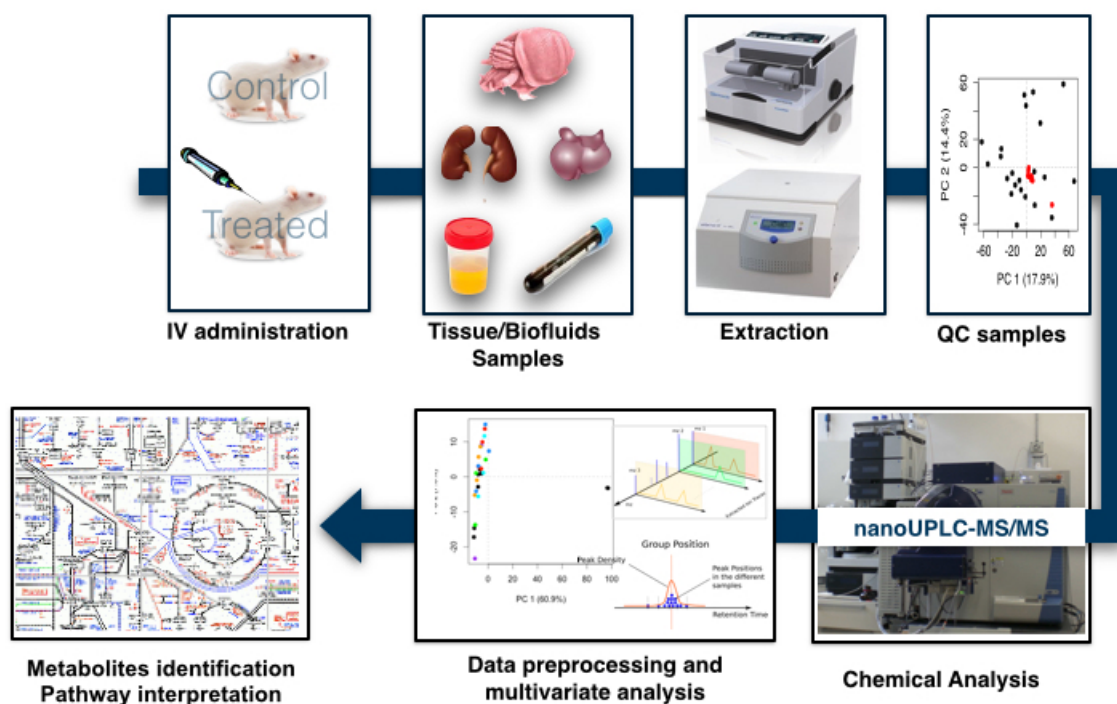


Figure 5.1 Metabolomic workflow for untargeted experiment.

### Organ collection and extract preparation

Immediately after sampling, 5 mL of blood was transferred into ice-cold (-20 °C), deoxygenated aqueous 95 % methanol in a ratio 1:9 (v/v). The urine was weighed and transferred into ice-cold, deoxygenated aqueous 95 % methanol at a ratio of 1:9 (w/v). Frozen brain was grounded under cryogenic conditions (-196° C) to 5 µm particles in a CryoMill (Retsch, Germany), using a single 25 mm i. d. steel ball (30 seconds, 25/sec frequency). The pulverized tissue was rapidly transferred (without thawing) into ice-cold, deoxygenated aqueous 95 % methanol at a ratio of 1:9 (w/v). *trans*-Cinnamic acid-d<sub>5</sub>, as internal standard, was dissolved in the aqueous methanol at concentration of 0.1 mg/L for the monitoring of the extraction protocol.



All samples were extracted with an orbital shaker for 10 min at room temperature. The methanol extracts were then centrifuged for 5 min at 3600 rpm at 4 °C, decanted under a stream of nitrogen in 50 mL dark glass vessels and stored at -80 °C.

To assess the most suitable solvent mixture for the Ultra performance liquid chromatography–quadrupole time-of-flight analysis, different solvent mixtures were evaluated for brain matrix, as previously described (Gika & Theodoridis, 2011; G. Theodoridis et al., 2012). The total ion current (TIC) chromatograms were used for visual inspection and fast scrutiny of the data. Tryptophan peaks in extracted ion chromatograms (XIC) for each solvent mixture(s) were subsequently examined in terms of size, shape and retention time (Figure 5.2).

All samples were filtered through 0.2 µm PVDF filters (Millipore) and injected into a UPLC/QTOF-MS system.

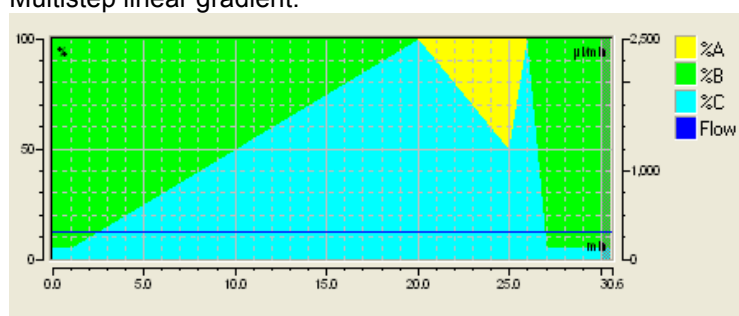
#### **Ultra performance liquid chromatography–quadrupole time-of-flight analysis**

Analysis was carried out using a Dionex UPLC, coupled via an electrospray ionization (ESI) interface to a LTQ Orbitrap XL QTOF-MS (Thermo Scientific, San Jose, CA USA), operating in W-mode and controlled by Masslynx 4.1. with the chromatographic conditions summarized in Table 5.1. Mass spectrometric data were collected by separate runs in positive and negative ESI mode. The scan cycle started with a full scan mass spectrum (MS) mode at a resolving power of 30,000 (with a scan window divided in two scan events: 100-550 m/z, and 500-1500 m/z). Based on pre-scan information from the full scan MS, a second injection with Data Dependent MS<sup>n</sup> scan (a FullScan Mode as referenced scan event with three scan events with MS<sup>n</sup> as Data Dependent Scan, each at a resolving power of 7500), was performed.

**Table 5.1 Chromatographic and spectrometric conditions.**

HPLC	Dionex 3000 Nano HPLC
Column	Kinetex 2.6 µm C18 100 Å
Column temperature	4° C
Injection volume	10 µL
Eluent flux	0.3 mL/min
Solvent A	0.1% formic acid in isopropanol
Solvent B	0.1% formic acid in mQ water
Solvent C	0.1% formic acid in acetonitrile

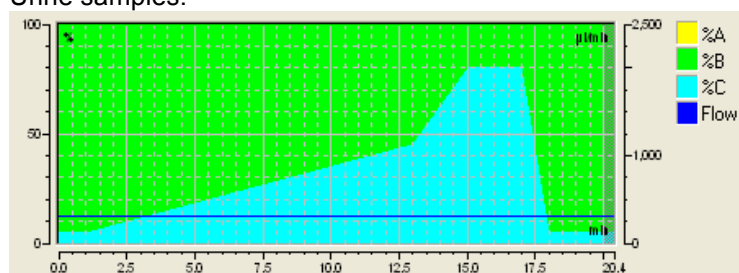
Multistep linear gradient:



	Retention [min]	Flow [µl/min]	%B	%C	Curve
1	0.000	300.000	95.0	5.0	
2	0.000	300.000	95.0	5.0	5
3	1.000	300.000	95.0	5.0	5
4	20.000	300.000	0.0	100.0	5
5	25.000	300.000	0.0	50.0	5
6	26.000	300.000	0.0	100.0	5
7	27.000	300.000	95.0	5.0	5
8	30.000	300.000	95.0	5.0	5

Gradient

Urine samples:



	Retention [min]	Flow [µl/min]	%B	%C	Curve
1	0.000	300.000	95.0	5.0	
2	0.000	300.000	95.0	5.0	5
3	1.000	300.000	95.0	5.0	5
4	13.000	300.000	55.0	45.0	5
5	15.000	300.000	20.0	80.0	5
6	17.000	300.000	20.0	80.0	5
7	18.000	300.000	95.0	5.0	5
8	20.000	300.000	95.0	5.0	5

Mass spectrometer	LTQ Orbitrap XL QTOF-MS
Source Voltage	5.00 kV (positive) 3.50 kV (negative)
Source Current	100.00 $\mu$ A
Capillary Voltage	30.00 V
Tube Lens	110 V
Mass range	100-550 m/z and 500-1500 m/z
Capillary Temp	320.00° C
APCI Vaporizer Temp	0.00° C
Sheath Gas Flow	35.00 a.u.
Aux Gas Flow	5.00 a. u.
Sweep Gas Flow	0.00 a. u.

### **Quality control**

Twenty-two samples of each investigated tissue were randomized before injection. To correct for batch effects and to allow the equilibration of the analytical system, a blank solution (solvent, 5  $\mu$ L) was injected every twelve samples. Furthermore, pooled Quality Control (QC) samples, prepared from each tissue, were injected several times during the experiment to monitor drifts in the analytical pipeline.

The stability of the retention times, areas and heights was checked in all injections for the signal of the internal standard (rosmarinic acid-d<sub>7</sub>) added to the samples, which was considered suitable to check the global stability of the process. The stability was confirmed also by injecting a standard mixture of 11 compounds (G. A. Theodoridis et al., 2012) at the beginning and at the end of the analyses of each tissue, both in positive and in negative ESI mode.

### **Data Analysis Workflow**

#### **MS data acquisition, conversion, and storage**

Raw untargeted metabolomic data were transformed to the open mzXML format by the ProteoWizard 2.1.x suite (Holman et al., 2014; Kessner et al., 2008). After conversion, the data have been stored and organized as a specific ISA-Tab text file, implemented by the cross-platform ISACreator software (Rocca-Serra et al., 2010). All data preprocessing and analysis was performed within the R software environment for statistical computing and

graphics (The R Core Team, 2014). In particular, data import and export, preprocessing and visualization were performed with metaMS, a package that implement a pipeline for untargeted GC-MS and LC-MS metabolomics (Wehrens et al., 2014). MetaMS is based on the open source packages xcms (Smith et al., 2006) and CAMERA (Kuhl et al., 2012).

### **Data processing**

All runs apart from the solvent and the standard injections were selected. The data with retention times lower than 1 min and higher than 21 min were disregarded, annotation was not performed. The data were preprocessed with a set of parameters optimized for the specific chromatographic and instrumental conditions (Orbitrapstefano.Rdata).

### **Statistical analysis**

Several types of scaling method were evaluated, and a total ion current (TIC) normalization was performed prior to the multivariate analysis, to account for small differences in the efficiency between the different samples within the analytical run. Unsupervised principal component analysis (PCA), was used to identify major outliers (removed from further analysis).

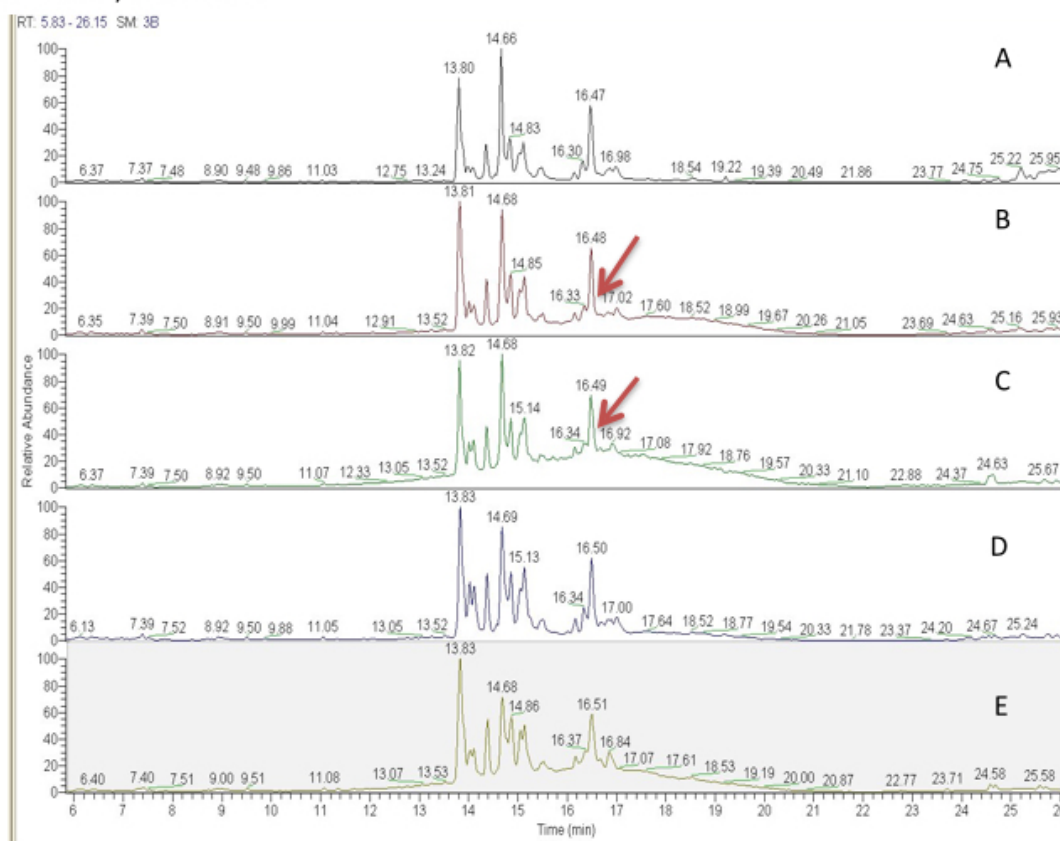
Univariate analysis (e.g. Student's t test, ANOVA) with a multiple testing corrections was performed to reduce the inclusion of false discoveries when undertaking the multiple comparisons: *p*-values were corrected using false discovery rate (FDR) adjustments of Benjamini-Hochberg (Benjamini & Hochberg, 1995) with  $FDR < 0.10$  or  $< 0.05$ .

## Results and discussion

### Efficiency of extraction solvent

The choice of solvent in which metabolites are extracted from tissues plays a crucial role in untargeted investigations. In the present study, experiments were performed to evaluate the efficiency of various solvent combinations for extracting metabolites from samples of complex multicompartiment systems (Kim & Verpoorte, 2010) such as the brain. The best response was achieved with aqueous methanol (3:7, v/v), which improved the solubility of hydrophilic metabolites. Practical issues in the extraction procedure were also considered. The formation of emulsions had to be avoided because they were unfavorable for subsequent chromatographic analysis and could compromise method repeatability by introducing bias (see Figure 5.2 and Table 5.2 for details). The optimum solvent ratios provided richer chromatograms with higher levels of information.

### ZOOM – TIC m/z 500-1500



## ZOOM – TIC m/z 100-500

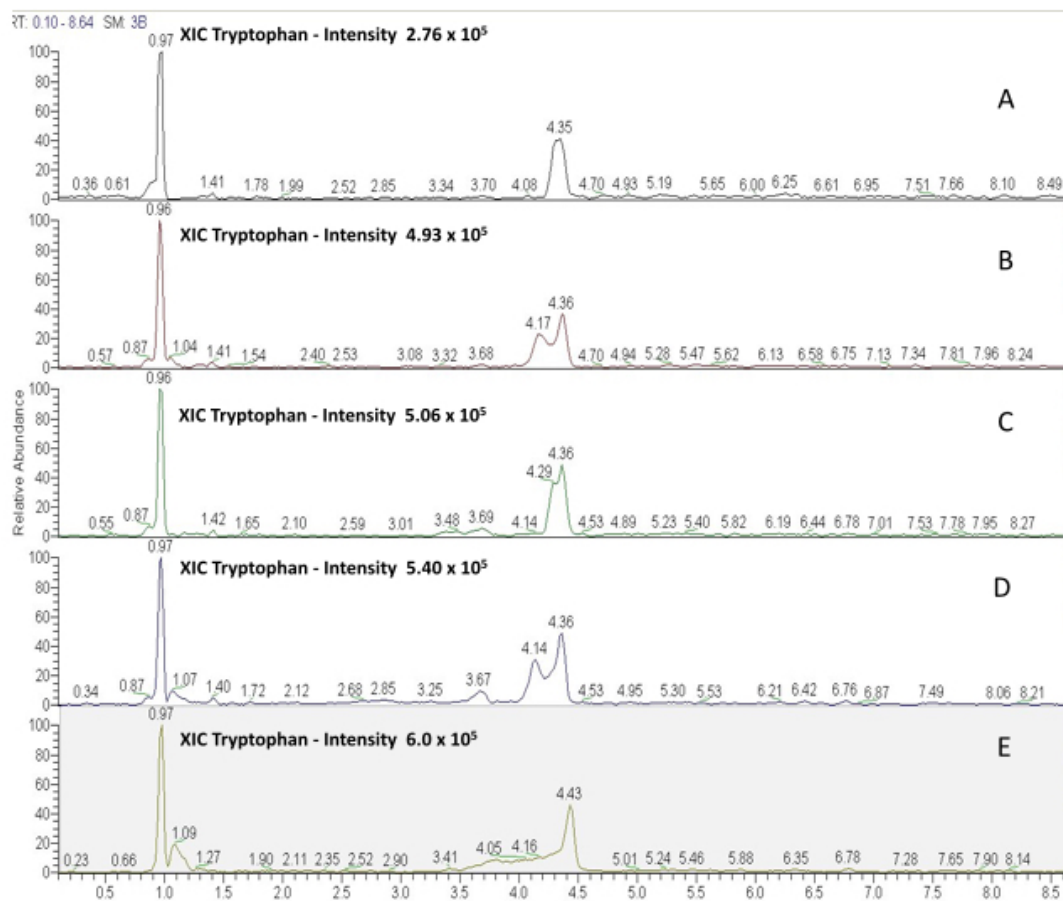
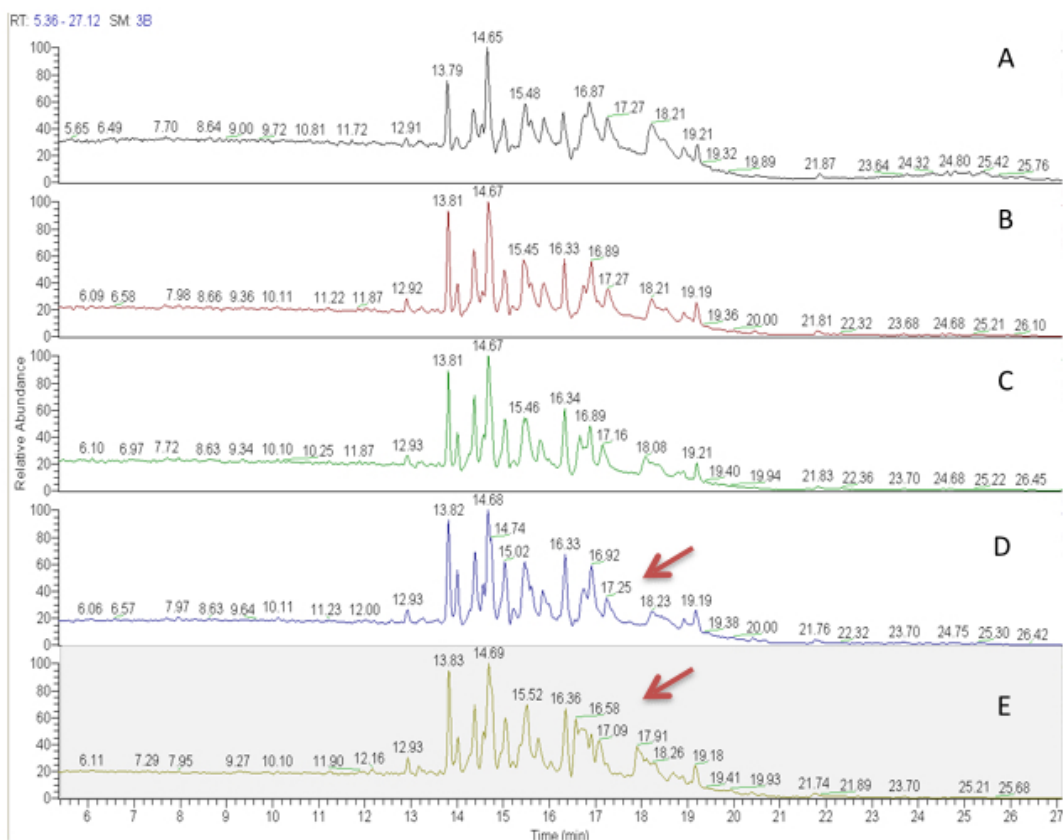


**Figure 5.2 (Previous pages) Efficiency of extraction solvent for brain tissue.** Pre-concentration of the brain matrix (1:2, 1:8) did not bring significant improvement of the signal intensity. Different water content in the final solution does not impact compounds for  $rt > 10$  min, with changes only in the relative intensity. Any addition of water after evaporation produced deterioration of the matrix and peak shape worsening. For more details see Table 5.2.

**Table 5.2 Summary of different solvent ratios.**

<b>TIC</b>	<b>MeOH</b>	<b>H<sub>2</sub>O</b>	<b>Preconcentration</b>	<b>Solution</b>	<b>XIC Tryptophan</b>
A	0.7	0.3	/	<i>slightly opaque</i>	good peak shape
B	0.7	0.3	2:1	<i>opaque</i>	double peak shape
C	0.5	0.5	2:1	<i>completely opaque</i>	good peak shape
D	0.7	0.3	15:4	<i>opaque</i>	double peak shape
E	1	/	5:1	<i>clear</i>	peak shape fronting

### **Data preprocessing**

Following data acquisition, the obtained mass spectra were subjected to various data preprocessing methods, i.e. mathematical operations, in order to facilitate and enhance the subsequent data analysis. Data preprocessing by metaMS generated six annotated peak tables. Each peak table reports retention time ( $rt$ ) and mass/charge ratio ( $mz$ ) value for each feature, isotope annotation (*isotope*), common adducts (*adduct*), and the group number (*pcgroups*). The latter was obtained by clustering the features considering their retention time and the correlation between the extracted ion chromatograms to identify co-eluting ions. As a result of this procedure, the features were grouped into groups that are likely to be related to the same metabolite. The peak tables generated by metaMS were used as data matrices for further statistical analysis.

### **Extraction and number of features**

Brain, plasma and urine extracts were compared in terms of the extracted features in ESI+ and ESI- mode. The total number of extracted features detected in ESI+ was 2193 in brain, 2417 in plasma and 4304 in urine. On the other hand, the total number of features detected in ESI- was 1140 in brain, 1328 in plasma and 2846 in urine.

Urine showed the highest number of detected features in both ionization modes. The distribution in the space defined by the  $m/z$  ratio and chromatographic retention time of the experimental features obtained in ESI positive mode, evidenced that most of them were generated from highly hydrophilic, polar compounds eluting in the earliest part of the

chromatogram, as well as hydrophobic metabolites, eluting in the final part of the gradient (Figure 5.3).

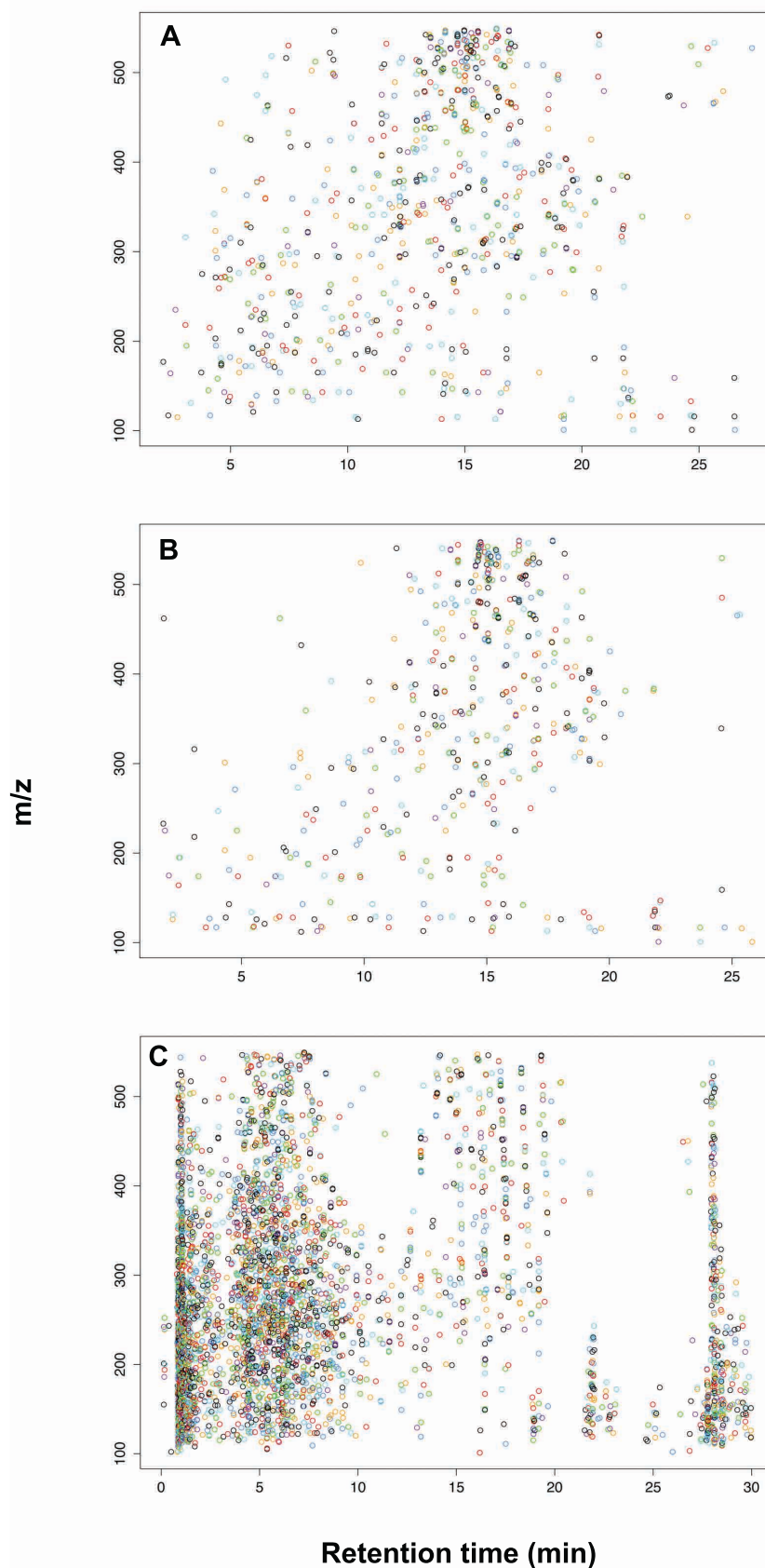


**Figure 5.3** Distribution in the space defined by the  $m/z$  ratio and chromatographic retention time of the experimental features obtained in ESI positive mode for the extracts from blood (A), brain (B), and urine (C) of adult male rats. The samples were collected 0.25(0); 2(0); 15(0); 20(0); min after intravenous administration of 667 nmol cyanidin 3-glucoside.



Although the number of features does not correlate directly with the number of metabolites, it's considered to be "proportional" to metabolites. Ionization process generates several ions from the same neutral molecule. In almost all cases, tens of different features in the data matrix represented each molecule. This redundancy is typical of a so-called "*fat*" data matrix, in which the number of samples is (much) smaller than the number of variables. Consequently, statistical tools used for data reduction had to deal with the multiplicity problem, which actually limited the capacity of finding robust and consistent biomarkers.

### **Quality assessment**

PCA was used to check analytical stability in relation to the biological variability of the samples. This type of analysis is commonly applied to multivariate metabolomics datasets in which several variables (signals in a mass spectrum arising from metabolites) are processed simultaneously for a certain number of samples (Nicholson et al., 1999; Worley & Powers, 2013). Each variable  $n$  ( $n > 1$ ) can be considered a unique dimension; thus, each sample can be represented in  $n$ -dimensional space. However, such space is quite difficult to visualize and interpret; therefore, PCA reduces the dimensionality via a projection technique so that individual samples can be compared in a lower (e.g., two-dimensional) space called a PCA score plot. The score plots for the brain, blood, and urine datasets are displayed in Figure 5.4, 5.5, and 5.6, respectively. The points in the figure show the positions of the various samples in the plane of higher variance. On the plot, the separation of the samples obtained at different time points after treatment is clearly visible. The averaging of intersample features provided evidence of marked inter-individual variability. However, the Quality Controls (QCs) constituted a tight cluster in the middle of the "real" samples only in the urine dataset. This behavior is an indication of robust analytical reproducibility because it shows that the variability due to the analytical platform (the spread of the QC points) is much smaller than the biological variability among samples (Franceschi et al., 2014). Accounting for the influence of confounding factors, figure 5.7 demonstrates how the integral of the TIC varied over the full analytical run of 30 injections (~12 h). As expected, the efficiency of the instrument was constant. This plot does not indicate the presence of particularly critical injections, which would have required the reinjection of some of the samples.

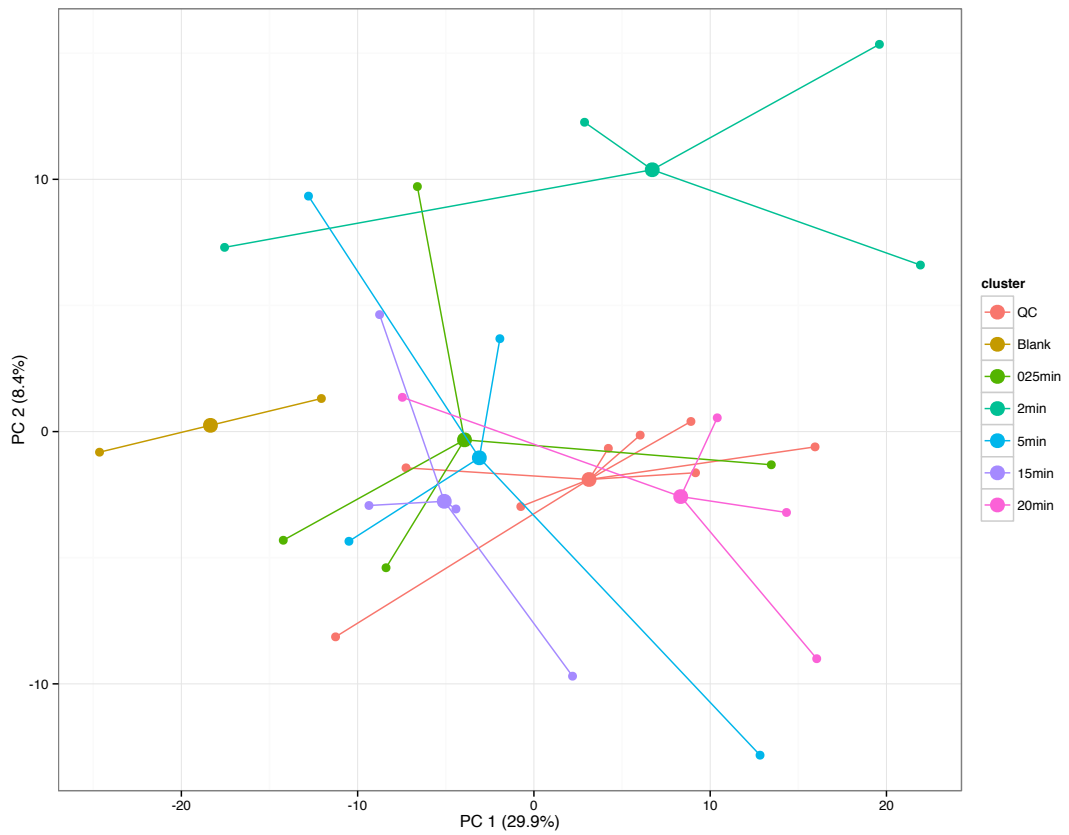
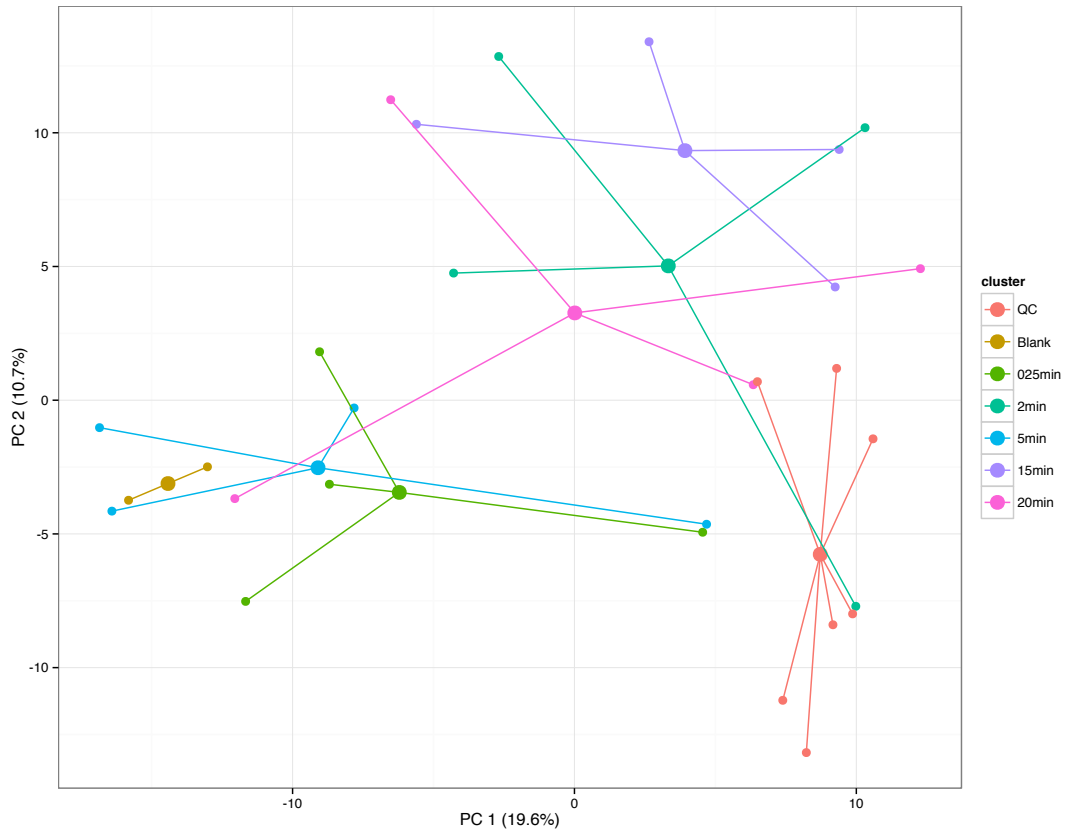


**Figure 5.4. Principal components analysis scores plots for blood extract in negative (down) and positive (up) scan mode. Different colors are used to identify the different sample classes (time points) and the QCs.**

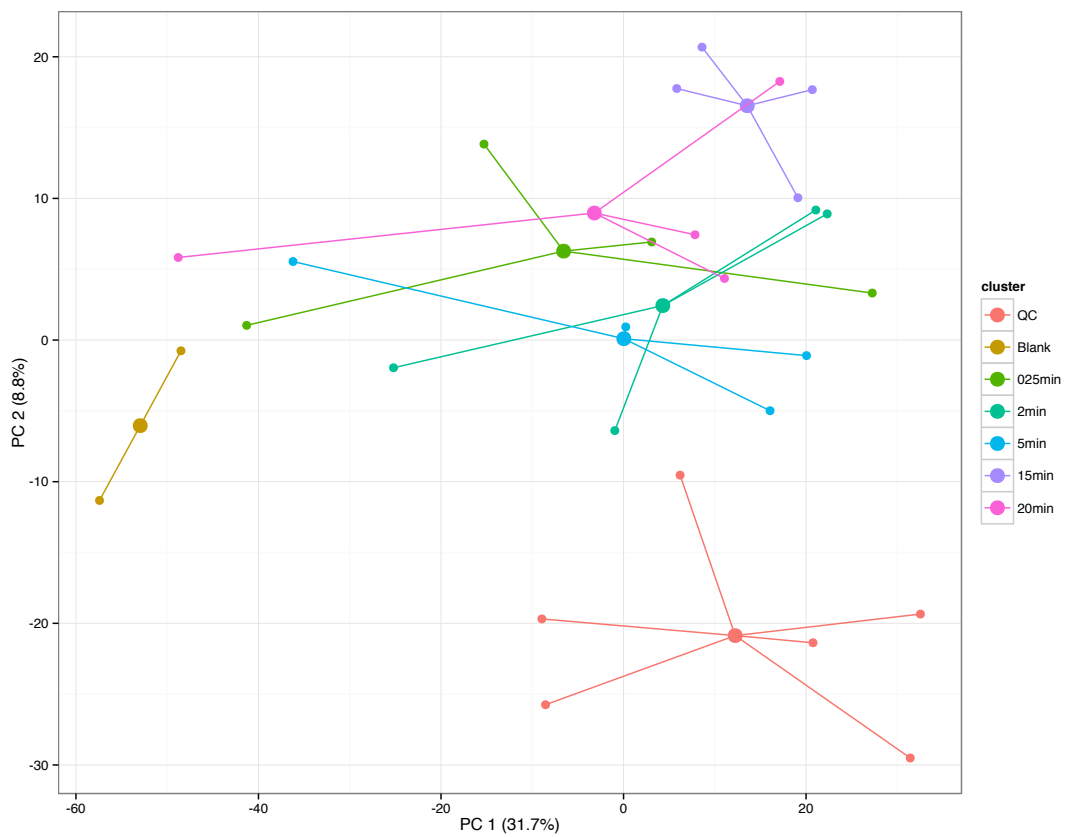
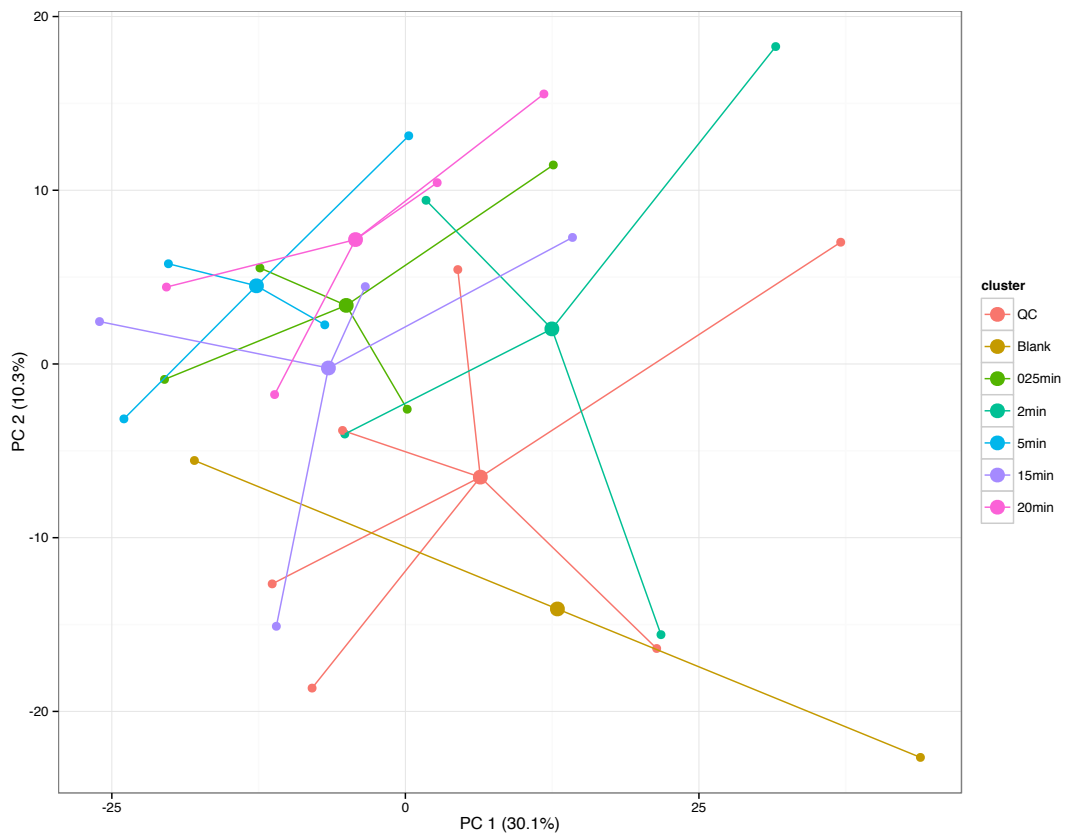


**Figure 5.5** Principal components analysis scores plots for brain extract in negative (up) and positive (down) scan mode. Different colors are used to identify the different sample classes (time points) and the QCs.

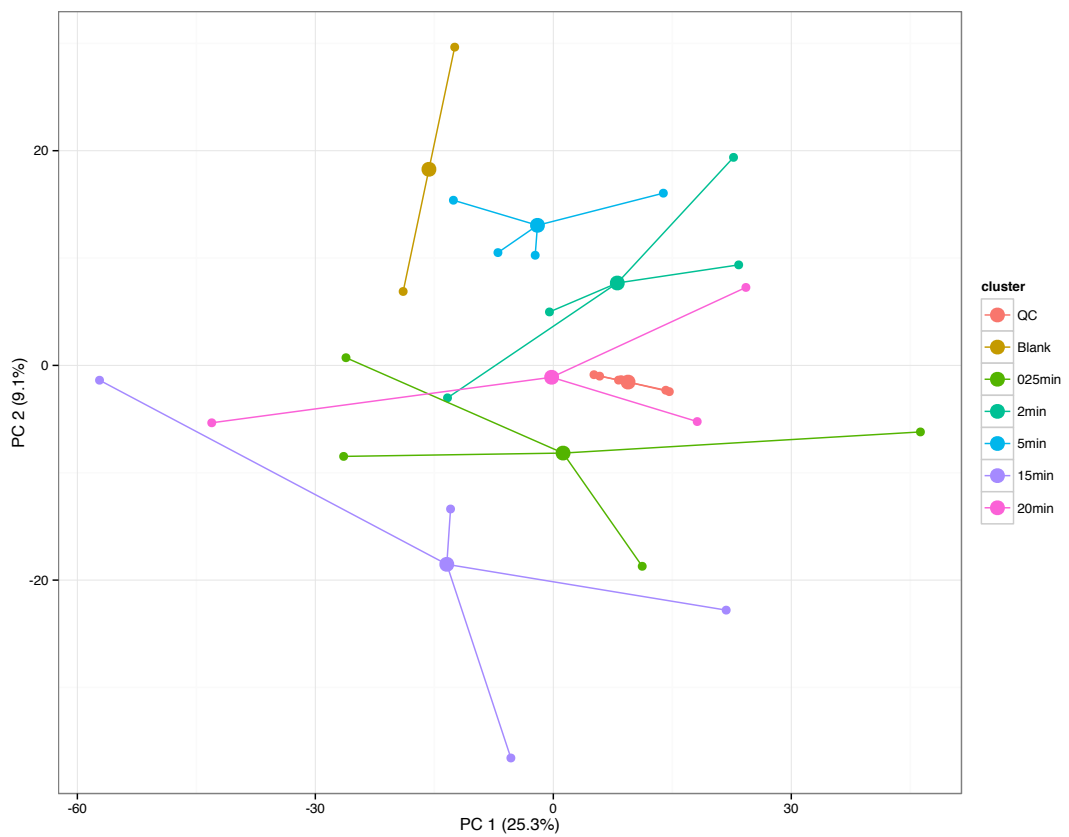
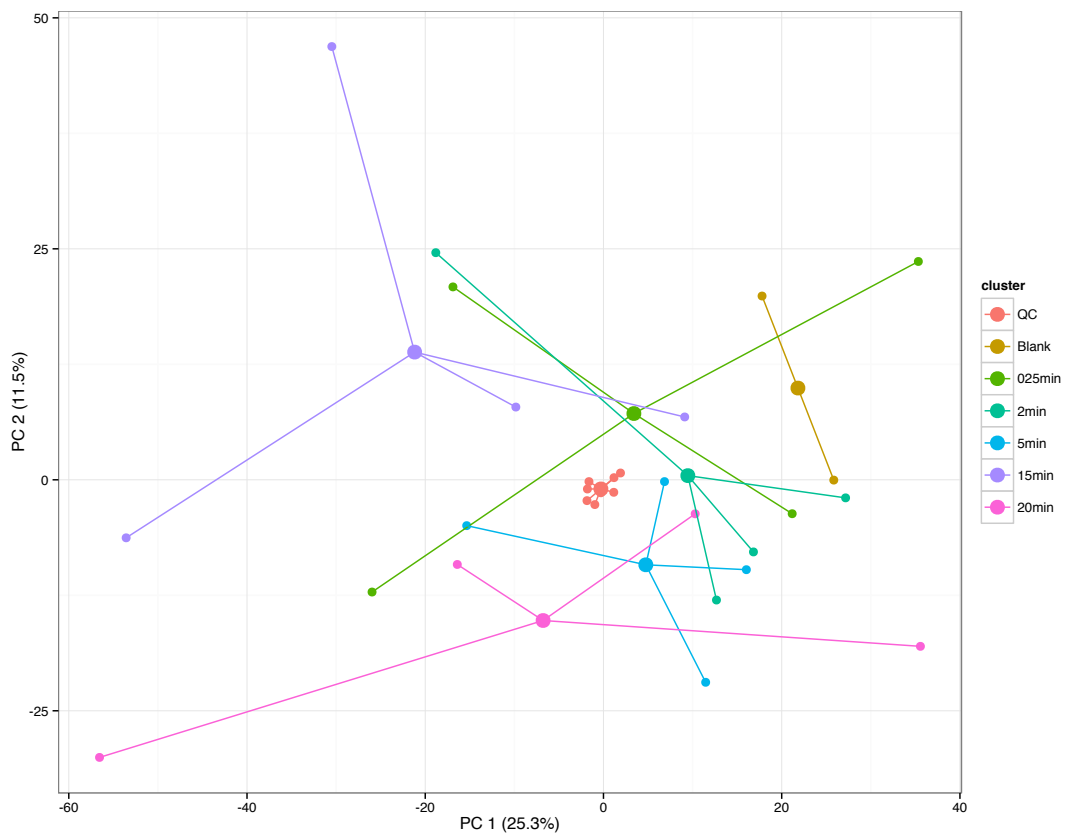


**Figure 5.6** Principal components analysis scores plots for urine extract in negative (down) and positive (up) scan mode. Different colors are used to identify the different sample classes (time points) and the QCs.

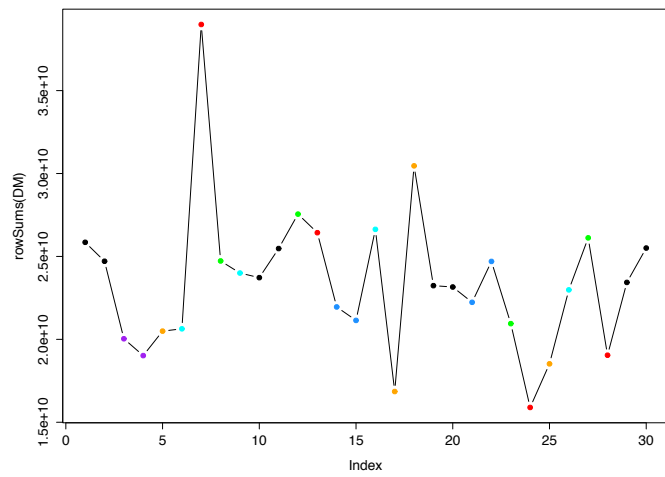
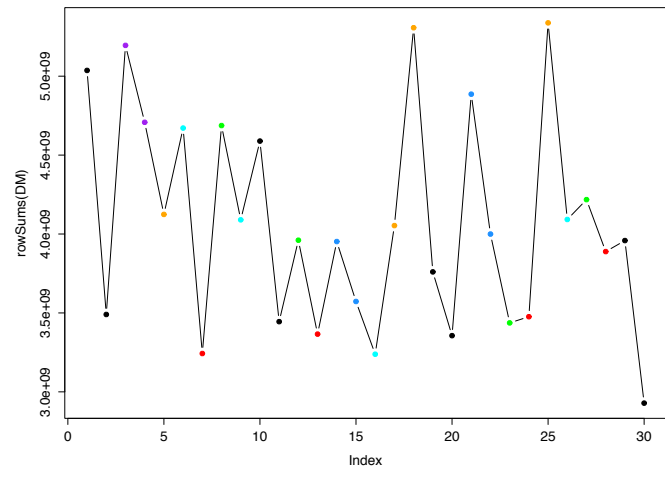
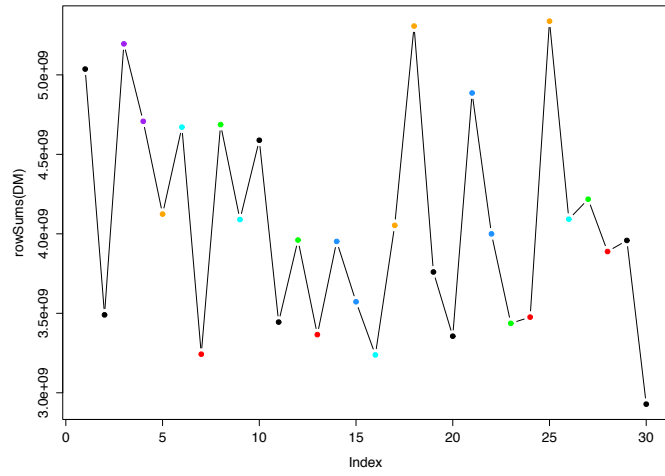


**Figure 5.7** Variation of the integral of the TIC over the analytical run for blood (A), brain (B), and urine (C) extracts.

## Univariate and multivariate statistical methods

We first conducted PCA on each of three complete datasets (brain, plasma, and urine), and then tested the significance of any group separation. Several statistical tests were used to provide a framework for the interpretation of the untargeted data analysis, which allowed us to filter significantly changed features between groups via univariate testing such as a *t*-test or ANOVA with FDR at a level of 5% or 10% correction for multiple testing (Benjamini & Hochberg, 1995). A list of the features that passed the various filtering methods is given in Table 5.2.

Initially we compared observations between the first and last time points (0.25–20 min) with the Student's *t*-test. Correlations were then evaluated using a linear regression model. Looking at the slope factor, we undertook a first inspection if we found metabolic variations consistent with cyanidin 3-glucoside treatment. We obtained no features for the brain and blood dataset in positive/negative scan mode and three features for the urine dataset in positive scan mode only.

However, with this approach we risked losing a physiological hormetic-like response (U-shaped). Thus, we jointly tested all of the differences between time points (using multivariate ANOVA) and then discarded pairs of time points that were not jointly significant before applying the FDR. Correlations were then evaluated using a quadratic regression model. In this case, we obtained three features from the brain dataset and two from the blood dataset in negative scan mode. The features in the urine dataset in positive scan mode numbered 74. Discriminating features obtained for the brain, blood, and urine datasets are reported in Figures 5.8, 5.9 and 5.10, respectively. At the end of the analysis, the *pcgroup* of each identified feature was examined to identify co-eluting ions.

Placing statistically significant findings from data analysis into a biological context requires the assignment of features to their metabolite identities. The association of the groups of obtained features to specific metabolites, commonly referred as annotation, is the biggest challenge for untargeted metabolomics experiments. To determine the identity of the features of interest, we first searched for the accurate mass of a compound in an online chemical structure database. However, a database match denoted only a putative metabolite assignment that was impossible to confirm by comparing the retention time and tandem MS data of standard compounds to those of the features of interest. On the contrary, the raw data supplemented by a set of standardized metadata and organized into a coherent repository were made available on the MetaboLights server (Haug et al., 2013) for use in further analysis.

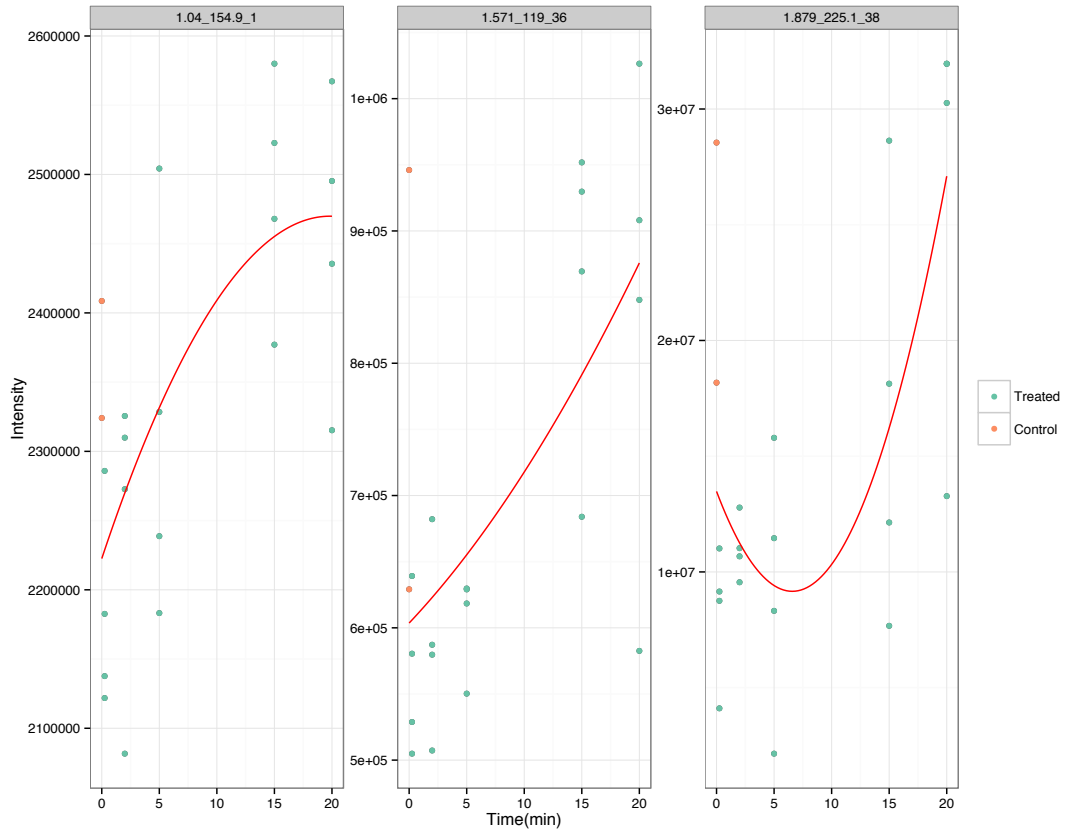


Figure 5.8 Discriminating features identified in brain extracts.

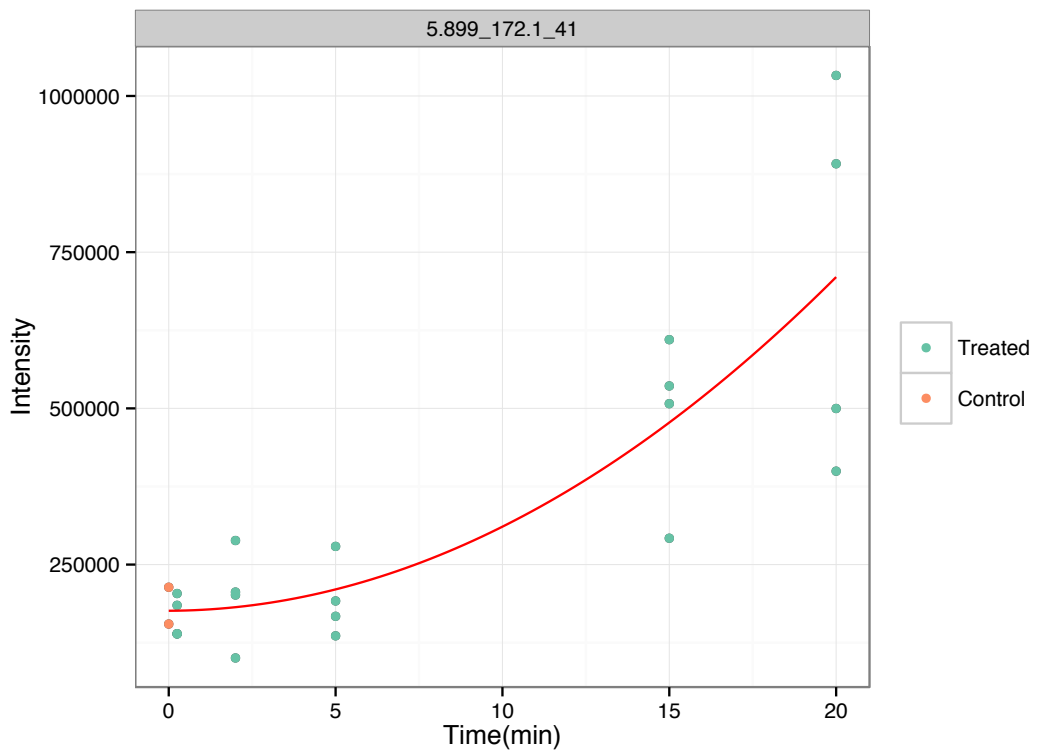
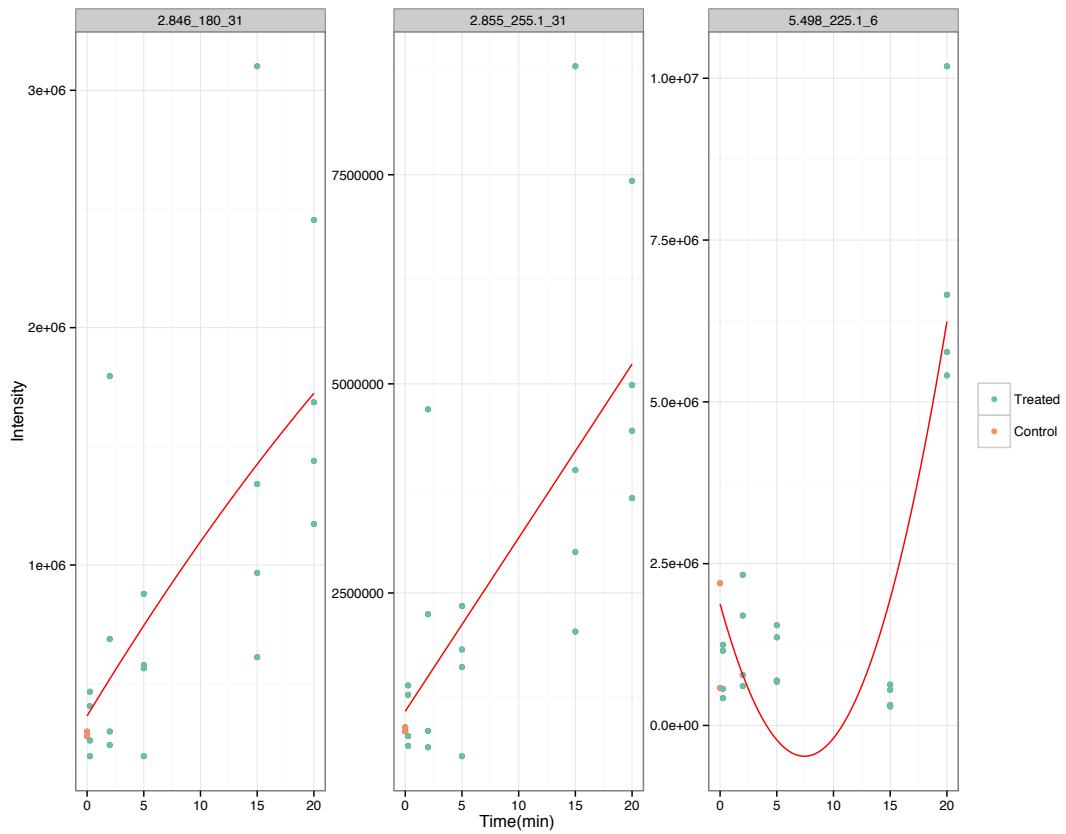


Figure 5.9 Discriminating feature identified in blood extracts.



**Figure 5.10** First 3 discriminating features identified in urine extracts.

## Conclusions

The data analysis workflow presented here allowed us to examine the efficacy of different imputation methods for finding significantly changed features via multivariate and univariate testing. The challenge of correctly reducing a “fat” and redundant data matrix to a “manageable” list of features was successfully overcome.



Table 5.3 List of discriminating features identified.

Dataset	pcgroup	isotopes	mz	rt
Brain	1		1.549.282	1.039.905
	36		1.190.235	1.571.006
	38		2.250.609	1.879.433
Blood	41		172.0977	5.89945
Urine	19		1.710.992	0.9208375
	10		1.370.760	0.9692217
	10		4.131.044	10.515.000
	10		1.270.501	10.624.933
	10		4.131.377	10.839.533
	55		1.768.845	11.073.217
	17	[163][M+1]+	2.461.451	12.161.825
	45		2.750.939	19.560.333
	20	[338][M+1]+	3.601.130	20.711.917
	20	[338][M]+	3.591.092	20.716.167
	20		1.800.583	20.720.500
	20	[338][M+2]+	3.611.052	20.724.417
	67		3.050.624	22.801.917
	58		2.891.096	23.737.667
	11		2.901.127	23.747.000
	11		3.731.063	24.290.583
	37	[122][M]+	2.240.739	26.518.667
	37	[122][M+1]+	2.250.772	26.519.833
	37	[122][M+2]+	2.260.697	26.538.667
	31		1.780.895	28.149.167
	31		1.800.476	28.464.083
	31	[187][M]+	2.550.797	28.548.833
	31	[187][M+1]+	2.560.831	28.724.167
	40		4.131.373	31.043.167
	113		4.291.322	32.847.833
	39		3.271.008	38.080.500
	39	[241][M]+	2.861.107	38.254.417
	39	[241][M+1]+	2.871.141	38.268.500
	39		3.731.063	38.320.917
	29	[245][M+2]+	2.911.160	39.357.917
	29	[245][M+1]+	2.901.126	39.397.750
	29		2.710.989	39.409.250
	29	[245][M]+	2.891.095	39.536.917
	13		2.831.111	41.355.333
	13	[386][M+2]+	4.151.338	41.821.000
	13	[386][M+1]+	4.141.410	41.891.167
	13	[386][M]+	4.131.374	41.918.833
	13		3.731.249	42.044.500
	13		2.460.907	42.434.333
	13		2.290.642	42.443.333
13		2.650.641	42.444.000	
13		1.491.072	42.919.500	
13		4.651.410	43.072.250	
13		2.280.689	43.163.833	
1		2.401.545	44.254.167	
1		2.120.740	44.254.167	
1		1.420.320	44.254.333	
1	[440][M]+	4.792.029	44.254.333	
1	[440][M+1]+	4.802.064	44.254.333	
1	[151][M+1]+	2.411.084	44.254.417	
1		1.640.528	44.254.500	
1	[151][M+2]+	2.421.010	44.254.833	
1		1.520.528	44.257.333	
1	[151][M+3]+	2.431.042	44.257.750	
1	[80][M]+	1.940.634	44.258.167	
1		2.421.123	44.268.000	
1		1.250.292	44.277.833	
1		1.940.998	44.277.833	

1	[151][M]+	2.401.051	44.277.833
1	[332][M]2+	3.541.168	44.337.833
1	[332][M+1]2+	3.546.187	44.425.833
1	[42][M]+	1.660.684	44.426.500
1		2.380.899	44.438.750
1	[120][M]+	2.220.948	44.482.667
1		1.530.606	44.495.667
1		2.081.332	44.785.417
30		4.431.480	46.505.750
30		2.750.939	46.699.500
9		3.411.258	47.298.667
9	[381][M+1]+	4.071.388	47.317.500
9	[84][M]+	1.960.791	47.667.500
9		4.451.459	47.681.500
9	[84][M+2]+	1.980.748	47.694.083
9	[84][M+1]+	1.970.809	47.777.833
9		4.201.143	48.089.500
9	[409][M]+	4.471.251	48.132.500
9	[409][M+1]+	4.481.287	48.183.500
16	[392][M+1]+	4.281.203	48.355.833
16	[392][M]+	4.271.167	48.369.917
124		1.460.599	49.246.167
124		3.470.365	49.246.750
59	[38][M+1]+	1.640.898	49.386.667
59	[38][M]+	1.630.865	49.524.833
59		4.021.151	49.576.167
21		3.871.042	49.818.500
21		2.580.795	49.997.667
21	[289][M]+	3.170.624	50.069.167
21		3.621.202	50.091.500
21	[269][M]2+	3.051.045	50.174.000
21	[269][M+2]2+	3.061.080	50.220.500
21		1.800.476	50.460.833
21		4.701.408	50.679.000
15		4.881.514	51.009.833
15	[354][M+1]+	3.731.139	51.169.083
15	[331][M+1]+	3.551.041	51.171.833
15	[331][M]+	3.541.005	51.241.250
15	[354][M+2]+	3.741.076	51.257.000
15		1.390.448	51.265.750
15	[185][M+3]+	2.571.199	51.296.167
15	[354][M]+	3.721.111	51.331.167
15	[185][M+1]+	2.551.242	51.355.000
15		1.800.840	51.362.917
15	[185][M]+	2.541.208	51.363.167
15	[185][M+2]+	2.561.167	51.363.167
15		3.571.199	51.622.750
15		4.031.157	51.765.250
15		3.421.119	51.769.500
15		4.021.233	51.818.000
15		2.470.949	51.837.833
15		2.720.773	51.845.833
71		3.561.162	51.902.167
71		4.011.198	51.954.500
71		1.980.946	52.401.167
8		3.101.219	52.698.833
8		2.000.375	52.764.500
8		2.771.095	52.867.500
8		2.281.053	52.889.417
8		4.611.405	53.076.833
8		4.310.942	53.093.833
5		2.241.600	53.592.333
5	[444][M+2]+	4.851.866	53.592.833
5	[30][M+1]+	1.540.568	53.692.833
5		1.610.420	53.742.667
5		1.370.419	53.759.833
5		2.240.859	53.772.750

5		1.350.263	53.793.000
5		1.230.262	53.799.167
5	[60][M+1]+	1.820.516	53.816.167
5	[129][M+1]+	2.271.095	53.821.250
5	[27][M+1]+	1.520.609	53.861.167
5	[30][M]+	1.530.534	53.876.750
5	[129][M]+	2.261.062	53.886.667
5	[60][M]+	1.810.483	53.905.167
5	[58][M+1]+	1.800.559	53.927.833
5	[124][M+1]+	2.251.137	53.927.833
5	[487][M]+	5.441.416	53.964.167
5	[487][M+1]+	5.451.451	53.964.167
5	[27][M]+	1.510.575	54.053.333
5	[58][M]+	1.790.525	54.095.333
6	[123][M+1]+	2.250.985	54.983.500
6	[123][M+2]+	2.260.908	55.154.250
33		2.421.210	55.365.333
33		3.851.249	55.582.833
7		1.220.963	56.676.833
7		2.351.264	56.799.333
14	[483][M]+	5.412.024	57.327.667
14	[483][M+1]+	5.422.059	57.331.167
14		2.331.198	57.334.500
14	[210][M+1]+	2.721.023	57.334.500
14	[210][M]+	2.710.991	57.379.833
14		1.500.661	57.382.917
14	[246][M+2]+	2.911.162	57.385.833
14	[153][M]+	2.431.041	57.402.667
14		3.470.731	57.402.667
14	[246][M+1]+	2.901.127	57.501.167
14	[246][M]+	2.891.095	57.517.667
14		4.651.411	57.858.250
14		2.671.162	57.945.000
14		3.241.376	58.426.333
4	[323][M+2]+	3.460.945	59.175.833
4	[323][M]+	3.440.985	59.205.833
4	[323][M+3]+	3.470.979	59.212.667
4	[61][M]+	1.810.683	59.793.500
4	[61][M+1]+	1.820.714	59.884.000
4	[61][M+3]+	1.840.673	59.889.250
4		1.130.054	59.897.167
4		1.530.732	59.901.500
26		2.281.218	60.011.167
26		2.261.260	60.023.000
26	[389][M+1]+	4.171.232	60.064.000
26		5.461.759	60.524.167
76		3.220.922	60.986.167
76		3.671.776	60.997.833
76		3.221.198	61.013.667
43	[190][M]+	2.561.366	61.519.667
43	[190][M+1]+	2.571.398	61.523.667
43	[240][M]+	2.860.930	61.765.000
43		4.291.511	61.778.500
43		4.421.349	61.907.833
43		4.521.305	61.950.333
43		5.051.125	61.984.000
73		4.931.818	62.486.000
73		2.090.378	62.651.167
73	[251][M]+	2.950.747	62.652.833
73		3.401.325	62.654.500
73	[251][M+1]+	2.960.781	62.659.333
73		3.170.566	62.664.750
112		3.600.934	63.061.833
112		1.470.916	63.105.583
2		3.450.212	63.232.833
2		5.042.095	63.495.417
2		2.210.518	63.595.333

2	[181][M]+	2.531.005	63.755.500
2		1.210.885	63.756.000
2		1.340.963	63.756.000
2	[40][M+1]+	1.650.563	63.756.000
2	[40][M+2]+	1.660.486	63.756.000
2	[40][M]+	1.640.528	63.756.167
2		2.211.104	63.756.167
2	[117][M+1]+	2.221.138	63.756.167
2		2.231.064	63.756.167
2		2.231.169	63.756.167
25		3.760.705	64.648.333
25		1.650.910	64.650.250
205		3.211.358	65.203.333
153		4.741.609	65.575.167
153		2.411.546	65.737.667
153		1.780.862	65.764.000
38		2.395.768	65.950.000
38		4.781.459	65.950.167
38	[437][M+1]+	4.751.907	66.133.167
38	[231][M+1]+	2.820.625	66.464.250
38		2.630.485	66.491.167
38	[231][M]+	2.810.591	66.494.667
44		4.431.663	67.389.167
44		4.271.166	67.720.667
44		4.321.042	67.874.500
44		3.821.250	68.120.833
44		2.526.028	68.521.500
36		3.961.685	68.917.667
36		3.871.040	69.409.167
36	[180][M+1]+	2.521.246	69.474.167
82		3.881.059	69.823.833
82		2.561.001	69.832.667
82	[232][M]+	2.810.954	69.959.333
82		3.261.533	69.984.333
82	[232][M+1]+	2.820.988	69.992.500
85		3.101.219	71.103.417
85		2.870.460	71.129.167
85	[202][M+1]+	2.660.674	71.137.667
85	[202][M]+	2.650.641	71.147.667
85	[202][M+2]+	2.670.599	71.163.500
114		4.561.253	71.945.667
91		1.930.430	72.213.667
91		1.350.804	72.582.833
91		2.430.686	72.739.667
54		3.220.858	76.216.000
49		3.591.787	76.606.667
49	[448][M+1]+	4.941.853	76.738.167
49	[448][M+3]+	4.961.805	76.738.667
49	[448][M]+	4.931.821	76.747.667
49	[448][M+2]+	4.951.768	76.750.917
116		2.490.693	77.977.333
126		4.711.615	78.280.333
34	[182][M+2]+	2.550.963	79.187.333
34	[182][M+1]+	2.541.039	79.201.833
34		2.690.955	79.205.833
34	[182][M]+	2.531.005	79.282.917
34		2.350.900	79.369.333
34		1.640.705	79.497.833
149		1.711.491	80.427.833
149		2.790.434	81.322.833
89		4.100.839	82.198.667
89		2.341.037	82.744.500
89		2.950.383	82.791.500
135	[472][M+1]+	5.261.575	83.652.250
135	[472][M]+	5.251.541	83.715.417
61		2.810.954	85.447.833
100	[374][M+1]+	3.971.081	87.133.000

100	[374][M]+	3.961.044	87.157.667
74		4.651.871	88.661.667
88	[362][M+1]+	3.811.949	90.404.917
88	[362][M]+	3.801.914	90.409.083
88		3.851.468	90.473.583
63		2.710.875	91.708.250
63		2.941.635	91.716.167
63	[175][M+1]+	2.501.089	91.720.500
63	[175][M]+	2.491.056	91.721.000
108		1.230.239	96.435.167
108	[171][M+1]+	2.491.226	96.513.667
108	[171][M]+	2.481.193	96.623.833
111		2.670.798	99.831.667
211		2.330.742	107.392.667
178		2.971.332	123.604.167
81		4.523.942	174.139.167

---

## Bibliographic references

- Benjamini, Y., & Hochberg, Y. (1995). Controlling the false discovery rate: a practical and powerful approach to multiple testing. *Journal of the Royal Statistical Society. Series B (Methodological)*, 289-300.
- Directive 2010/63/EU of the European Parliament and of the Council of 22 September 2010 on the protection of animals used for scientific purposes. (2010). Official J Eur Union Retrieved from <http://eur-lex.europa.eu/LexUriServ/LexUriServ.do?uri=OJ:L:2010:276:0033:0079:en:PDF>.
- Franceschi, P., Mylonas, R., Shahaf, N., Scholz, M., Arapitsas, P., Masuero, D., . . . Wehrens, R. (2014). MetaDB a Data Processing Workflow in Untargeted MS-Based Metabolomics Experiments. *Front Bioeng Biotechnol*, 2, 72. doi: 10.3389/fbioe.2014.00072
- Gika, H., & Theodoridis, G. (2011). Sample preparation prior to the LC-MS-based metabolomics/metabonomics of blood-derived samples. *Bioanalysis*, 3(14), 1647-1661. doi: 10.4155/bio.11.122
- Haug, K., Salek, R. M., Conesa, P., Hastings, J., de Matos, P., Rijnbeek, M., . . . Steinbeck, C. (2013). MetaboLights--an open-access general-purpose repository for metabolomics studies and associated meta-data. *Nucleic Acids Res*, 41(Database issue), D781-786. doi: 10.1093/nar/gks1004
- Holman, J. D., Tabb, D. L., & Mallick, P. (2014). Employing ProteoWizard to Convert Raw Mass Spectrometry Data. *Curr Protoc Bioinformatics*, 46, 13 24 11-19. doi: 10.1002/0471250953.bi1324s46
- Kessner, D., Chambers, M., Burke, R., Agus, D., & Mallick, P. (2008). ProteoWizard: open source software for rapid proteomics tools development. *Bioinformatics*, 24(21), 2534-2536. doi: 10.1093/bioinformatics/btn323
- Kim, H. K., & Verpoorte, R. (2010). Sample preparation for plant metabolomics. *Phytochem Anal*, 21(1), 4-13. doi: 10.1002/pca.1188
- Kuhl, C., Tautenhahn, R., Bottcher, C., Larson, T. R., & Neumann, S. (2012). CAMERA: an integrated strategy for compound spectra extraction and annotation of liquid chromatography/mass spectrometry data sets. *Anal Chem*, 84(1), 283-289. doi: 10.1021/ac202450g
- Nicholson, J. K., Lindon, J. C., & Holmes, E. (1999). 'Metabonomics': understanding the metabolic responses of living systems to pathophysiological stimuli via multivariate statistical analysis of biological NMR spectroscopic data. *Xenobiotica*, 29(11), 1181-1189. doi: 10.1080/004982599238047
- Rocca-Serra, P., Brandizi, M., Maguire, E., Sklyar, N., Taylor, C., Begley, K., . . . Sansone, S. A. (2010). ISA software suite: supporting standards-compliant experimental annotation and enabling curation at the community level. *Bioinformatics*, 26(18), 2354-2356. doi: 10.1093/bioinformatics/btq415

- Smith, C. A., Want, E. J., O'Maille, G., Abagyan, R., & Siuzdak, G. (2006). XCMS: processing mass spectrometry data for metabolite profiling using nonlinear peak alignment, matching, and identification. *Anal Chem*, 78(3), 779-787. doi: 10.1021/ac051437y
- The R Core Team. (2014). R: A Language and Environment for Statistical Computing. Vienna, Austria: R Foundation for Statistical Computing.
- Theodoridis, G., Gika, H., Franceschi, P., Caputi, L., Arapitsas, P., Scholz, M., . . . Mattivi, F. (2012). LC-MS based global metabolite profiling of grapes: solvent extraction protocol optimisation. *Metabolomics*, 8(2), 175-185. doi: 10.1007/s11306-011-0298-z
- Theodoridis, G. A., Gika, H. G., Want, E. J., & Wilson, I. D. (2012). Liquid chromatography-mass spectrometry based global metabolite profiling: a review. *Anal Chim Acta*, 711, 7-16. doi: 10.1016/j.aca.2011.09.042
- Wehrens, R., Weingart, G., & Mattivi, F. (2014). metaMS: an open-source pipeline for GC-MS-based untargeted metabolomics. *J Chromatogr B Analyt Technol Biomed Life Sci*, 966, 109-116. doi: 10.1016/j.jchromb.2014.02.051
- Worley, B., & Powers, R. (2013). Multivariate analysis in metabolomics. *Current Metabolomics*, 1(1), 92-107.

#### **Acknowledgment of activities undertaken**

The preparation of samples and QCs for LC-MS analysis was undertaken by the author. The LC-MS analysis was then run by Dr Mattia Gasperotti and Dr Marynka Ulaszewska at the Metabolomics platform within the Food and Quality Nutrition Department of Fondazione Edmund Mach (FEM). The pre-processing, pre-treatment and the statistical analysis of the untargeted LC-MS data were undertaken by the author under the supervision of Dr Pietro Franceschi. PK analysis was conducted by the author.

**Section III - Development and  
characterization of a SERS method for the  
assessment of ROS/RNS in living cells**



# **Chapter 6. Reactive oxygen species detection in aqueous environments with SERS-based nanosensors**

## **Chapter Overview**

In this chapter we propose a novel SERS-based nanosensor (NS) for the detection of ROS in aqueous environments. The NS was based on gold nanoparticles (AuNPs), a widely used substrate due to its ease of preparation and efficient enhancement of Raman signal (Munro et al., 1995). NS were obtained by coating citrate-reduced AuNPs with oxidation-sensitive reporter molecules. Three SERS active molecules, namely 6-Amino-6'-hydroxy-3H-spiro[2-benzofuran-1,9'-xanthene]-3,3'(9a'H)-dione (6AF), 1,2-Diamino-9,10-anthraquinone (DAQ), and 2,3-Naphthalenediamine (DAN), were used in this work. Various ROS/RNS can induce a chemical change in the structure of the molecules adsorbed onto the surface of gold nanoparticles (Au-NPs), and hence reflected in SERS fingerprint. The preparation of 6AF-, DAQ-, and DAN-coated Au nanoparticles (6AF-, DAQ- and DAN-AuNPs), their characterization using UV-Vis spectrophotometry and SERS spectroscopy, and their applicability as sensors for ROS/RNS detection are reported here. All of them have been found to undergo oxidation reaction in buffered aqueous solutions, but only the 6AF-AuNPs could be shown to be an efficient SERS sensor, so allowing the measurement of specific ROS/RNS under versatile experimental conditions.

## Experimental section

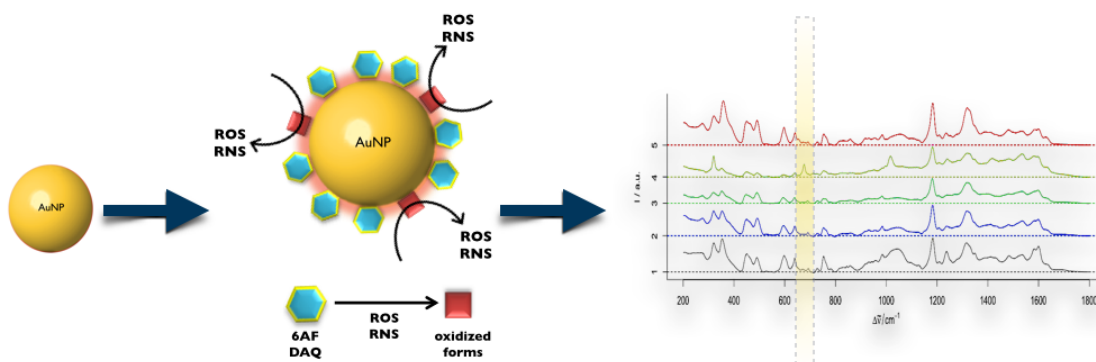


Figure 6.1 Schematic diagram of the SERS-based nanosensor for sensing  $O_2^{\bullet-}$ .

### Materials

Sodium tetrachloroaurate (III) dehydrate ( $AuCl_4 \cdot Na_2H_2O$ ), sodium citrate tribasic dihydrate ( $Na_3C_6H_5O_7 \cdot 2H_2O$ ), 6-Amino-6'-hydroxy-3H-spiro[2-benzofuran-1,9'-xanthene]-3,3'(9a'H)-dione (6AF,  $C_{20}H_{13}NO_5$ ), 1,2-Diamino-9,10-anthraquinone (DAQ,  $C_{14}H_{10}N_2O_2$ ), 2,3-Naphthalenediamine (DAN,  $C_{10}H_8N_2$ ), 1,4,7,10,13,16-Hexaoxacyclooctadecane (18-Crown-6,  $C_{12}H_{24}O_6$ ), potassium superoxide ( $KO_2$ ), 2,2-Azobis(2-amidinopropane) dihydrochloride (ABAP,  $[=NC(CH_3)2C(=NH)NH_2]_2 \cdot 2HCl$ ), hydrogen peroxide ( $H_2O_2$ ), ethanol (EtOH) and all solvents used were purchased from Sigma-Aldrich and used without further purification. Peroxynitrous acid, sodium salt ( $ONO_2 \cdot Na$ ) in 0.3 M NaOH solution was purchased from Cayman Chemicals (Ann Arbor, MI). MilliQ water was used for the preparation of all solutions.

Hank's balanced salt solution (HBSS) was purchased from EuroClone (Wetherby West, Yorkshire, UK). Dulbecco's Modified Eagle's Medium (DMEM), and Roswell Park Memorial Institute medium (RPMI) 1640, were obtained from Gibco, Invitrogen (Paisley, Scotland, UK). Phosphate buffered saline (PBS) was prepared as following: 6.03 mM  $Na_2HPO_4$ , 3.91 mM  $NaH_2PO_4$  and 139 mM NaCl (Carlo Erba, Milan, Italy) were dissolved in MilliQ water

and pH was adjusted to 7.4 with HCl. CaF<sub>2</sub> microscope slides were purchased from Crystal GmbH (Berlin, Germany).

### **Raman Instrumentation**

Spectroscopic measurements were done using an InVia Raman system (Renishaw, Wotton-under-Edge, UK). The sample was deposited, as pure powder or in the form of a 50  $\mu$ L drop, on a UV-grade CaF<sub>2</sub> microscope slide and put under the Raman microscope. The laser source (785 nm, 200 mW, diode laser) was focused on the sample, with a 10x objective (N.A. 0.25), and the Raman spectrum was collected with a 10s exposure.

### **Cit-AuNPs preparation**

The synthesis was performed using the Turkevich/Frens method (Turkevich et al., 1951), with slight modifications. Briefly, in a 250 mL round-bottom flask equipped with a condenser, 90 mL of mQ water was brought to boil and 10 mL of 0.1% HAuCl<sub>4</sub> was added under vigorous stirring for 1 minute. Rapid addition of 4 mL of 1% sodium citrate solution to the stirred gold chloride solution resulted in a color switch from pale yellow to dark wine red. The color switch occurred over several minutes. The solution was maintained for 30 minutes at boiling temperature and then removed from the heating bath. Stirring was continued until the solution reached room temperature. This pure solution of citrate-capped gold nanoparticles (Cit-AuNPs) was then used for the further functionalization.

### **Preparation of functionalized-AuNPs**

#### ***Preparation of Au-nanoparticles coated with 6-Amino-6'-hydroxy-3H-spiro[2-benzofuran-1,9'-xanthene]-3,3'(9a'H)-dione (6AF)***

A 6AF stock solution was prepared dissolving 6AF in dehydrated methanol to obtain a final concentration of 3 mM. 6AF solutions were prepared by properly diluting the stock solution with mQ water, or phosphate buffered solution (PBS, pH 7.4) to achieve the desired final concentration (300 nM - 300  $\mu$ M). Extreme care was taken to avoid 6AF photo-degradation upon light exposure: all dilutions were done in a dark room with red safelight illumination.

Then, 50 mL of the 6AF solution were added to 50 mL of Cit-AgNPs previously diluted 1:25 with mQ water. To remove 6AF excess, the mixture was centrifuged in 1.5 mL polypropylene eppendorf tubes at 6708 x g for 20 minutes, the supernatant was removed and fresh mQ water was added. This washing procedure was repeated 3 times.

#### ***Preparation of Au-nanoparticles coated with 1,2-Diamino-9,10-anthraquinone (DAQ)***

A DAQ stock solution was prepared dissolving DAQ in in anhydrous dimethyl sulfoxide to obtain a final concentration of 5 mM. DAQ solutions were prepared by properly diluting the stock solution with mQ water, or phosphate buffered solution (PBS, pH 7.4) to achieve the desired final concentration (500 nM - 500  $\mu$ M). Extreme care was taken to avoid DAQ photo-degradation upon light exposure: all dilutions were done in a dark room with red safelight illumination.

Then, 50 mL of the DAQ solution were added to 50 mL of Cit-AgNPs previously diluted 1:25 with mQ water. In order to remove DAQ excess, the mixture was centrifuged in 1.5 mL polypropylene eppendorf tubes at 6708 x g for 20 minutes, the supernatant was removed and fresh mQ water was added. This washing procedure was repeated 3 times.

#### ***Preparation of Au-nanoparticles coated with 1,2-Naphthalenediamine (DAN)***

A DAN stock solution was prepared dissolving 6AF in in anhydrous dimethyl sulfoxide to obtain a final concentration of 7 mM. DAN solutions were prepared by properly diluting the stock solution with mQ water, or phosphate buffered solution (PBS, pH 7.4) to achieve the desired final concentration (700 nM - 700  $\mu$ M). Extreme care was taken to avoid DAN photo-degradation upon light exposure: all dilutions were done in a dark room with red safelight illumination.

Then, 50 mL of the DAN solution were added to 50 mL of Cit-AgNPs previously diluted 1:25 with mQ water. In order to remove DAN excess, the mixture was centrifuged in 1.5 mL polypropylene eppendorf tubes at 6708 x g for 20 minutes, the supernatant was removed and fresh mQ water was added. This washing procedure was repeated 3 times.

## **Nanoparticles characterization**

To check repeatability between different preparations, all colloids were characterized by UV–Visible absorption spectroscopy, using a Lambda 20bio UV–Vis spectrometer (Perkin- Elmer, Monza, Italy). UV-vis absorption spectra were acquired between 350 nm and 700 nm. Samples were prepared by diluting 10 times the citrate-reduced gold nanoparticles stock solution with mQ water in a 3 mL cuvette.

To check coating stability against aggregation in different physiological buffer, UV-vis absorption spectra were recorded on a Synergy H1 – Hybrid Multi-Detection Reader between 350 nm and 700 nm. Samples were prepared by diluting 10 times the functionalized-AuNPs solution with mQ water, PBS, HBSS, respectively, in a 96-well microplate.

## **Measurement for ROS specificity and sensitivity**

The response of the probe was measured immediately after treatment with different concentrations of the appropriate ROS or RNS at room temperature. In each case, 5  $\mu\text{L}$  of ROS/RNS (details are explained below) were added to 45  $\mu\text{L}$  of 6AF-/DAQ-/ or DAN-AuNP solution. The final oxidant concentrations were between 5 nM and 5  $\mu\text{M}$  except for  $\text{H}_2\text{O}_2$  (5 nM - 500  $\mu\text{M}$ ). All experiments were performed in quadruplicate using the 6AF-/DAQ-/DAN- AuNPs in mQ water and in PBS at 14.4  $\mu\text{M}$  (6AF), 210  $\mu\text{M}$  (DAQ), or 350  $\mu\text{M}$  (DAN) concentration. Because of the probes' pH sensitivity, the same experiments were repeated with pure 0.3 M NaOH to confirm that the observed responses were from the oxidant species and not from basic pH. This change was then subtracted from that induced by ROS/RNS.

## **Generation of ROS/RNS**

### ***Hydrogen Peroxide ( $\text{H}_2\text{O}_2$ )***

A 30% (w/w) hydrogen peroxide solution was used as received without further purification. From this solution a 0.1 M stock solution was prepared in water. This solution was prepared immediately prior to use and added to the f-AuNPs solutions to give the desired final  $\text{H}_2\text{O}_2$  concentrations (5 nM - 500  $\mu\text{M}$ ).

### ***Generation of alkyl peroxy radical (ROO<sup>•</sup>)***

Following Setsukinai's method (Setsukinai et al., 2003), ROO<sup>•</sup> was generated by thermolysis of 2,2-Azobis(2-amidinopropane)dihydrochloride (ABAP), in the solution, under elevated temperature (37° C). The estimated ROO<sup>•</sup> concentration was about 5 nM - 5 μM

### ***Superoxide anion (O<sub>2</sub><sup>•-</sup>)***

According to the method of Valentine et al. (Valentine & Curtis, 1975) O<sub>2</sub><sup>•-</sup> was generated chemically, using ionization of potassium superoxide (KO<sub>2</sub>) in aqueous solution. Briefly, 60 mg of 18-Crown-6 were dissolved in 10 mL dry DMSO and then 7 mg of KO<sub>2</sub> were quickly introduced into the flask using a syringe to avoid contact with air humidity. The mixture of reagents was stirred with a Teflon-coated magnetic stirring bar for 1 h to give a pale yellow solution of 10 mmol/L O<sub>2</sub><sup>•-</sup>. The O<sub>2</sub><sup>•-</sup> concentrated solution could be stored at 0° C for weeks without major decomposition. Superoxide anion concentration was determined by UV spectrometry at 250 nm ( $\epsilon=2686 \text{ M}^{-1}\text{cm}^{-1}$ ). The appropriate dilution of the stock solution was made to give the desired final superoxide anion concentration (5 nM - 5 μM).

### ***Peroxynitrite (ONOO<sup>-</sup>)***

The peroxynitrite stock solution (0.3 M NaOH) was diluted 100 folds in 0.3 M NaOH solution, kept in dry ice and melted for use immediately before the experiment. The actual concentration of peroxynitrite was measured by UV spectrometry at 302 nm ( $\epsilon=1670 \text{ M}^{-1}\text{cm}^{-1}$ ), before using it in any experiments. The appropriate dilution of the stock solution was made to give the desired final peroxynitrite concentrations (0.5 - 10 μM)

### **Data Processing**

Data were acquired using the software WiRE 3.2 (Renishaw). All data preprocessing and analysis was performed within the R software environment for statistical computing and graphics (The R Core Team, 2014). In particular, data import and export, preprocessing and visualization were performed with the hyperSpec package (Beleites & Sergio, 2014) for R, along with the ggplot2 package (Ginestet, 2011) for graphical display.

The preprocessing consisted of three steps: i) cosmic rays identification and removal, ii) baseline correction iii) smoothing interpolation and intensity vector-normalization. For the baseline correction, smoothing splines were automatically fitted through the supporting points of the whole spectral range and then subtracted from each spectrum of the dataset using function `spc.rubberband`, and peak picking was performed using `detectPeaks` from package MALDIquant (Gibb & Strimmer, 2012).

For O<sub>2</sub><sup>•-</sup>-quantification, the intensity at the maximum of the 680 cm<sup>-1</sup> band of the 6AF SERS spectrum was chosen for calibration purposes. The calibration curve, the 95% confidence interval for the calibration, the limit of detection (LOD) and the limit of quantification (LOQ) were calculated using chemCal (Ranke, 2014). The use of weighted regression for calibration was considered and checked, but it was found not necessary, as the standard deviation of SERS intensity was not increasing with concentration in the interval used for calibration.

## Results and discussion

In SERS, the laser irradiation of gold nanoparticles can induce localized surface plasmon resonances (SPRs) at a nanostructured surface, which generates enhanced electromagnetic fields. If molecules are brought into close proximity to such nanoparticles (e.g., via adsorption), a large enhancement of the Raman scattering signal can be observed.

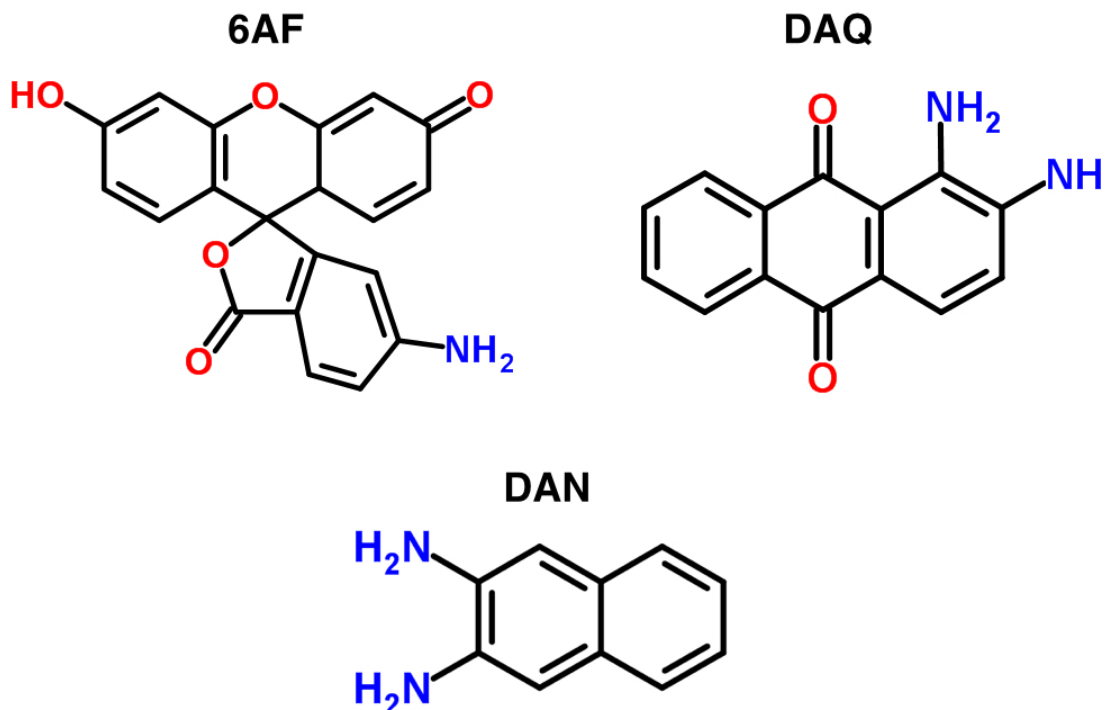


Figure 6.2 Structures of the three probes.

The molecular structure of solid 6-amino-6'-hydroxy-3H-spiro[2-benzofuran-1,9'-xanthene]-3,3'(9a'H)-dione (6AF), 1,2-diamino-9,10-anthraquinone (DAQ), and 2,3-naphthalenediamine (DAN) are presented in Figure 2, and their Raman spectra at a 785-nm excitation wavelength appear Figures 3, 4, and 5, respectively. Raman spectra were also acquired at 514 nm (data not shown), at which a strong fluorescence background was recorded as might be expected considering the intense color of the aqueous solutions of 6AF, DAQ, and DAN. SERS characterizations of 6AF, DAQ, and DAN were obtained under different experimental settings with various outcomes.

Keeping in mind our final goal of ROS/RNS intracellular detection, we selected probes that are best excited in the near-infrared region (785 nm) to reduce the native fluorescence background and take advantage of this particularly convenient feature for studying biological



specimens (i.e., low autofluorescence of proteins, robust tissue penetration) (Weissleder, 2001).

To probe our proposed mechanism for ROS/RNS detection, we used Raman spectroscopy to characterize the reporter molecules on gold nanoparticle (AuNP) surfaces. Raman spectroscopy can characterize the vibrational modes of individual bonds and offers insight into chemical structure. Its signals were easily detected in our experiments owing to the surface-enhanced Raman scattering by molecules on the plasmonic gold surfaces.

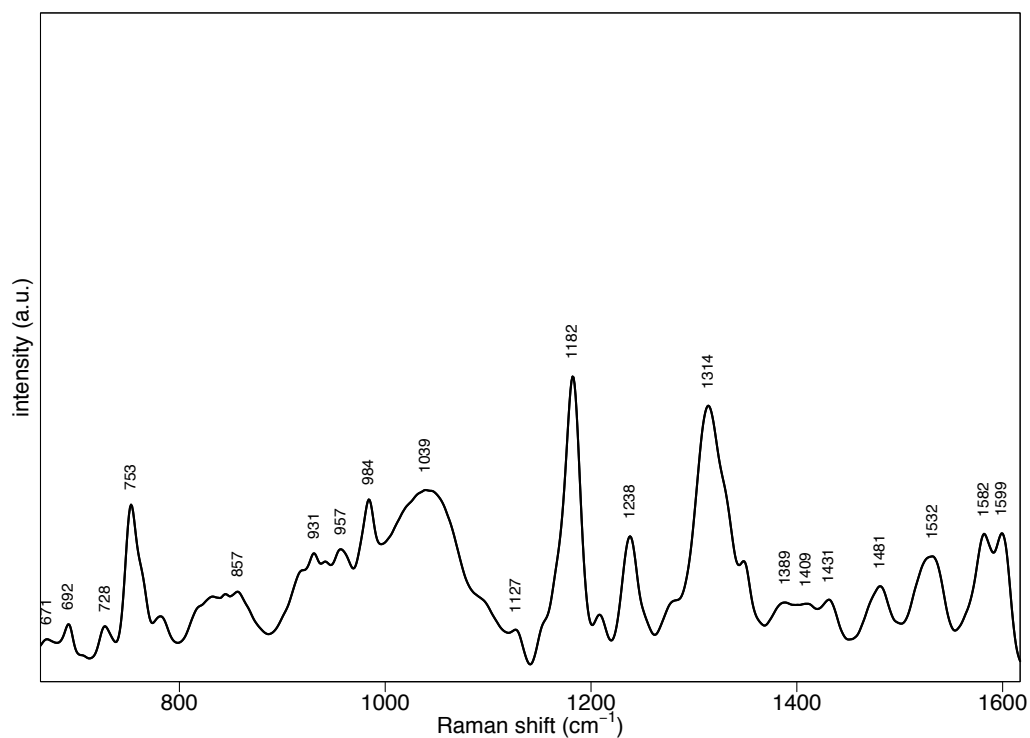


**Figure 6.3 SERS of 6AF solution in PBS.**

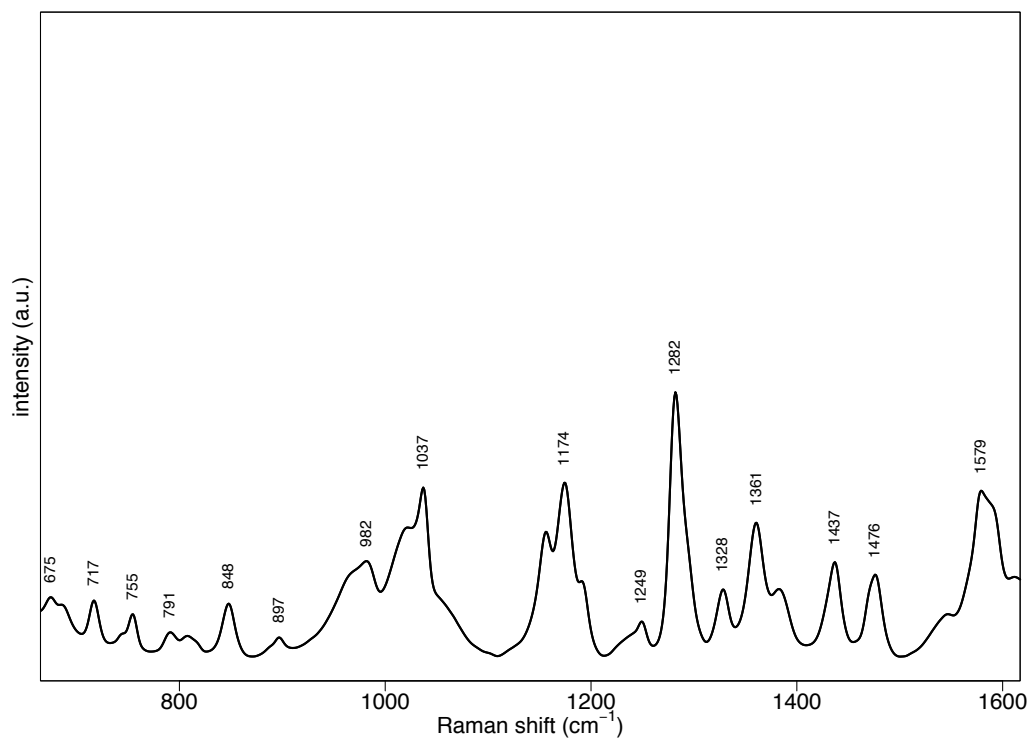


Figure 6.4 SERS of DAQ solution in PBS

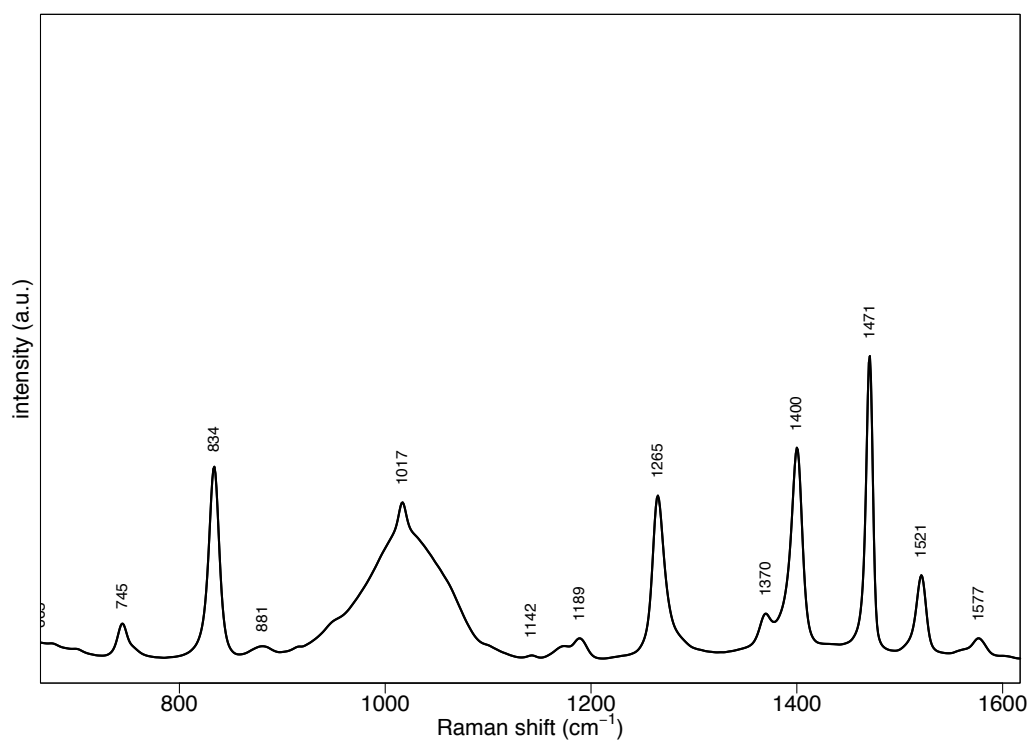


Figure 6.5 SERS of DAN solution in PBS.

## Characterization

AuNPs exhibit surface plasmons sensitive to the size, coating, and polydispersity of AuNPs in solution (Eustis & El-Sayed, 2006; Glomm, 2005). Hence, some information about AuNPs can be obtained by examining the SPR peak present on their absorption spectra.

Citrate AuNPs had an absorption maximum at 535 nm, which indicated that the average diameter of the nanoparticles was approximately 50 nm, consistent with previously reported values (He et al., 2005). This estimation, obtained using the ratio  $A_{\lambda_{\max}}/A_{\lambda_{450}}$ , applied only to AuNPs coated with citrate, and therefore could not be used for 6AF-, DAQ-, or DAN-coated AuNPs. However, the SPR peak of the latter nanoparticles showed a slight shift with respect to those of the citrate-reduced nanoparticles, so the size of 6AF-, DAQ-, or DAN-coated AuNPs was interpreted to have changed during the ligand-exchange reaction. This assumption was checked with subsequent SERS experiments.

## Ligand exchange

The stabilization of AuNPs originates from Au/ligand interaction at the gold particle surface. Citrate is one of the weakest ligands, providing only limited stability to the nanoparticles. On the contrary, the interaction at the AuNP surface is increasingly stronger with phosphine, amine, and thiol functions (Leff et al., 1996).

Because 6AF, DAQ, and DAN contain a primary amine, they were expected to produce relatively stable AuNPs via direct interaction of their amino groups with AuNP surface atoms. Thus, no modification of the ligands was required. Owing to their stronger interaction (compared with that of citrate) with gold, the amine groups of 6AF, DAQ, and DAN readily displaced citrate from the surface of previously prepared citrate-reduced AuNPs.

To determine the ligand concentration yielding the best SERS signal, we collected a series of SERS spectra for various concentrations of the three coating agents and obtained curves depicting the intensity of the band with the highest signal in the SERS spectrum as a function of ligand concentration. The characteristic vibrational modes of each ligand began to appear and increase in intensity as a consequence of the increasing extent of AuNP coating.

The 6AF SERS intensities at  $1182\text{ cm}^{-1}$  as a function of 6AF concentration are reported in Figure 5A. The 6AF curve has a slope factor of 1.718 at concentrations below  $10^{-5}\text{ M}$ . At high concentrations, the working curve approaches a limiting value, presumably corresponding to

surface saturation. Above this value, large but less reproducible SERS signal intensities were observed.

The DAQ SERS intensities at  $1282\text{ cm}^{-1}$  as a function of DAQ concentration are reported in Figure 5B. As shown in the figure, the curve is very steep. The DAN SERS intensities at  $834\text{ cm}^{-1}$  as a function of DAN concentration are reported in Figure 5C. The intensity did not vary appreciably as a function of DAQ and DAN concentrations, and the intensity values showed large dispersions.

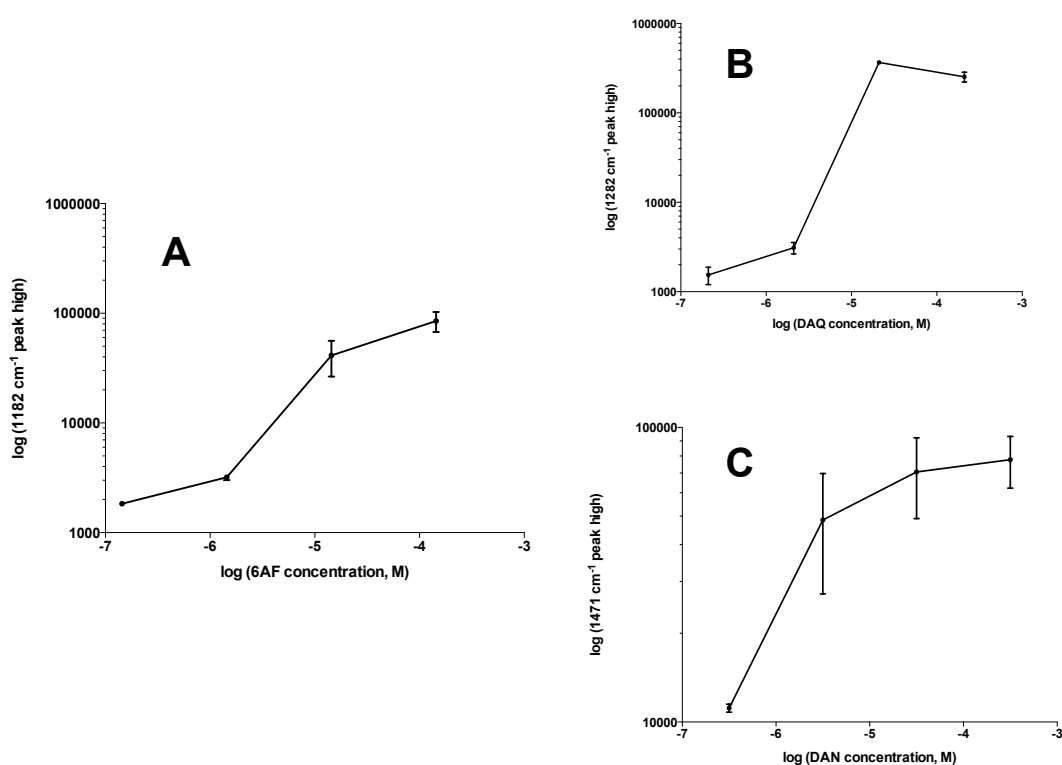


**Figure 6.6** A. Concentration dependence of the 6AF 1182 SERS intensity. B. Concentration dependence of the DAQ 1282 SERS intensity. C. Concentration dependence of the DAN 1471 SERS intensity. Each data point represents the average intensity of the characteristic peak from four spectra. The standard deviation is shown by the error bars (n=4).

### **Specificity and sensitivity of ROS detection**

To evaluate oxidation-dependent changes in vibrational modes, we incubated 6AF-, DAQ-, and DAN-AuNPs with various biologically relevant reactive species including,  $O_2^{\bullet-}$ , hydrogen peroxide, ABAP (for alkyl peroxy radical  $[ROO^{\bullet}]$  and peroxynitrite  $[ONOO^{\bullet-}]$ ). All of these reporter molecules underwent oxidation reactions in buffered aqueous solutions, which changed their structures and were in turn reflected in the specific spectral differences shown in Figures 6 and 7.

Repeatable concentration-dependent changes were identified only in the 6AF SERS spectrum after the addition of  $O_2^{\bullet-}$ , which revealed the sensibility of the nanosensor (NS) for the superoxide anion radical. Thus, to verify the feasibility of this method for quantitative analysis, we collected a series of SERS spectra only for  $O_2^{\bullet-}$  at various concentrations and constructed a calibration curve (i.e., SERS intensity as a function of concentration). The maximum intensity of the  $680\text{ cm}^{-1}$  band of the 6AF SERS spectrum was chosen for calibration purposes. The concentration-dependent calibration curves for the in vitro detection efficiency of 6AF-AuNPs for various ROS/RNS are presented in Figure 8.

The lowest  $O_2^{\bullet-}$  concentration measured was 1 nM, which is on the same order of magnitude as that of the lowest concentration previously reported in results obtained with other techniques (Woolley et al., 2013). For concentrations between 1 nM and 1  $\mu\text{M}$ , the correlation between spectrum intensity and superoxide anion radical concentration was linear (Figure 8), with a coefficient of determination ( $R^2$ ) of 0.9935. For concentrations lower than 1 nM, the spectrum showed no  $O_2^{\bullet-}$  vibrational bands. The limit of detection (the lowest quantity of analyte that can be distinguished from a blank value within a stated confidence limit) and limit of quantification (the lowest amount of analyte in a sample that can be quantitatively determined with suitable precision and accuracy) calculated from the calibration curve were 103 nM and 229 nM, respectively.

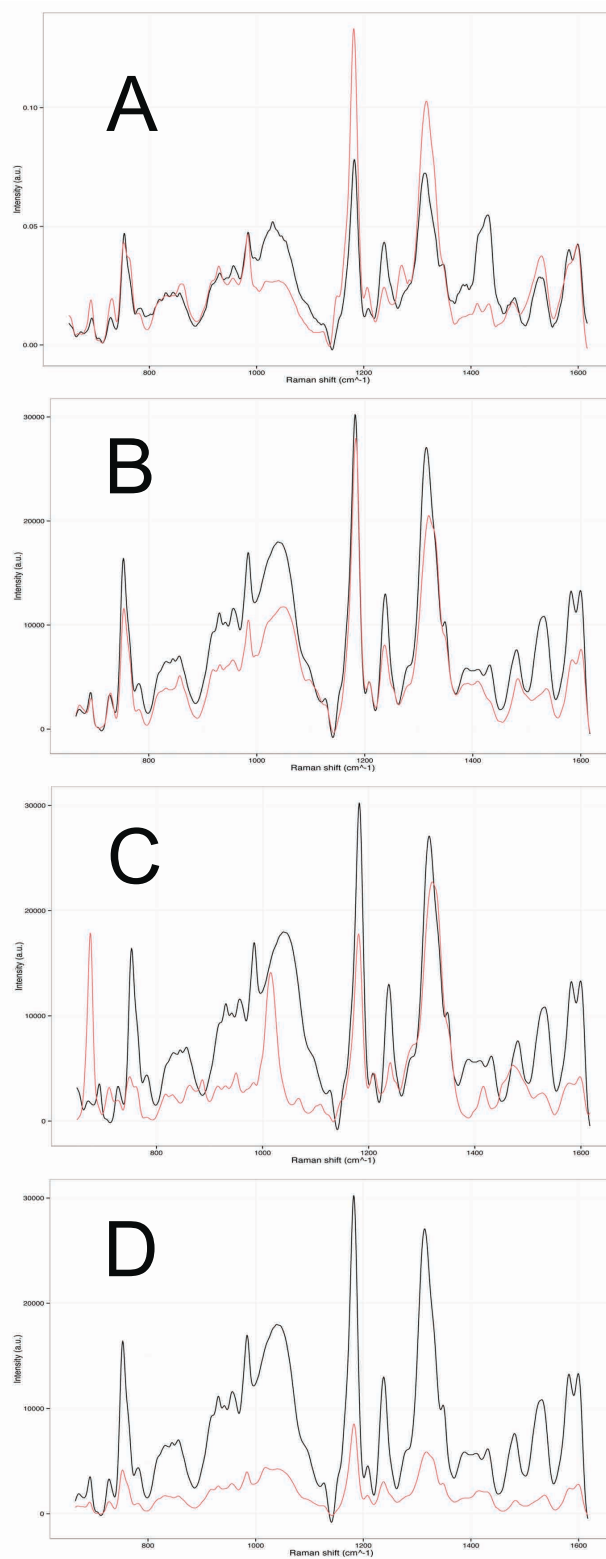
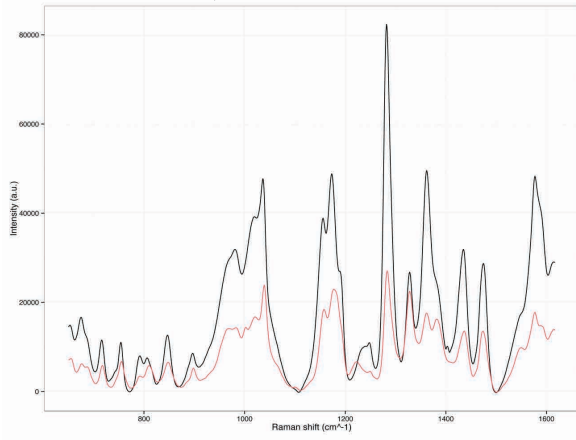


**Figure 6.7** Representative SERS spectra observed for 6AF-AuNPs under different redox conditions. **A.** ABAP; **B.** ONOO; **C.** O<sub>2</sub><sup>\*-</sup>; **D** H<sub>2</sub>O<sub>2</sub>.

# DAQ



# DAN

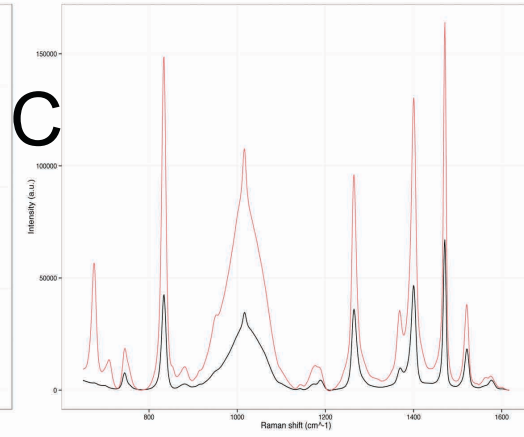
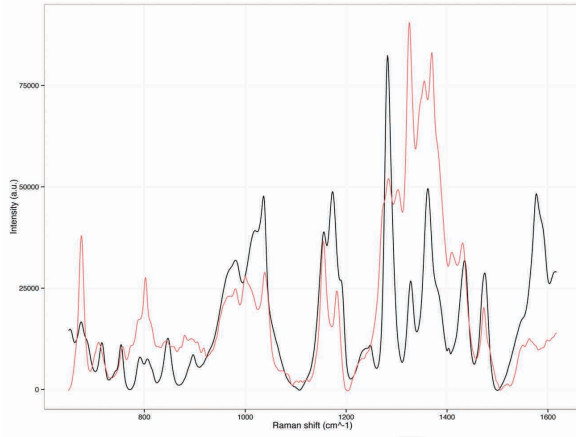
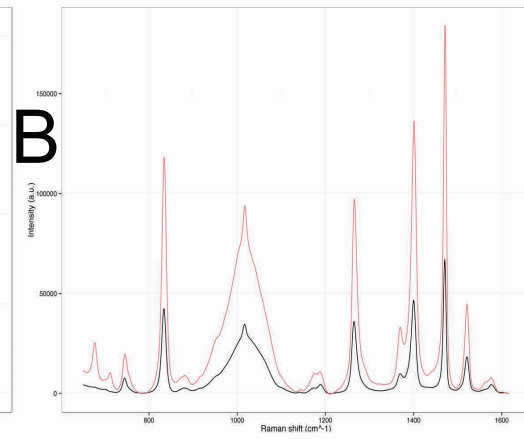
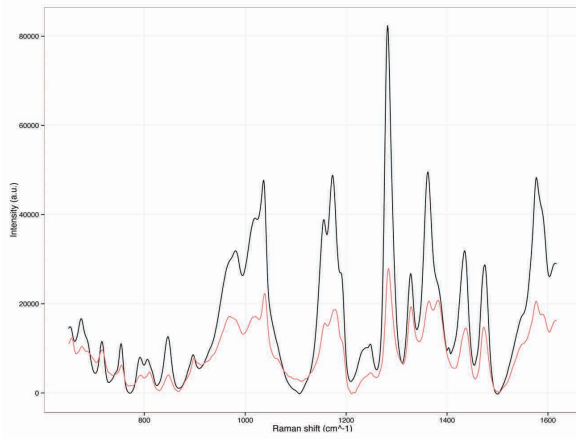
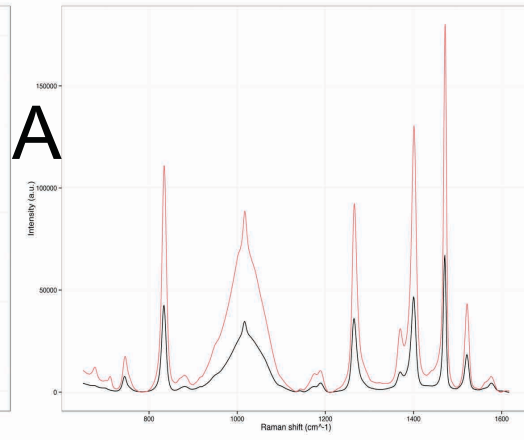


**Figure 6.8** Representative SERS spectra observed for DAQ-/ and DAN-AuNPs under different redox conditions. **A.** O<sub>2</sub>\*-; **B.** H<sub>2</sub>O<sub>2</sub>; **C.** ONOO<sup>-</sup>.

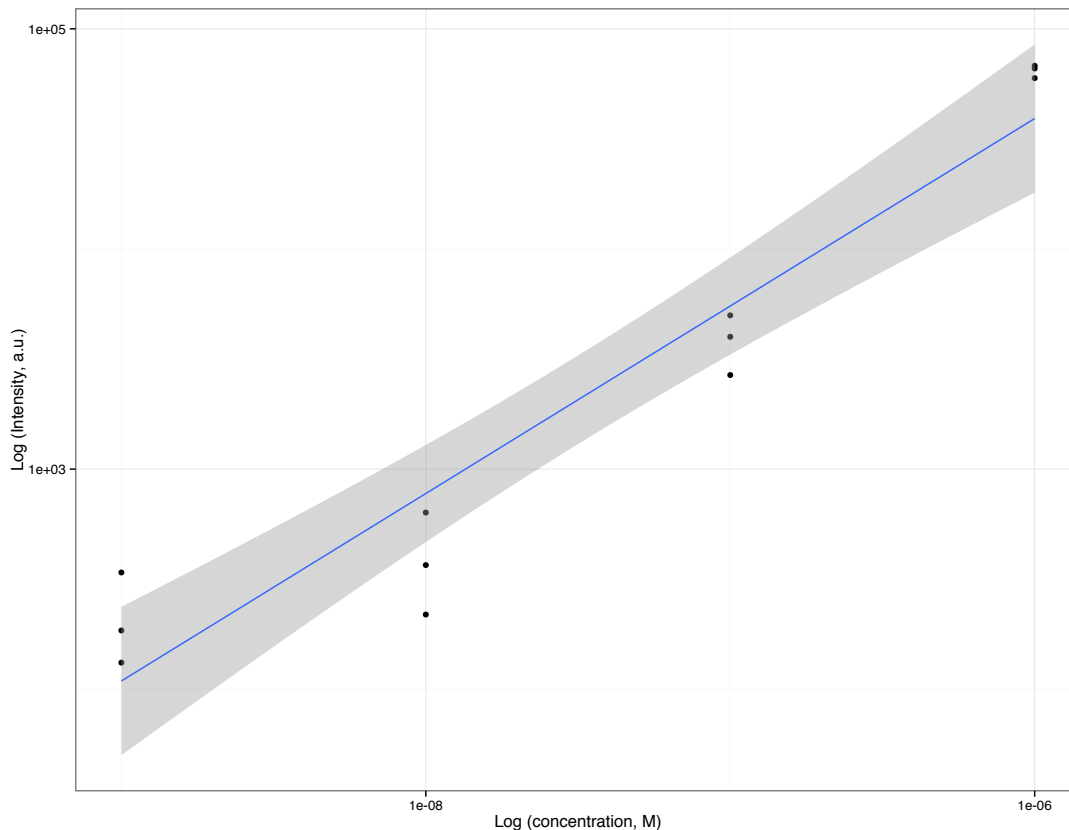


**Figure 6.9** Calibration curve on a log-log scale of  $680\text{ cm}^{-1}$  band peak intensity vs.  $O_2^{\bullet-}$  concentrations. The solid line is the linear fitting line, with the 95 % confidence interval for the calibration (gray shadow).

### Stability in physiological buffer

Keeping in mind our final goal of ROS/RNS intracellular detection using the SERS-based NS, we tested their stability in several physiological buffered solutions and cell culture media. 6AF-capped gold nanoparticles showed no sign of aggregation, even after few hours, differently from what seen with cit-AuNPs. This result confirms the exchange of citrate with 6AF and opens the possibility of using the NS for cellular applications. Table 1 reports the absorption maximum of 6AF-AuNPs recorded over prolonged periods of time in mQ water, PBS, HBSS, DMEM and RPMI, respectively.



**Table 6.1 Absorption maximum of 6AF-AuNPs over prolonged periods of time.**

	<b>mQ water</b>	<b>PBS</b>	<b>HBSS</b>	<b>DMEM</b>	<b>RPMI</b>
10 min	560 nm	588 nm	558 nm	588 nm	588 nm
5hour	560 nm	560 nm	560 nm	560 nm	560 nm
10hour	560 nm	560 nm	560 nm	560 nm	560 nm
24hour	560 nm	560 nm	560 nm	560 nm	560 nm
72 hour	560 nm	560 nm	560 nm	560 nm	560 nm

## **Conclusions**

6AF-coated AuNPs were prepared, and consistent results of SERS analysis showed that they exhibited selective and concentration-dependent signals after exposure to for  $O_2^{\cdot-}$ . We concluded that the detection sensitivity of the SERS-based NS for  $O_2^{\cdot-}$  had values comparable to those obtained with commonly used spectrophotometric methods. Furthermore, 6AF-AuNPs exhibited good stability in physiological buffered solutions and cell culture media. These results open the possibility of using these SERS-based NSs to study the production of ROS inside single living cells. Furthermore, a refinement of this method may allow for the multimodal analysis of a complex array of ROS/RNS. The potential for studying the dynamic relations between, for instance, superoxide and hydrogen peroxide, would greatly advance knowledge of redox dynamics.

## Bibliographic references

- Beleites, C., & Sergio, V. (2014). HyperSpec: a package to handle hyperspectral data sets in R. *R package version 0.98-20140523*.
- Eustis, S., & El-Sayed, M. A. (2006). Why gold nanoparticles are more precious than pretty gold: Noble metal surface plasmon resonance and its enhancement of the radiative and nonradiative properties of nanocrystals of different shapes. *Chem Soc Rev*, 35(3), 209. doi: 10.1039/b514191e
- Gibb, S., & Strimmer, K. (2012). MALDIquant: a versatile R package for the analysis of mass spectrometry data. *Bioinformatics*, 28(17), 2270-2271. doi: Doi 10.1093/Bioinformatics/Bts447
- Ginestet, C. (2011). ggplot2: Elegant Graphics for Data Analysis. *Journal of the Royal Statistical Society Series a-Statistics in Society*, 174, 245-245. doi: Doi 10.1111/J.1467-985x.2010.00676\_9.X
- Glomm, W. R. (2005). Functionalized gold nanoparticles for applications in bionanotechnology. *Journal of Dispersion Science and Technology*, 26(3), 389-414. doi: Doi 10.1081/Dis-200052457
- He, Y. Q., Liu, S. P., Kong, L., & Liu, Z. F. (2005). A study on the sizes and concentrations of gold nanoparticles by spectra of absorption, resonance Rayleigh scattering and resonance non-linear scattering. *Spectrochimica Acta Part a-Molecular and Biomolecular Spectroscopy*, 61(13-14), 2861-2866. doi: Doi 10.1016/J.Saa.2004.10.035
- Leff, D. V., Brandt, L., & Heath, J. R. (1996). Synthesis and characterization of hydrophobic, organically-soluble gold nanocrystals functionalized with primary amines. *Langmuir*, 12(20), 4723-4730. doi: Doi 10.1021/La960445u
- Munro, C. H., Smith, W. E., Garner, M., Clarkson, J., & White, P. C. (1995). Characterization of the Surface of a Citrate-Reduced Colloid Optimized for Use as a Substrate for Surface-Enhanced Resonance Raman Scattering. *Langmuir*, 11(10), 3712-3720. doi: 10.1021/la00010a021
- Ranke, J. (2014). chemCal: Calibration functions for analytical chemistry. *R package version 0.1-34*.
- Setsukinai, K., Urano, Y., Kakinuma, K., Majima, H. J., & Nagano, T. (2003). Development of novel fluorescence probes that can reliably detect reactive oxygen species and distinguish specific species. *Journal of Biological Chemistry*, 278(5), 3170-3175. doi: Doi 10.1074/Jbc.M209264200
- The R Core Team. (2014). R: A Language and Environment for Statistical Computing. Vienna, Austria: R Foundation for Statistical Computing.
- Turkevich, J., Stevenson, P. C., & Hillier, J. (1951). A study of the nucleation and growth processes in the synthesis of colloidal gold. [10.1039/DF9511100055]. *Discussions of the Faraday Society*, 11(0), 55-75. doi: 10.1039/DF9511100055
- Valentine, J. S., & Curtis, A. B. (1975). A convenient preparation of solutions of superoxide anion and the reaction of superoxide anion with a copper (II) complex. *Journal of the American Chemical Society*, 97(1), 224-226. doi: 10.1021/ja00834a058
- Weissleder, R. (2001). A clearer vision for in vivo imaging. *Nature Biotechnology*, 19(4), 316-317. doi: Doi 10.1038/86684
- Woolley, J. F., Stanicka, J., & Cotter, T. G. (2013). Recent advances in reactive oxygen species measurement in biological systems. *Trends in Biochemical Sciences*, 38(11), 556-565. doi: 10.1016/j.tibs.2013.08.009

# **Chapter 7. Cellular response and sensor development**

## **Chapter overview**

In chapter 7 the SERS-based nanosensor (NS) have been further refined for SERS-mapping technique with the ultimate goal to enable real-time intracellular observations of ROS in living cells. Nanoparticle Tracking Analysis and TEM were performed to characterize the dimensions and the cell distribution of the NS. The biocompatibility was assessed in different cell lines and, finally, a method for monitoring differences in the presence of ROS/RNS in living cells was described.

## Experimental section

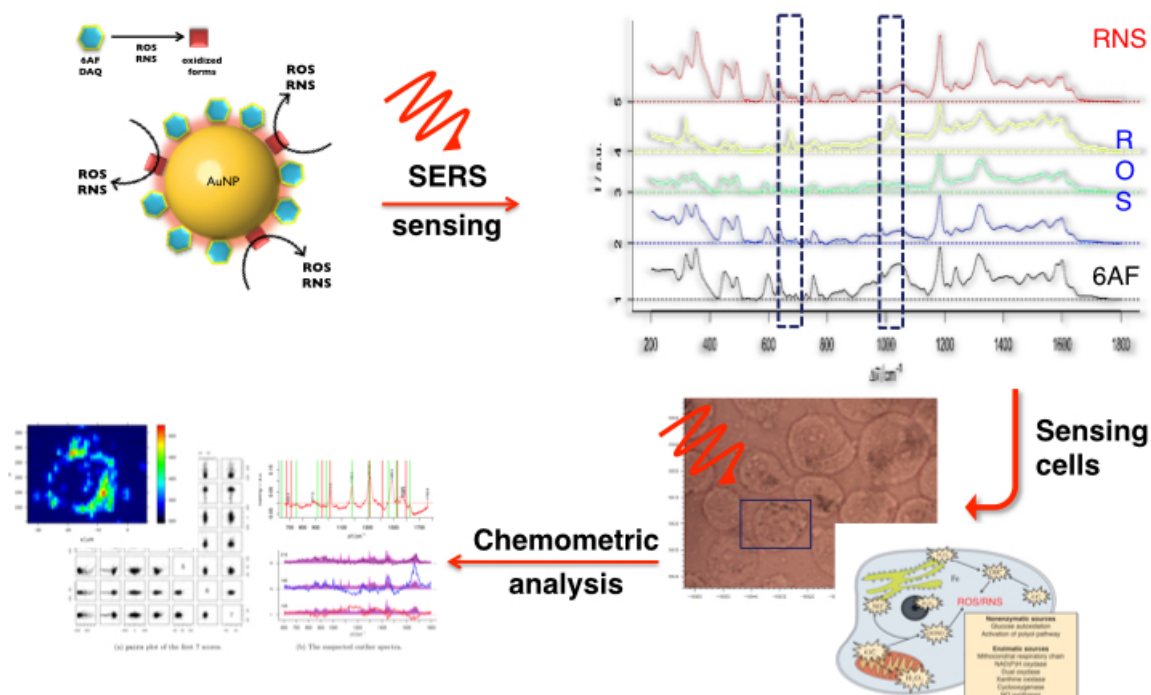


Figure 7.1 Schematic diagram of the SERS-based nanosensor development workflow for ROS sensing in living cells.

## Materials

Sodium tetrachloroaurate (III) dehydrate ( $\text{AuCl}_4\text{-Na } 2\text{H}_2\text{O}$ ), sodium citrate tribasic dihydrate ( $\text{Na}_3\text{C}_6\text{H}_5\text{O}_7 \cdot 2\text{H}_2\text{O}$ ), Thionyl chloride ( $\text{SOCl}_2$ ), 3-mercaptopropionic acid (3-MPA,  $\text{C}_3\text{H}_6\text{O}_2\text{S}$ ), 6-Amino-6'-hydroxy-3H-spiro[2-benzofuran-1,9'-xanthene]-3,3'(9a'H)-dione (6AF,  $\text{C}_{20}\text{H}_{13}\text{NO}_5$ ), 2,2-Azobis(2-amidinopropane) dihydrochloride (ABAP,  $[\text{=NC}(\text{CH}_3)\text{C}(\text{=NH})\text{NH}_2]_2 \cdot 2\text{HCl}$ ), ethanol (EtOH), and all solvents used were purchased from Sigma-Aldrich and used without further purification. Dulbecco's Modified Eagle's Medium (DMEM), Roswell Park Memorial Institute medium (RPMI) 1640, AlamarBlue® and all cell culture reagents were obtained from Gibco, Invitrogen (Paisley, Scotland, UK). HEPES-buffered Tyrode's solution (HBTS) was prepared as follow: NaCl, 150 mM; glucose, 10 mM; HEPES, 10 mM; KCl, 4.0 mM;  $\text{MgCl}_2$ , 1.0 mM;  $\text{CaCl}_2$ , 1.0 mM (purchased from Sigma-Aldrich) were dissolved in MilliQ water and pH was adjusted to 7.4 with NaOH. Milli-Q water was used for the preparation of all solutions.  $\text{CaF}_2$  microscope slides were purchased from Crystal GmbH (Berlin, Germany).

### **Cit-AuNPs preparation**

The synthesis was performed using the Turkevich/Frens method (Turkevich et al., 1951), with slight modifications. Briefly, in a 250 mL round-bottom flask equipped with a condenser, 90 mL of mQ ultrapure water was brought to boil and 10 mL of 0.1% HAuCl<sub>4</sub> was added under vigorous stirring for 1 minute. Rapid addition of 4 mL of 1% sodium citrate solution to the vigorously stirred gold chloride solution resulted in a color change from pale yellow to dark wine red. The color change occurred over several minutes. The solution was maintained for 30 minutes at boiling temperature and then removed from the heating bath. Stirring was continued until the solution reached room temperature. Before the reduction process all glassware was cleaned using concentrated HNO<sub>3</sub> and then chromic acid (2.77 g K<sub>2</sub>Cr<sub>2</sub>O<sub>7</sub> in 100 mL H<sub>2</sub>SO<sub>4</sub>), and carefully rinsed with Milli-Q water.

### **Preparation of Au-nanoparticles coated with 6-Amino-6'-hydroxy-3H-spiro[2-benzofuran-1,9'-xanthene]-3,3'(9a'H)-dione (6AF)**

30 μM 6AF aqueous solution was prepared. Then, under vigorous stirring, 50 mL of the 6AF solution were added to 50 mL of Cit-AuNPs previously diluted 1:10 with Milli-Q water. In order to remove the coating agent excess, the two mixtures were centrifuged in 1.5 mL polypropylene eppendorf tubes at 6708 x g for 20 minutes, the supernatant was removed, and fresh Milli-Q water was added. This washing procedure was repeated 3 times. The resulting coated-nanoparticles dispersion is stable against aggregation up to 72 h.

Before their use for SERS experiments, the stock dispersion of coated nanoparticles was pelleted by centrifugation and removal from each eppendorf tube of 1.3 mL of the supernatant with a micropipette, resulting in a concentrated aqueous dispersion of coated nanoparticles.

### **Nanoparticles characterization**

#### **Spectroscopic measurements**

UV-vis absorption spectra were recorded on a Synergy<sup>TM</sup> H1 – Hybrid Multi-Detection Reader between 350 nm and 700 nm. Samples were prepared by diluting 10 times the functionalized-AuNPs stock solution with different buffers in a 96-well microplate.

### **Nanoparticle-tracking Analysis**

All samples were diluted hundredfold by mQ water immediately before starting Nanoparticles Tracking Analysis (NTA). Measurements were performed under trigger mode with a NanoSight LM10 Nanoparticle Analysis System (NanoSight, Amesbury UK), equipped with a scattering cell with red laser (approx. 40 mW at  $\lambda = 638$  nm). NanoSight software version NTA 1.5 was used for data accumulation and analysis. The samples were injected into the sample chamber with 2.5 mL sterile syringes (SD Plastidek, Spain) until the liquid reached the tip of the nozzle. Data was recorded using a 20 $\times$  objective and 60-second video clips, with manual shutter and gain adjustments, but the parameters were kept at the same for all comparison samples. Three video measurements were conducted for each sample to obtain the mean size of the nanoparticles and the associated standard deviation. All measurements were performed at room temperature.

The Stokes–Einstein equation was used to calculate the sphere-equivalent hydrodynamic diameter ( $d$ , m) from the measured diffusion coefficient ( $D$ ,  $\text{m}^2 \text{s}^{-1}$ ):

$$d = \frac{kT}{3\pi\eta D}$$

where  $k$  is the Boltzmann constant ( $\text{J K}^{-1}$ ),  $\eta$  is the solvent viscosity ( $\text{kg s}^{-1} \text{m}^{-1}$ ) and  $T$  is the absolute temperature (K).

### **Raman Instrumentation**

SERS maps were collected using an InVia Raman microscope (Renishaw plc, Wotton-under-Edge, UK) equipped with high-power near infrared diode laser (Renishaw plc, and Toptica Photonics AG, Germany) delivering between 90 and 120 mW of laser power at the sample.

The  $\text{CaF}_2$  slide supporting the samples was mounted on a ProScan II motorized stage (Prior, Cambridge, UK) under the microscope.

A thermoelectrically cooled charge coupled device (CCD) camera was used for detection. Spectra of a silicon reference sample (SigmaAldrich, UK) and a neon light source (Renishaw plc, UK) were taken to calibrate the wavenumber scale. Single spectra were obtained in the 600–1700  $\text{cm}^{-1}$  region and consist of 1019 data points each. Maps were taken as previously reported (Bonifacio et al., 2010). Briefly, a manually selected region, corresponding to a single cell, was mapped with steps of 1  $\mu\text{m}$ , each spectrum of the map was obtained in 0.3 s

upon excitation with a 735 nm laser, in the 600–1800  $\text{cm}^{-1}$  region and consisted of 1272 data points. The quantity of spectra for each map varied dependent on the size of cells.

### **Cell culture**

The SH-SY5Y human neuroblastoma cell line was obtained from the American Type Culture Collection (Manassas, VA). Cells were cultured in Dulbecco's modified Eagle's medium (DMEM) supplemented with 10% (v/v) heat-inactivated fetal bovine serum (FBS), 1% (v/v) L-glutamine, 0.05 mg/mL penicillin, and 0.05 mg/mL streptomycin and were maintained at 37 °C with 95% humidified air and 5% CO<sub>2</sub>. Cells in culture dishes were used for experiments after reaching 80% confluence.

C2C12 mouse adherent myoblasts were grown in Dulbecco's modified Eagle's medium (DMEM) supplemented with heat-inactivated 10% fetal bovine serum (FBS), 2mM L-glutamine, 0.05 mg/mL penicillin, and 0.05 mg/mL streptomycin, 0.5% anti-mycoplasma and 25 mM Hepes, and were maintained at 37 °C with 95% humidified air and 5% CO<sub>2</sub>.

Human endothelial-like immortalized cells (EA.hy926) were cultured in DMEM supplemented with 10% (v/v) heat-inactivated fetal calf serum (FCS), 1% (v/v) L-glutamine, 0.05 mg/mL penicillin, and 0.05 mg/mL streptomycin. Cultures and were maintained at 37 °C with 95% humidified air and 5% CO<sub>2</sub>.

CRL-2278 RAW 264.7 gamma NO(-) murine monocytic/macrophagic cell line was purchased from American Type Culture Collection (ATCC, Rockville, MD). CRL-2278 RAW 264.7 gamma NO(-) cells were cultured in a 24-well plate at a density of  $1 \times 10^5$  cells/mL in RPMI-1640 medium with 2 mM L-glutamine and modified to a final concentration of 4.5 g/L glucose, 1.5 g/L sodium bicarbonate, 10 mM Hepes, 1 mM sodium pyruvate, and 10% (v/v) fetal bovine serum (FBS).

### **Toxicity Assay**

The cytotoxicity of various concentrations of 6AF-AuNPs was evaluated using AlamarBlue<sup>®</sup> (Invitrogen) assay, according to the manufacturer's suggestions. Viable cells convert the cell permeable nonfluorescent oxidized compound resazurin to the highly fluorescent- reduced resorufin, which is an indicator of cellular metabolic activity.

This assay is commonly used to determine the extent of cell viability in cultures after various treatments (Rampersad, 2012). Briefly, cells were grown in a 96-well plate in 100  $\mu$ L of DMEM supplemented with FBS. After 24 h seeding, cells were incubated with various concentrations (from 2 nM to 200  $\mu$ M) of 6AF-modified gold probes for 44 h, and cell viability assay was carried out. After treatments, the assay was performed by replacing the culture media with a 10% AlamarBlue solution in DMEM. Reduction of AlamarBlue was determined spectrophotometrically after 3-4 h. (excitation 440 nm, emission 485 nm). The untreated cells were used as a positive control (i.e., 100% viable), and all values from the experiment were correlated with this set of data. The results were analyzed either by one-way or two-way ANOVA followed by Bonferroni's multiple comparison tests.

### **Cellular Uptake**

Cellular uptake was mainly analyzed by transmission electron microscopy (TEM). In TEM, an image is generated from the electrons beam transmitted through the specimen after the interactions between the electrons and specimen (Hawkes, 1985). This technique enables one to verify fine structures as small as an atom owing to the small wavelength of electrons. For TEM analysis cells were grown on coverslips under the same conditions as for Raman spectroscopy. Briefly, cells were grown in a 6-well tissue culture plate at a concentration of  $4.4 \times 10^6$  and were incubated overnight with 6AF-AuNPs ( $5.0 \times 10^8$  particles/mL) in FBS-free media to allow uptake of the nanosensors. After a brief rinse in PBS, cells attached to a glass surface were fixed with 2.5% glutaraldehyde in 0.1M phosphate buffer, pH 7.3, for 10min at room temperature, and then for 20min at 41C. Cells were then rinsed in 0.1 M PBS, pH 7.3, post fixed with 1% osmium tetroxide in the same buffer for 1h at 4° C, dehydrated in ascending alcohols, and then treated with propylene oxide. After embedding in Araldite (Electron Microscopy Sciences, Ft. Washington, PA, USA), ultrathin sections of the cell were cut with a Reichert OM ultramicrotome. Sections were stained with uranyl and lead citrate, and then examined with an electron microscope Jeol 100S (JEOL, Peabody, MA, USA). The image-analysis tool JMicroVision version 1.2.7 ([www. jmicrovision.com](http://www.jmicrovision.com)) was used for analysis of TEM images (Roudit N. JMicroVision: image analysis toolbox for measuring and quantifying components of high-definition images. Version 1.2.7. 2008. Available from: <http://www.jmicrovision.com>. Accessed June 16, 2014).



### **Intracellular SERS experiments**

All SERS mapping experiments were made using living cells, according to the literature (Palonpon et al., 2013). Briefly, 10 000 cells were seeded on a 25 x 25 x 1mm CaF<sub>2</sub> coverslip in a cell culture dish (6 cm in diameter) containing DMEM and incubated for two days at 37° C in a humidified 5% CO<sub>2</sub> atmosphere. AuNPs or 6AF-AuNPs were added to FBS-free DMEM (to a final concentration of 0.45 - 5.0 x 10<sup>8</sup> particles/mL) and incubated with cells overnight. The next day before SERS measurements, cells were rinsed three times with HBTS to remove excess of nanoparticles in the medium. Typical cell medium containing phenol red, has fluorescence that hinders the Raman signals. In addition, various types of biomolecules in the serum can be a source of possible background signal for SERS mapping. Thus, during SERS mapping, the cell culture medium was replaced with HBTS. Two control experiments were carried out to exclude auto fluorescence of cells and to exclude the contribution of normal Raman signal of the dye non-conjugated to AuNPs.

### **Antioxidant screening**

For antioxidant screening experiment, Cyanidin 3-glucoside (C3G) was always freshly dissolved in DMSO and used immediately. The final concentration of DMSO in the culture medium during different treatments was <0.1% (v/v). Sub-confluent cells were treated for 1 h in serum-free medium with 25 µM of C3G, whereas all control cells were treated with 0.1% DMSO only. After this incubation time, cells were washed three times with HBTS under sterile conditions, to avoid the presence of C3G during SERS measurements. Cells were then incubated for 30 minutes with 5 mM 2,2'-Azobis(2-methylpropionamide) dihydrochloride (ABAP) dissolved in HBTS to induce oxidative stress. ABAP is a commonly used azo initiator that can initiate both free radical and nucleophilic oxidations (Werber et al., 2011). At the end of the exposition, cells have been immediately processed for SERS mapping measurements.

### **Data Processing**

All data preprocessing and analysis was performed within the R software environment for statistical computing and graphics (The R Core Team, 2014) and in-house written scripts. In particular, data import and export, preprocessing and visualization were performed with the

hyperSpec package (Beleites & Sergo, 2014) for R, along with the lattice (Cheshire, 2010), and ggplot2 package (Ginestet, 2011) for graphical display.

### **Data acquisition, conversion, and storage**

The preprocessing consisted of four steps: i) cosmic rays identification and removal, ii) baseline correction iii) smoothing interpolation, and iv) intensity vector-normalization. For the baseline correction, a linear baseline was fit automatically to the whole spectral range and was subtracted from each spectrum of the dataset using function modpolyfit from package baseline (Hovde Liland & BjÅ, 2015), and peak picking was performed using detectPeaks from package MALDIquant (Gibb & Strimmer, 2012). Each spectrum was normalized to its mean spectral intensity across all wavenumbers in order to account for fluctuations in laser intensity.

### **Statistical analysis**

After preprocessing, the spectral contribution of cellular background was subtracted applying a cutoff threshold to intensity of single peaks. All the pixels with intensity  $i$  below this cutoff were set to zero. Next, a mean spectrum was generated by taking the arithmetic mean of the processed spectra. In addition to univariate testing, multivariate statistical methods were adopted for data interpretation. High dimensionality is one of the major obstacles to statistical analysis of spectroscopic data. PCA was performed on the mean spectra derived from the four groups of treatment.

## Results and discussion

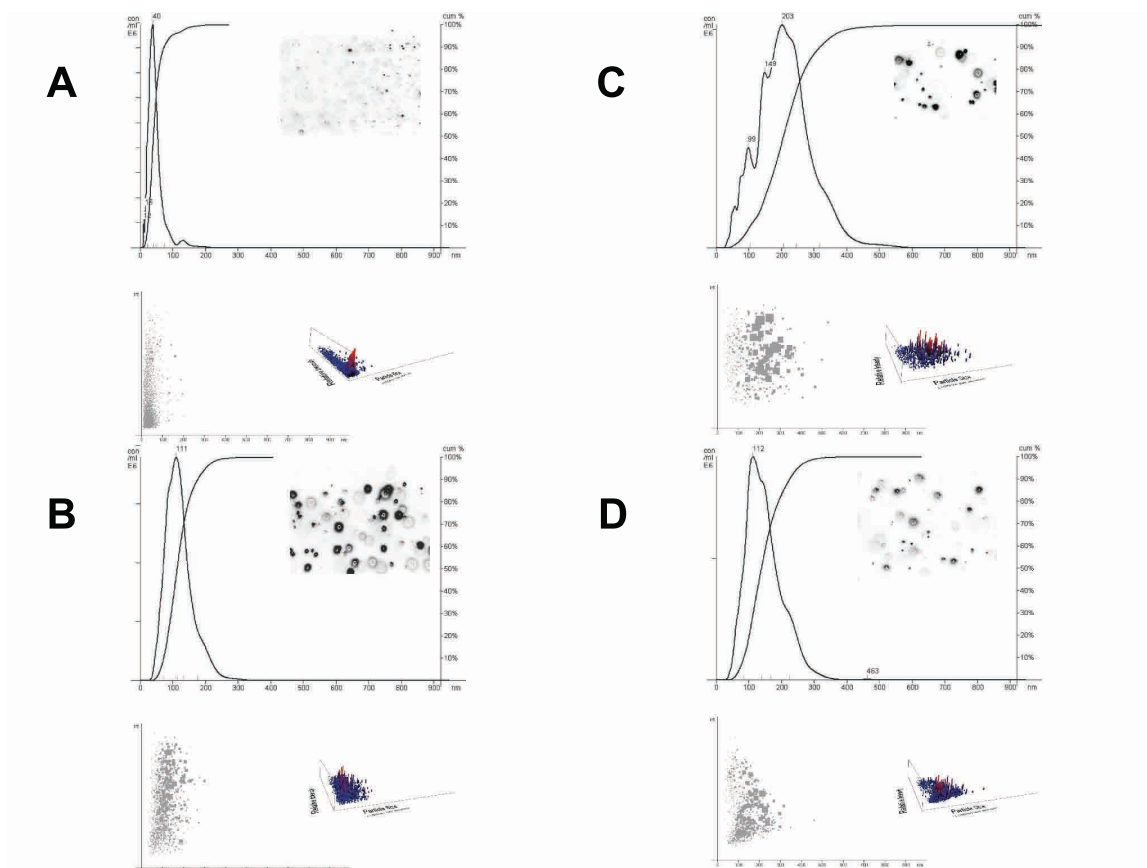


**Figure 7.2 Nanoparticles Tracking Analysis.** **A.** Cit-NPs in mQ-water. **B** 6AF-NPs in mQ-water. **C.** Cit-NPs in DMEM. **D.** 6AF-NPs in DMEM

### Nanoparticle Tracking Analysis (NTA)

Distributions of the hydrodynamic diameters of the 6AF-AuNPs in the different samples were measured by the NTA method. This technique efficiently measures the velocity of tiny particles within the fluid streams moving at the velocity of the fluid. NTA allows nanoparticles to be sized in suspension on a particle-by-particle basis, with higher resolution and therefore better understanding of aggregation than other methods such as dynamic light scattering (DLS) and differential centrifugation sedimentation (DCS) (Montes-Burgos et al., 2009).

Table 1 shows the average diameter values and the concentration obtained by NTA for the citrate- and 6AF- capped AuNPs samples in mQ H<sub>2</sub>O, and after centrifugation and re-suspension in DMEM culture medium. All samples exhibit similar asymmetric distribution curves with slow decaying tails towards large particle diameters, but with different distribution widths (Figure 1). The pH of the DMEM culture medium at 37°C was 7.46 and.

In all instances, the pH of the culture medium decreased slightly when the particles were re-suspended therein; however the observed decreases were not biologically significant.

The NTA data demonstrates that the integrity of the 6AF-AuNPs suspended in cell culture medium was maintained as compared to the 6AF-NPs in water, with minimal signs of particle aggregation present.

**Table 7.1** The average diameters of the citrate-/ (Cit-AuNPs) and 6AF- (6AF-AuNPs) capped gold nanoparticles, obtained by nanoparticle-tracking analysis (NTA) measurements of the NPs samples in mQ water and in DMEM.

	<b>Average diameter (nm) ± SD</b>		<b>Concentration (nps/mL)</b>	
	mQ water	DMEM	mQ water	DMEM
Cit-AuNPs	43 ± 23	203 ± 94	8.56E8	2.85E8
6AF-AuNPs	111 ± 40	112 ± 53	5.55E8	3.42E8

### **Stability**

The stability of Au-NPs-size distribution was examined by repeating NTA measurements of the same samples after 1, 24, and 48 hours. In all these measurements, bimodal curves were obtained very similar to those obtained in the first measurement carried out right after the AuNPs were generated.

### **Cytotoxicity and cellular uptake**

To evaluate the cytotoxicity of the nanosensor, an AlamarBlue assay in Human endothelial-like immortalized cells (EA.hy926) was performed with nanosensor concentration in the range 2 nM - 200 μM (Figure 2). The viability of cells incubated with 6Af-AuNPs for up to 3 days was tested and compared with cells left untreated. According to the experimental observations, the cell viabilities were all more than 90% compared to the control experiments.

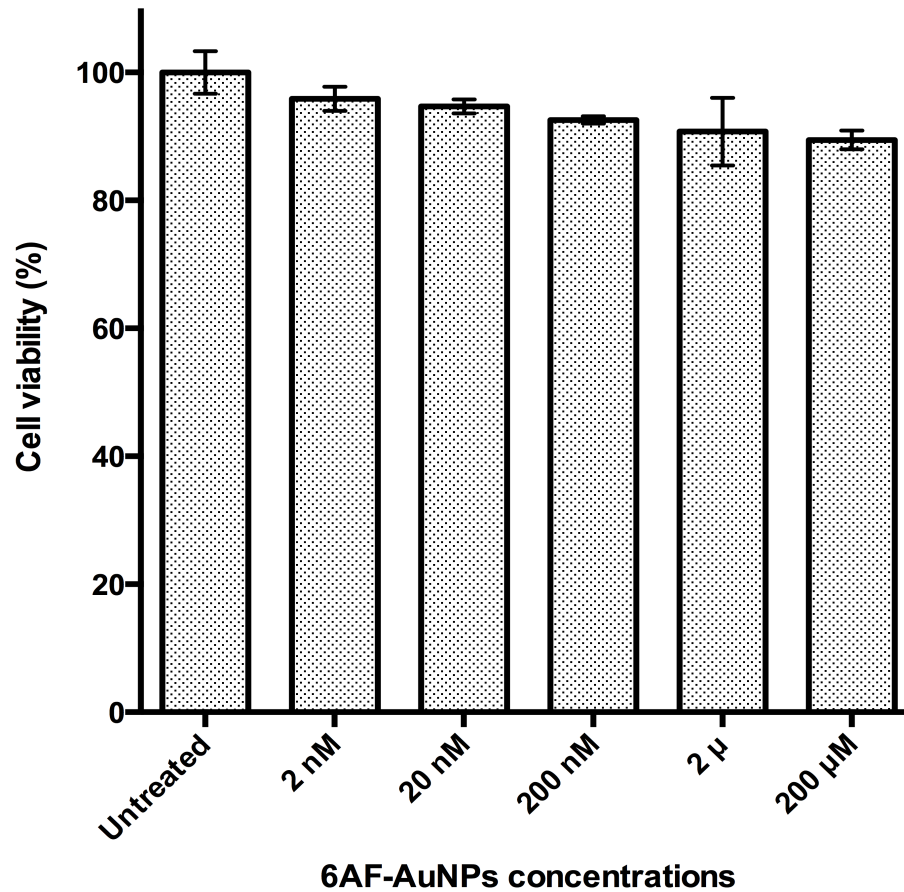


Figure 7.3 AlamaBlue assay of human EA.hy926 cells in the presence of different concentrations of the nanosensor (n=6).

TEM (Figure 3) confirmed that, when 6Af-NS were taken up by the cells of all of four cell lines in serum-free DMEM growth media. It should be noted that the 6AF-AuNPs were predominantly in the cytoplasm and neither encapsulated in vesicles nor coated in lipids. We could observe aggregates of nanoparticles inside cells, which appear as dark spots of the same dimension (~100 nm) measured by NTA. Since no sign of aggregation of AuNPs have been observed in the cell culture medium, therefore we concluded that aggregation was induced inside the endocytotic compartments.

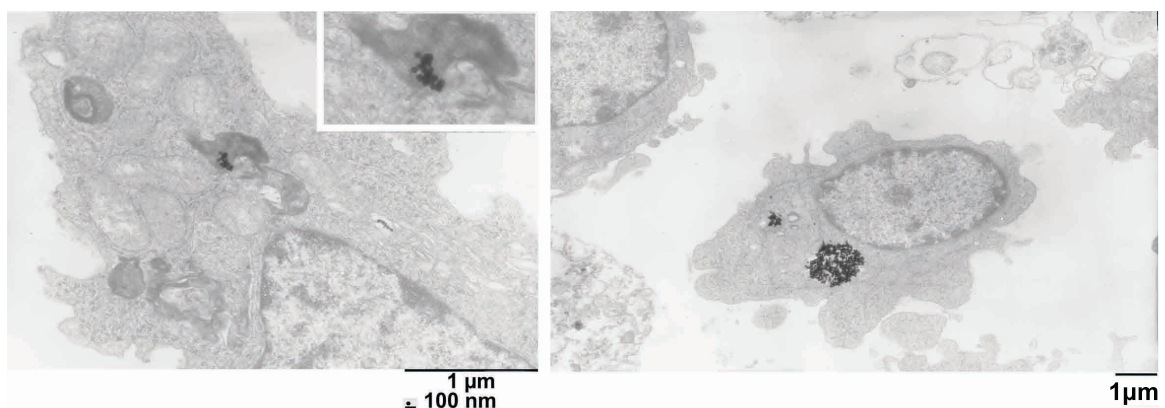


Figure 7.4 TEM images of 6AF-NPs in RAW cells.

While the exact mechanism of uptake remains a matter of investigation, these findings are in agreement with previous studies of nanoparticle uptake which found that nanoparticles can enter cells through a variety of pathways resulting in accumulation in the cytoplasm and may be linked to physical factors such as electrostatics or van der Waals forces (Geiser et al., 2005; Rosi et al., 2006; Rothen-Rutishauser et al., 2007; Schaeublin et al., 2011).

### **Intracellular Surface-Enhanced Raman Spectroscopy with 6AF-AuNPs**

The NSs used in this study were designed to be excited with lasers in the near-infrared region (see previous chapter for details), which has excellent transmittance through tissue. To investigate the potential chemical information gathered from the molecular vibrations of biomolecules, we performed SERS mapping for SH-SY5Y cells incubated with 6AF-AuNPs. The control groups were the cell cultures incubated in label-free medium and medium containing 6AF. For both groups, no Raman signal was recorded (data not shown). According to previously reported results, the use of 735-nm laser excitation and short integration time (0.3 s) does not provide intracellular chemical information without SERS support. SERS cellular mapping measurements provided a spectrum for every pixel interrogated within a single cell (Sathuluri et al., 2011).

The intensity of single peaks or peak regions assigned to a particular molecular vibration(s) within a field of interest were used to generate pseudo-color images showing the spatial distribution of chemical species within the cell (Figure 4). Similar to what has been reported by Salvati (Salvati et al., 2011) and Jaworska (Jaworska et al., 2015), after the uptake of nanoparticles containing high concentrations of a labile dye, the dye molecules are randomly spread across the intracellular space, whereas the dye conjugated to nanoparticles is spatially localized.

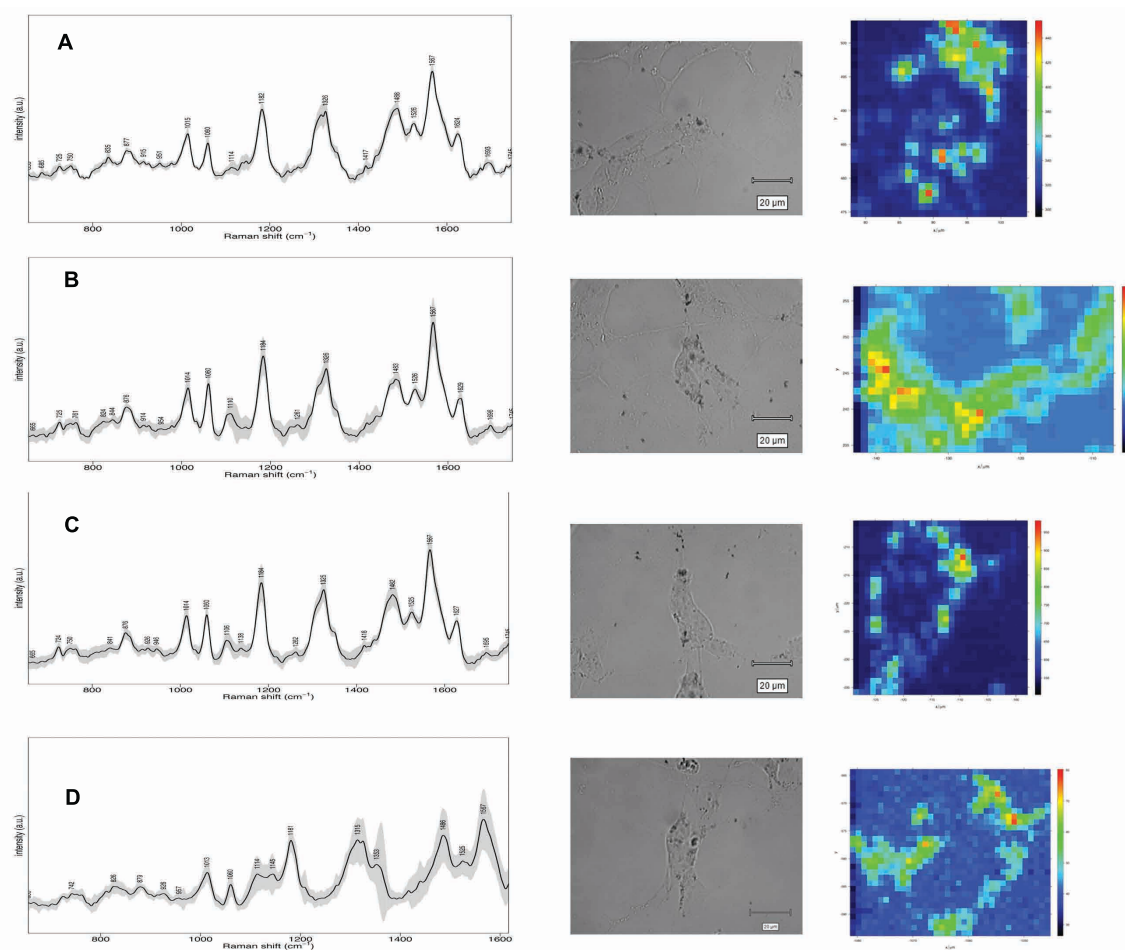


**Figure 7.5** SERS mean spectra extracted from cluster maps of SH-SY5Y cells incubated with 6AF-AuNPs (A); stressed with ABAP (D); in the presence (B) or not (C) of pre-treatment with C3G, along with a microphotography of a cell and a total intensity maps before pre-processing.

Intracellular measurements are affected by the length of time required for cellular NS uptake before SERS mapping. The SERS bands of 6AF were observed in the spectra recorded for incubation times up to 48 h. Their cellular distributions in the cluster maps implicate a decrease in the concentration of 6AF-AuNP particles after a long incubation time (48 h). However, because the SERS spectra for each incubation time also show the presence of bands attributed to various biomolecules, we hypothesized that a detachment of the 6AF molecules from the enhancing surface of the gold occurred in favor of other biomolecules in close vicinity to hot spots.

In preliminary studies probing 6AF-AuNP response in Eahy926 cells, we observed the SERS signal of the dye after only 3 h of incubation, whereas SERS bands originating from various biomolecules were observed up to 16 h. This result indicates that the conjugation of 6AF to nanoparticles is stable in the cellular environment up to a few hours.

### **Assays of oxidative stress**

SERS mapping generates large and complex datasets, thus creating the need for adequate data reduction and analysis. PCA is a suitable tool for these data manipulations, and it also facilitates sample group discrimination in SERS mapping (Llabjani et al., 2011; Martin et al., 2010). The authors suggested that the number of spectra should be several times greater than the number of variables/features in the dataset. Because the number of spectra ( $n = 4112$ ) for each map was almost five times the number of variables (865 data points), we applied PCA.

PCA generates loadings and score plots from the derived PCs of the initial or preprocessed data. The obtained PC loadings are correlation coefficients between the original data and PC scores. PC loadings identify the importance of each variable (i.e., peak in a SERS spectrum). The correlation of a variable to a PC reflects its contribution to the variation in the dataset. Therefore, plots of PC loadings reveal vibrational modes (wavenumbers) corresponding to the variation, which allows for distinction between groups. Thus, we applied PCA to our hyperspectral data to fulfill two aims: data reduction to fewer dimensions and objective distinction between cell groups (control cells [ctrl], stressed with ABAP with [test] or without [stress] protective C3G pre-treatment [c3g]).

PCA was performed on a data matrix containing 173 mean SERS spectra, which were collected from the four treatment groups (ctrl = 38; stress = 59; c3g = 38; test = 38). To allow for group classification, we applied PCA to mean-centered, vector-normalized individual datasets, and the first and second PC scores were plotted with data point coloration according to cell groups (Figure 5). To obtain the PC scores plot, we analyzed SERS spectra belonging to all cells without providing information about treatment type. Thus, any observed clustering of the spectra was considered unbiased and indicative of a common underlying biochemical signature for the particular treatment.



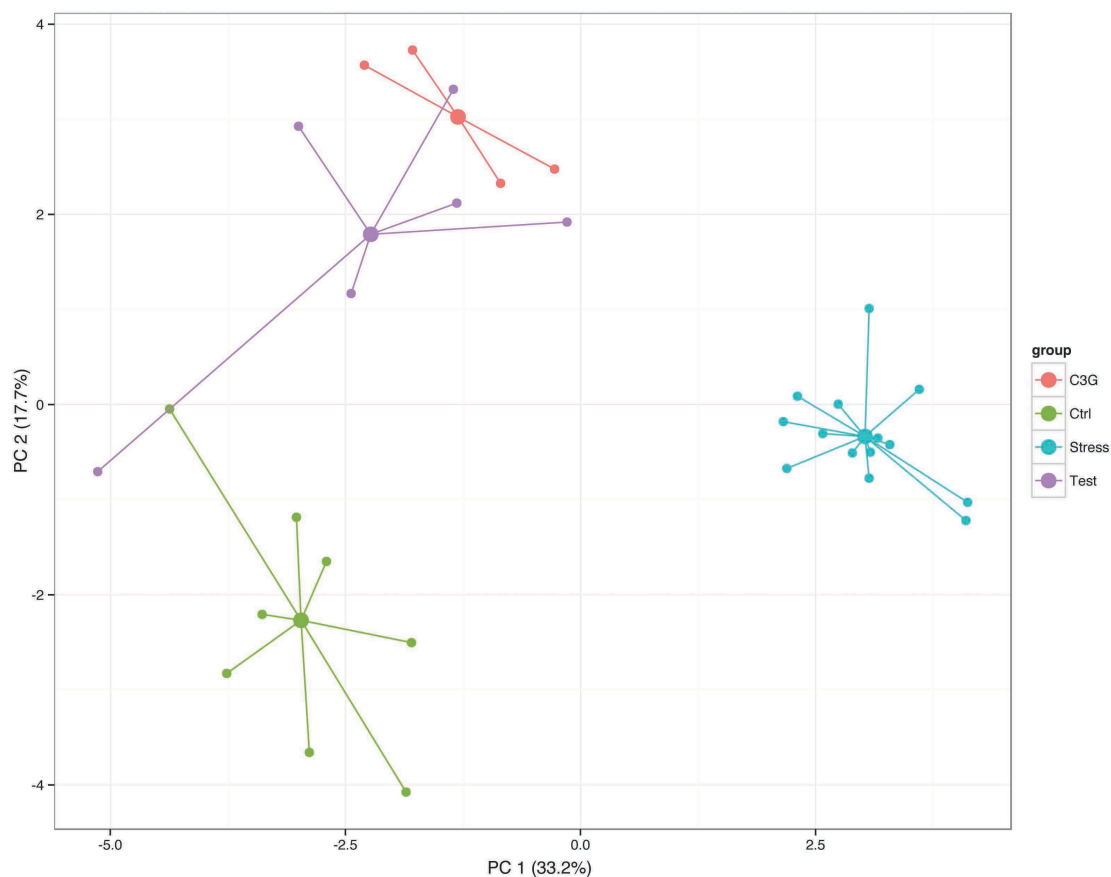


**Figure 7.6 PCA scores plot of mean spectra showing the interclass variance.** To obtain this scores plot, each cell in the dataset is treated as a class without specifying the four classes (i.e., control, pretreated with C3G, stressed with ABAP in presence or absence of C3G treatment). After PCA, individual cells' spectra were given a matching color in accordance with their original group types.

## Conclusions

SERS-based imaging techniques applied to small molecules complement the growing research field of single-cell metabolomics and can be used to interpret many key biological processes in cells. The results of this study suggest that our approach using 6AF-AuNPs and SERS mapping could contribute greatly to the future characterization of antioxidant activity in biomedical and food research. We showed that 6AF-AuNPs can be internalized by cells and have little or no cytotoxicity even at high probe concentrations (above micromolar levels). These versatile and simple ROS/RNS detection probes and assay platforms can be used to relate ROS/RNS detection with oxidative stress status in living cells.

Translating this proof of principle to clinical utility requires further studies, however. The next step must be the characterization of the cellular fingerprint for a biochemical interpretation of each SERS spectrum. Furthermore, combining multiple statistical analysis techniques with SERS mapping into an integrated platform would be a large step forward in the simultaneous measurement of intracellular ROS-generating events.

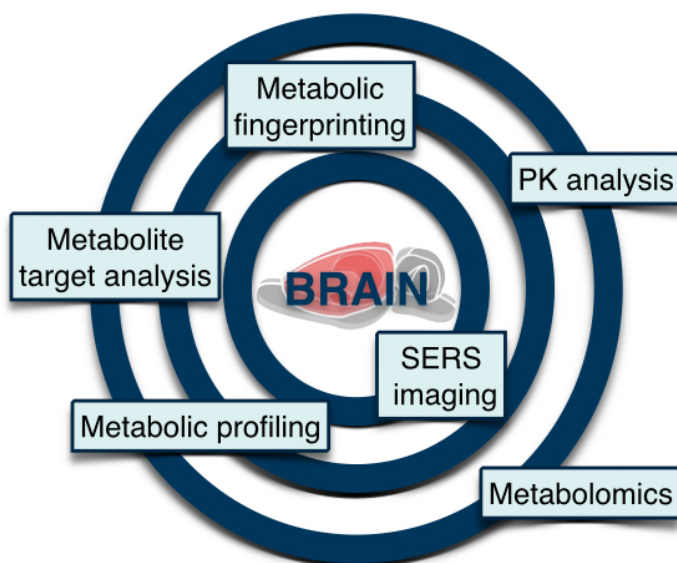
## Bibliographic references

- Beleites, C., & Sergo, V. (2014). HyperSpec: a package to handle hyperspectral data sets in R. *R package version 0.98-20140523*.
- Bonifacio, A., Beleites, C., Vittur, F., Marsich, E., Semeraro, S., Paoletti, S., & Sergo, V. (2010). Chemical imaging of articular cartilage sections with Raman mapping, employing uni- and multi-variate methods for data analysis. *Analyst*, *135*(12), 3193-3204. doi: 10.1039/c0an00459f
- Cheshire, J. (2010). Lattice: Multivariate Data Visualization with R. *Journal of the Royal Statistical Society Series a-Statistics in Society*, *173*, 275-276.
- Geiser, M., Rothen-Rutishauser, B., Kapp, N., Schurch, S., Kreyling, W., Schulz, H., . . . Gehr, P. (2005). Ultrafine particles cross cellular membranes by nonphagocytic mechanisms in lungs and in cultured cells. *Environ Health Perspect*, *113*(11), 1555-1560.
- Gibb, S., & Strimmer, K. (2012). MALDIquant: a versatile R package for the analysis of mass spectrometry data. *Bioinformatics*, *28*(17), 2270-2271. doi: Doi 10.1093/Bioinformatics/Bts447
- Ginestet, C. (2011). ggplot2: Elegant Graphics for Data Analysis. *Journal of the Royal Statistical Society Series a-Statistics in Society*, *174*, 245-245. doi: Doi 10.1111/J.1467-985x.2010.00676\_9.X
- Hawkes, P. W. (1985). *The Beginnings of electron microscopy*. Orlando: Academic Press.
- Hovde Liland, K., & BjÅ, r.-H. M. (2015). baseline: Baseline Correction of Spectra. Retrieved from <http://CRAN.R-project.org/package=baseline>
- Jaworska, A., Wojcik, T., Malek, K., Kwolek, U., Kepczynski, M., Ansary, A. A., . . . Baranska, M. (2015). Rhodamine 6G conjugated to gold nanoparticles as labels for both SERS and fluorescence studies on live endothelial cells. *Mikrochim Acta*, *182*, 119-127. doi: 10.1007/s00604-014-1307-5
- Llabjani, V., Trevisan, J., Jones, K. C., Shore, R. F., & Martin, F. L. (2011). Derivation by infrared spectroscopy with multivariate analysis of bimodal contaminant-induced dose-response effects in MCF-7 cells. *Environ Sci Technol*, *45*(14), 6129-6135. doi: 10.1021/es200383a
- Martin, F. L., Kelly, J. G., Llabjani, V., Martin-Hirsch, P. L., Patel, II, Trevisan, J., . . . Walsh, M. J. (2010). Distinguishing cell types or populations based on the computational analysis of their infrared spectra. *Nat Protoc*, *5*(11), 1748-1760. doi: 10.1038/nprot.2010.133
- Montes-Burgos, I., Walczyk, D., Hole, P., Smith, J., Lynch, I., & Dawson, K. (2009). Characterisation of nanoparticle size and state prior to nanotoxicological studies. *Journal of Nanoparticle Research*, *12*(1), 47-53. doi: 10.1007/s11051-009-9774-z

- Palonpon, A. F., Ando, J., Yamakoshi, H., Dodo, K., Sodeoka, M., Kawata, S., & Fujita, K. (2013). Raman and SERS microscopy for molecular imaging of live cells. *Nat Protoc*, 8(4), 677-692. doi: 10.1038/nprot.2013.030
- Rampersad, S. N. (2012). Multiple applications of Alamar Blue as an indicator of metabolic function and cellular health in cell viability bioassays. *Sensors (Basel)*, 12(9), 12347-12360. doi: 10.3390/s120912347
- Rosi, N. L., Giljohann, D. A., Thaxton, C. S., Lytton-Jean, A. K., Han, M. S., & Mirkin, C. A. (2006). Oligonucleotide-modified gold nanoparticles for intracellular gene regulation. *Science*, 312(5776), 1027-1030. doi: 10.1126/science.1125559
- Rothen-Rutishauser, B., Muhlfeld, C., Blank, F., Musso, C., & Gehr, P. (2007). Translocation of particles and inflammatory responses after exposure to fine particles and nanoparticles in an epithelial airway model. *Part Fibre Toxicol*, 4, 9. doi: 10.1186/1743-8977-4-9
- Salvati, A., Aberg, C., dos Santos, T., Varela, J., Pinto, P., Lynch, I., & Dawson, K. A. (2011). Experimental and theoretical comparison of intracellular import of polymeric nanoparticles and small molecules: toward models of uptake kinetics. *Nanomedicine*, 7(6), 818-826. doi: 10.1016/j.nano.2011.03.005
- Sathuluri, R. R., Yoshikawa, H., Shimizu, E., Saito, M., & Tamiya, E. (2011). Gold nanoparticle-based surface-enhanced Raman scattering for noninvasive molecular probing of embryonic stem cell differentiation. *PLoS One*, 6(8), e22802. doi: 10.1371/journal.pone.0022802
- Schaeublin, N. M., Braydich-Stolle, L. K., Schrand, A. M., Miller, J. M., Hutchison, J., Schlager, J. J., & Hussain, S. M. (2011). Surface charge of gold nanoparticles mediates mechanism of toxicity. *Nanoscale*, 3(2), 410-420. doi: 10.1039/c0nr00478b
- The R Core Team. (2014). R: A Language and Environment for Statistical Computing. Vienna, Austria: R Foundation for Statistical Computing.
- Turkevich, J., Stevenson, P. C., & Hillier, J. (1951). A study of the nucleation and growth processes in the synthesis of colloidal gold. [10.1039/DF9511100055]. *Discussions of the Faraday Society*, 11(0), 55-75. doi: 10.1039/DF9511100055
- Werber, J., Wang, Y. J., Milligan, M., Li, X., & Ji, J. A. (2011). Analysis of 2,2'-azobis (2-amidinopropane) dihydrochloride degradation and hydrolysis in aqueous solutions. *J Pharm Sci*, 100(8), 3307-3315. doi: 10.1002/jps.22578

## **Section IV - Conclusions & future directions**

## Targeting natural antioxidant compounds to the brain



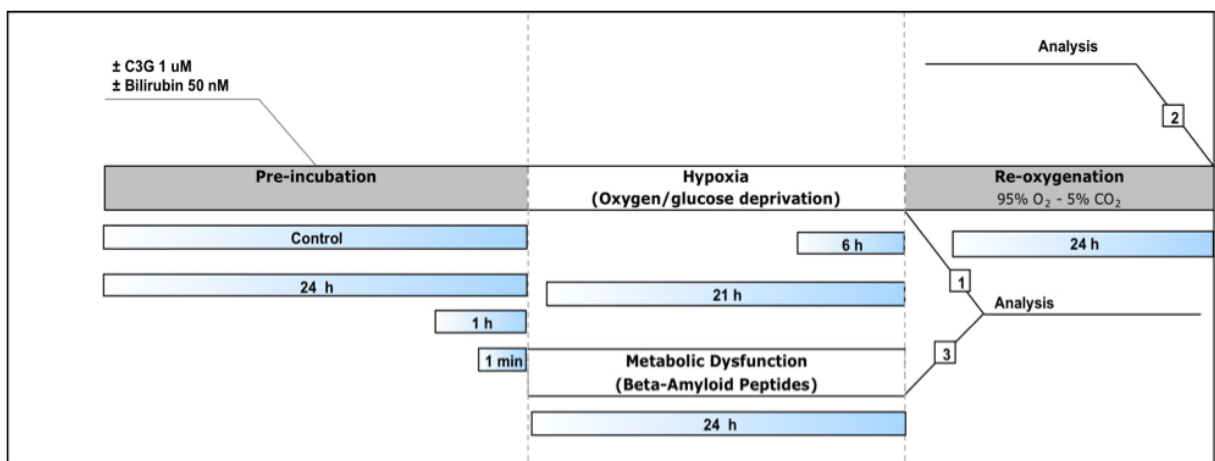
There is currently sparse evidence in literature describing the mechanistic relationship between dietary flavonoids, such as cyanidin 3-glucoside, and improved cognitive function. With this thesis, we have successfully conducted a multilevel integrated study that set the pharmacokinetic conditions to succeed in observing neuroprotective and cognitive enhancement activities in future *in vitro* and *in vivo* experiments. Furthermore, these conditions are important when designing and interpreting intervention trials in animals and humans, aimed at establishing the link between intake of anthocyanin-rich food/nutraceuticals and protection against age-related cognitive dysfunctions.

The data presented here could also be useful for awarding the rationale for using the flavonoid-rich diet and/or the pure dietary flavonoids as nutraceuticals to enhance neuroprotective pathways in healthy population. This preventive approach could be further incorporated into the interventions strategies to prevent oxidative stress-induced diseases. Ultimately, experiments will have an impact on society by contributing new knowledge in designing the recommended dietary guidelines for healthy brain aging.

## Future Direction

Given the heterogeneity of almost all biological systems, and the limitations of big untargeted experiments, it is evident here that there's a need for improved methods for measuring metabolomics in single cells, preferably noninvasively and *in vivo*.

Findings from SERS mapping will be implemented in the creation of an experimental model that simulates astrocyte metabolic dysfunction, mimicking the pathological mechanisms occurring in neurodegenerative disorders, in particular Parkinson's and Alzheimer's disease. Such model should find applications in basic studies but could also be exported to applied research, for example, when considering the cellular responses to New Chemical Entities.



- Cell culture  
Primary rat astrocytes, microglia and oligodendrocytes;
- Hypoxia-reoxygenation model [1-2]  
Oxygen-Glucose Deprivation (OGD);  
Hypoxic, Acidic, Ion-shifted (HAI)
- Beta-amyloid neurotoxicity model [3]  
 $\beta$ A 25-35,  $\beta$ A 1-42
- Analytical platform  
Cell viability assays (Alamarblue, Prestoblue, MTT)  
GSH/GSSG ratio measurement (UHPLC-MS/MS)  
ATP/ADP ratio measurement (fluorescence-based)  
ROS fingerprint (SERS mapping)

# Acknowledgments

The research work presented here is the fruit of working with many gifted scientists. It's with great humility and gratitude that I acknowledge the kindness and generosity of so many people who have helped me during my graduate studies.

First in line for many thanks is, obviously, my supervisor Sabina Passamonti, for her strength, support, thoughtful scientific discussions, and for the motivation that helped me to achieve my research goals.

I am grateful to thank Dr. Lovro Ziberna. For the last six years he has been my tutor, my critical audience, my motivational speaker, my information source (I'm still trying to moonwalk with Einstein), and, above all, my friend. Additionally, I would like to thank him for his patience in reading my manuscripts, flying across Europe.

I thank the present and former members of the research group with whom I shared a very pleasant time and also for their fruitful scientific discussions. Dr. Federica Tramer, the master of the lab, Dr. Antonella Bandiera, my first cell culture instructor, and prof. Paola D'Andrea, my last precious "guest". Then Ambra Delneri, Odeta Kalaja, Luisa Alessio, Antonio Filippi, Spela Moze, Raphael Okonji, Ayo Ademosun, Jovana Čvorović, Lucia Corich, and Desolah Ogonruku. I thank all of them for tolerating with all my monkey nonsense, for the caloric restriction and the snooty moments. We came from different backgrounds, disciplines, and countries with diverse cultures, yet grew to celebrate our differences. We worked, at times, in very tiny rooms, functioning on too little sleep and coffee, shared our meals, music, thoughts, fights, and dreams, laughed and learned, lost our tempers and found fortitude, and, through all of this, revealed and discovered the strengths and weaknesses of each other and ourselves. I would have had it no other way.

I thank other group members of the Department of Life Sciences in the C11 building of University of Trieste, who made friendly and relaxed work atmosphere. Special thanks to Sabrina Semeraro, Giancarlo Sannini and Ilenia D'agostino; they became a surrogate family to me during the last three years.

The wonderful people I have been privileged to work with in the Metabolomics group at the Edmund Mach Foundation (FEM) deserve my gratitude for training me in the ways of more analytically-oriented research. Special thanks to: my tutor, Dr. Fulvio Mattivi for the excellent scientific discussions and advice; Dr. Kajetan Trost for helping me to realize that being crazy

is not such a bad thing, and what should be my next big choice; dr. Marynka Ulaszewska for her expertise on the mass spectrometers; in the latter days of my work at FEM, I found myself asking Dr. Pietro Franceschi many questions. His door was always open and I appreciated his willingness to share his knowledge and his opinions. It is because of him that I can now manage the fundamental concept of “Academic Trimurti”. I would also like to thank Urska Vrhovsek, Mattia Gasperotti, Giulia Chitarrini, Domenico Masuero and my housemates, Federico, Livio, Hugo and Valerio.

Special thanks go Prof. Mojca Kržan, director of the Department of Pharmacology and Experimental Toxicology at the Medical Faculty of University of Ljubljana. During my placement there, I had the possibility to share with her many meaningful conversations. She made me aware that the hours spent redressing with the students all the basic theories in pharmacokinetics were never a waste of time.

I would like to thank dr. Andreja Vanzo of Agricultural institute of Slovenia for the assistance, coaching, and training she gave me in instrumental analysis and to dr. Vanessa Nicolin of the Department of Medicine, Surgery and Health Sciences for the TEM pictures.

I must give special recognition to dr. Annalisa Vicario, dr. Alois Bonifacio and prof. Valter Sergo for their encouragement and trust in my scientific abilities. Their guidance, encouragement, creative ideas helped me greatly to overcome the difficulties, which I encountered during my PhD.

Special thanks go to prof Joe Vinson, for his willingness to serve as external referee for my committee. He provided the insight I needed to continue and complete some of the aspects of these studies. Speaking with Dr. Vinson was always refreshing and his enthusiasm for his work was both contagious and encouraging. I would also like to give special thanks to prof Giacinto Scoles, as a student in his courses I realized how far I was from the truth.

Along the way, my colleagues at Graduate school of Nanotechnology became a very important part of my life. The members of the organizing committee of the First FVG PhD Symposium (Arianna Bellazzo, Anna Comel, Amna Abdalla Mohammed Khalid, Marienette Morales Vega, Francesca Nadalin, Emanuela Pitassi, Mattia Poletto, Clara Grudina Luca Caniparoli) and I shared many good times in a great adventure in Grado. It has been an honor.

I am deeply indebted to my friends for their presence during hard times, and for their moral and emotional support, or at least for their couches. Special thanks go to Fabio and Eliana,



Matteo, Cian, Anna, Il Matto, Mauretto, Cosimo and Maria, Pietro, Lida, Maja and Alessio, Randaz the President, Agnese, Marta, Sara, Fabio, Federica, Johnny and Misha.

My heartfelt gratitude goes to my big family for their love and encouragement.

All people mentioned above, and probably many others who I forgot to acknowledge, should know that this thesis is as much theirs as mine.

*“... and Thanks For All the Fish”.*

Stefano Fornasaro